Tribological Assessment of Hydrogels for Replacing Damaged Articular Cartilage

A dissertation

Submitted to the Faculty

of

Drexel University

by

Doruk Baykal

In partial fulfillment of the

Requirements for the degree

Of

Doctor of Philosophy

March 2013

Dedication

This dissertation is dedicated to my parents and the center of my universe, Burcu.

Acknowledgements

I would like to thank my advisor and mentor, Dr. Steven Kurtz, for making me a better engineer, writer, businessman and much more.

I would also like to acknowledge Dr. Banu Onaral, whose vision led me to where I am right now.

Thanks to Drs. Nancy Pleshko and Michele Marcolongo for their constant support and critical, yet, compassionate approach to my research.

Thanks to Ryan Siskey, who always provided me with solutions to the endless problems related to mechanical testing and fixtures.

I would also like to acknowledge Dr. Judd Day for his invaluable advice and teaching by example how to be a better scientist.

Thanks to Drs. Rahamim Seliktar, Adrian Shieh and Sriram Balasubramanian, who taught me how ask the relevant questions in order to improve the quality of this dissertation.

Finally, I would like to acknowledge my fellow IRC members, especially, Dan MacDonald, Dave Jaekel and Ryan Baxter, who made me a part of the team.

Table of Contents

List of Tables

List of Figures

Dissertation Abstract

Tribological Assessment of Hydrogels for Replacing Damaged Articular Cartilage
Doruk Baykal

In joint disorders, lesions may be limited to the joint surface. In such cases, replacing only the affected surface to preserve healthy tissue and cancellous bone is preferable to total joint arthroplasty. By employing a cartilage replacement material in focal defect repair or hemiarthroplasty applications, joint stability may be preserved while patient pain and joint dysfunction may be reduced. Hydrogels have been studied to replace damaged articular cartilage tissue. The motivation is that hydrogels may maintain natural joint lubrication due to their biphasic nature and their structure can be modified to mimic mechanical properties of articular cartilage. In order to assess the tribological properties of such a biphasic material, its lubrication mechanisms, the damage it causes on the opposing articular cartilage, and its wear properties under clinically relevant conditions were evaluated in the current dissertation. A biphasic model with linear-elastic solid matrix sufficiently predicted the material behavior of the family of tested hydrogels. Also, Stribeck analysis suggested that hydrogel-on-ceramic articulation was lubricated by a fluid film. Together, these findings suggested that, similar to articular cartilage, interstitial fluid pressurization was crucial to the viscoelasticity and lubrication properties of this biphasic material. Results indicated that biphasic materials with smaller aggregate moduli (spearman's rho=0.5; $p<0.001$) and larger permeability values (rho=-0.3; $p<0.001$) than those of the tested hydrogels in this study would produce lower coefficients of friction. Furthermore, collagen maturity and proteoglycan content as obtained by Fourier transform infrared spectroscopy were shown to decrease at the onset

of *in vitro* cartilage wear before surface damage occurred. Cartilage pins that articulated against cartilage and hydrogel yielded higher collagen maturity than cartilage on CoCr articulation in a physiologic pin on disc (POD) wear tester. However, only cartilage-on-cartilage articulation yielded higher proteoglycan content than cartilage-on-CoCr articulation. It was postulated that the cartilage articulations against cartilage, hydrogel and CoCr in the current research represented three distinct stages of in vitro wear of articular cartilage. Finally, submerged weights were found to be more suitable than wet weights in quantifying wear of hydrogels in spite of unwanted effects of swelling. Based on submerged weights, the wear rate of hydrogel articulations was -1.4 ± 8.3 mm^3 / MC, which was not statistically different than undetectable wear. The combination of coefficient of friction measurements, white light interferometry, and environmental scanning electron microscopy supported that wear generated was undetectable up to 5 million cycles of physiologic POD testing.

Introduction

Aseptic Loosening of Implants, Osteolysis and Revision Surgery

Joint replacements last 10 years in over 90% of patients and future demand for joint replacements is projected to increase [1]. In the US, more than 1 million joint disease patients underwent primary hip and knee joint replacement operations in 2010 alone [1]. Aseptic loosening of implants is a threat to the long-term success of joint replacements [1-3]. In 2005, the second most frequent cause for total knee arthroplasty revision in the States was implant loosening [4]. In addition, Kurtz et al. reported aseptic loosening to be the most prevalent reason for revision of retrieved hip implants with first generation highly-crosslinked Polyethylenes [5]. The revision rate for total joint arthroplasty is a significant economic burden to health care [1]. Revision surgeries constitute 10-20% of health care economies in Western countries [1].

Although no correlation between loosening and wear was found in a recent study on retrieved hip implants [5], wear of Ultra-High-Molecular-Weight Polyethylene (UHMWPE) is accepted as the cause of osteolysis and loosening [1-3, 6-9]. Even small amounts of wear can result in around 100 million microscopic UHMWPE pieces that enter the tissue daily [1, 6]. These submicron particles can induce adverse tissue reaction including foreign macrophage and giant cell reactions and can lead to bone resorption and osteolysis [1-3, 6, 7, 10]. In order to ensure longevity of total joints, *in vivo* wear debris generation must be minimized [2].

Various strategies have been employed by researchers to improve the wear resistance of UHMWPE in an attempt to increase implant longevity [11]. Modifying processing steps [12, 13], crosslinking followed by heat treatments and antioxidant

additives [6, 9, 14, 15], composites [16], alternative counter bearings [8, 17-20], and coatings of UHMWPE and the counter bearing [21, 22] were evaluated. Nevertheless, the wear rate of implants could not be reduced to such low values to practically stop wear and loosening in the lifetime of patients.

With the aim of minimizing *in vivo* wear debris generation, the clinical standard, UHMWPE-on-metallic femoral head, was challenged. Instead of UHMWPE, compliant materials, which would distribute loads and enhance fluid film lubrication, articulated against hard bearings [23-26]. Non-porous polyurethane [23], polyurethane composite with layers of varying elastic moduli [24], porous polyurethane foams [25] and elastomeric polyurethane [26] were among the compliant materials that were evaluated. Although compliant materials displayed low coefficients of friction when fluid film lubrication was maintained, their coefficients of friction [23, 25] and wear rates [26] increased significantly under physiologically relevant loading and velocity conditions.

Concern about longevity of total joint replacements has renewed interest in hemiarthroplasty for certain hip disorders and as an intermediate intervention [27, 28]. In certain conditions such as femoral neck fracture, localized chondral defects, trauma damage, shoulder fractures and avascular necrosis of the femoral head of younger patients, it may be preferable to remove only the affected joint surface instead of total joint arthroplasty [29-31]. Hemiarthroplasty is advantageous because it is less invasive, it preserves healthy tissue and bone [32], and allows faster recovery [29]. In addition to *in vivo* wear of the implant, an important concern in hemiarthroplasty is the wear of the opposing cartilage against the implant surface [29-31]. Cartilage articulation against hemiarthroplasty materials such as CoCr and alumina ceramic may lead to pain and

cartilage erosion [27, 29, 33]. Researchers have therefore investigated materials that could perform better than CoCr [27, 29], the primary material used for this procedure. Recently, biphasic materials, i.e., hydrogels, were proposed to replace damaged articular cartilage tissue [31, 34-40] and facilitate biphasic lubrication while articulating against the opposing cartilage surface [31, 35, 36, 40].

Structure and Function of Articular Cartilage

Articular cartilage is a soft tissue, which acts as the bearing material in diarthrodial joints [41-44]. It operates under high loads while producing low friction and wear [43-45]. Articular cartilage consists of chondrocytes and an extracellular matrix swollen with interstitial fluid [41, 43, 44] (Figure 1). The composition of the extracellular matrix varies with depth from surface and age [41, 46-48]. Cartilage function is determined by the interaction of its matrix constituents [47]. Depending on parameters such as age and location in the joint, 60-70% of the matrix consists of collagen whereas proteoglycan takes up 10-15% by dry weight [41, 43]. The interstitial fluid constitutes, on the other hand, 65-75% of articular cartilage [41, 43, 49]. Finally, chondrocytes constitute 5-10% of the wet weight of the extracellular matrix [47, 50]. Chondrocytes get their nutrients form the synovial fluid by diffusion; compression and relaxation of tissue lead to fluid exudation and uptake [47]. Proteoglycans are made up of a linear chain of hyaluronic acid that accommodates 50-100 glycosaminoglycans, which are negatively charged sulfate groups [41, 46, 50]. The charged glycosaminoglycans attract fluid [41], resist interstitial fluid flow and produce very low permeability in the range of 10^{-14} to 10^{-16} m^4/Ns [44, 50-52]. Fluid trapped in the proteoglycan network acts as a cushion against compression. Proteoglycan concentration is smallest in the superficial zone, maximum in

the middle zone and decreases in the deep zone [46, 48]. Due to high proteoglycan content, the middle zone contributes significantly to the compressive strength of the tissue [47]. Collagen network, on the other hand, provides the matrix with tensile load capability [44] and balances the swelling force of the proteoglycans [47, 50]. Cartilage collagen is composed of three polypeptide alpha chains that are covalently bonded [50] and is unable to form larger bundles [46]. This characteristic allows the collagen network to disperse through proteoglycans efficiently [46]. The orientation of collagen fibers varies with depth: the fibers are parallel to the surface in the superficial tangential zone; they are randomly placed in the middle zone and perpendicular to the surface in the deep zone [41, 46, 48]. In the superficial zone, collagen network and proteoglycans are strongly integrated to withstand tension. The zonal organization of constituents was shown to minimize the stresses on the tissue [46]. In addition to its role in the cartilage biomechanical functions, collagen in the superficial zone decreases the permeability of the tissue [47]. The disruption of this collagen layer was shown to result in a higher coefficient of friction for the tissue [51]. Synovial fluid is a non-homogeneous and non-Newtonian fluid due to the lubricant proteins [53, 54]. It lubricates the joint and reduces the coefficient of friction between articulating cartilage surfaces [53, 55, 56]. Two important constituents of synovial fluid are high molecular weight hyaluronate, which determines the viscosity of the fluid and lubricin, a glycoprotein responsible for the low coefficient of friction [51].

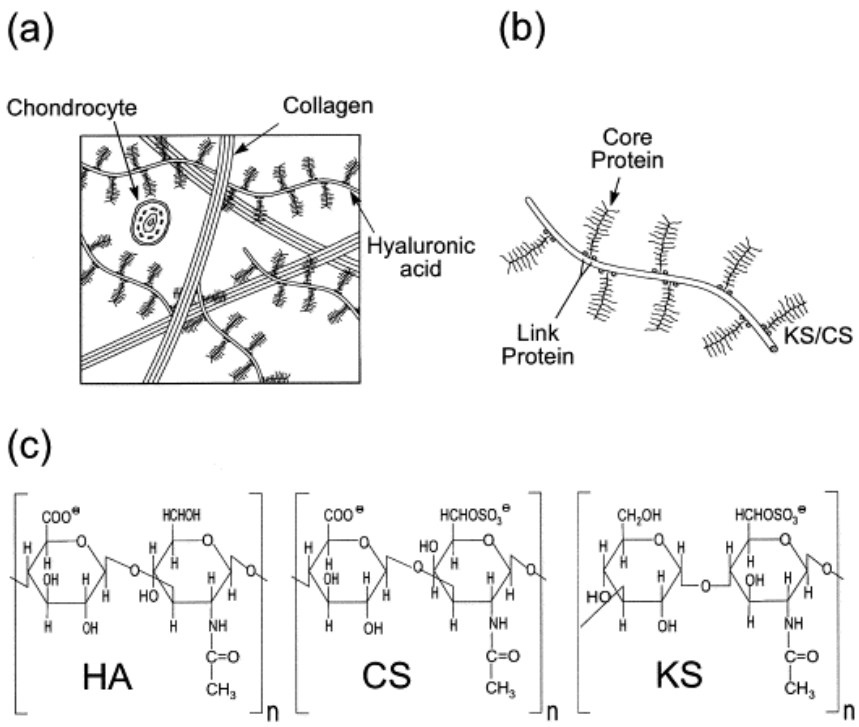

Figure 0-1) a- Matrix constituents of articular cartilage b- proteoglycan subunit c- chemical structures of hyaluronic acid, chondroitin sulfate and keratan sulfate are shown [57].

Articular cartilage cannot heal itself easily once it is damaged because it is avascular [47, 51]. Approximately 40 million Americans suffer from degenerative joint disease [40], whose estimated annual cost to the economy in lost wages and health care is about 1% of gross national product [40]. Osteoarthritis (OA), which is a degenerative disease of articular cartilage [58-60], is the leading cause of disability in United States [61]. In the UK, it is estimated that 15% of the population suffer from arthritis or related conditions [51]. The cost to the health and social services of this condition was 5.5 billion pounds in 1999 and 2000 alone [38]. OA causes pathological changes to the structure and contents of cartilage matrix [48, 58]. Surface fibrillation [52], loss of proteoglycans [51], increased water content [59], decreased collagen content and changes in collagen fibril orientation [59] at the onset of OA lead to mechanical and tribological changes resulting in matrix degradation. OA may also disrupt the rheological properties of synovial fluid

further affecting the lubrication of the joint [62]. When advanced levels of OA is reached, damaged articular cartilage tissue requires intervention [48]. OA, along with avascular necrosis [63], is the major indication for joint arthroplasty [48]. Rheumotoid arthritis, which is an autoimmune disorder leading to cartilage degeneration, can now be treated with disease-modifying antirheumatic drugs [64].

Although advanced stages of OA can be diagnosed by radiographic imaging, early stages that only involve cellular or molecular changes cannot easily be identified [60]. This information could assist surgeons in deciding between salvaging or removing cartilage during hemiarthroplasty operations [60]. Fourier Transform Infrared Spectroscopy (FTIRS) has been established as a powerful tool for cartilage evaluation [48, 65-70], including the use of mid-IR fiber optics for intact tissue evaluation [60, 71], and IR imaging of engineered cartilage constructs [72]. FTIRS is capable of spatially resolving multiple parameters simultaneously and is quantitative [48, 60, 67, 73-75]. Matrix constituents of cartilage have characteristic peaks in the infrared region between 1700-1000 cm^{-1} (Figure 2). For instance, the amide I absorbance (1595-1710 cm^{-1}) arises from the amide I carbonyl (C=O) stretch [48, 76, 77]. The infrared absorbance area between 985-1140 cm^{-1} is due to the proteoglycan sugar ring C-O absorbance [48, 70, 75]. FTIRS was employed to monitor molecular changes associated with degenerative cartilage structure and successfully differentiated healthy and early osteoarthritic cartilage before surface damage, such as clefts, fissures and fibrillations were apparent [60, 75]. Parameters such as collagen integrity, collagen content, proteoglycan content and collagen fibril orientation were used to compare control and osteoarthritic cartilage (Figure 3) [48].

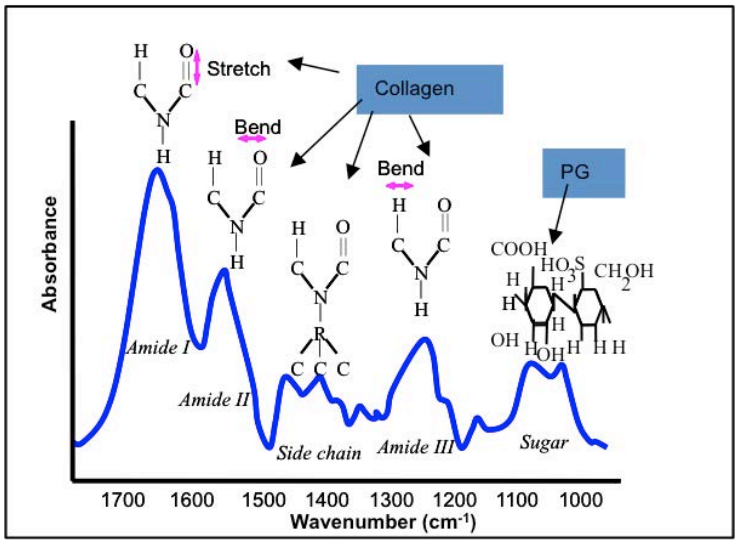

Figure 0-2) FTIR spectrum of cartilage provides molecular structure information about its matrix constituents. Courtesy of Arash Hanifi.

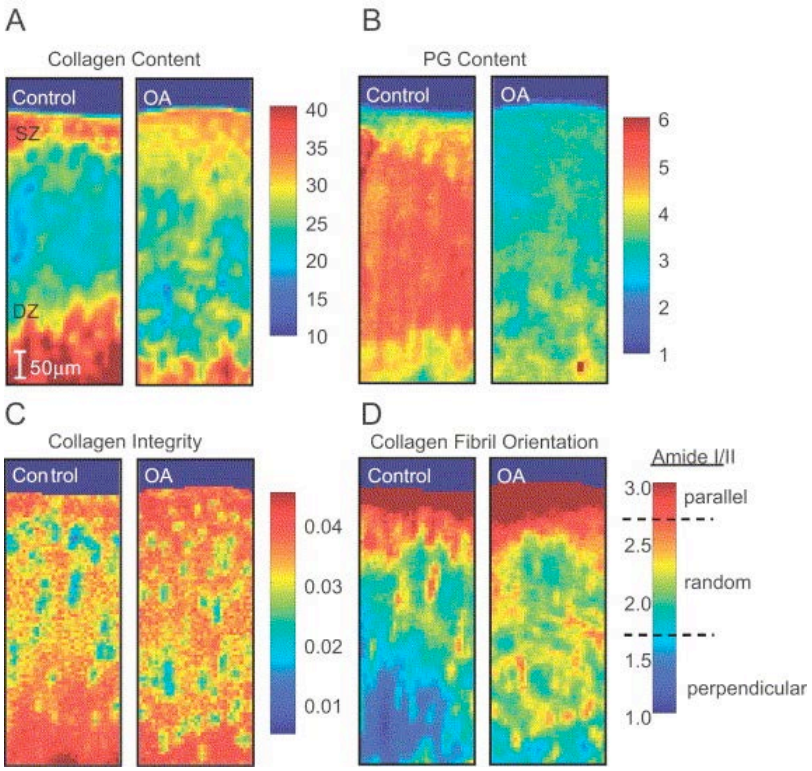

Figure 0-3) FT-IR images enables comparison of control and osteoarthritic cartilage in terms of collagen content, PG content, collagen integrity and collagen fibril orientation [48].

Hydrogel for Cartilage Replacement

Hydrogels are complex hydrophilic polymer networks that are swollen with water [23, 39, 78]. These networks contain ionic or covalent crosslinks [79]. Chain entanglements, hydrogen bonded structures, van der Waals forces and crystallites serve to crosslink hydrogels [79]. They have been used in various applications such as contact lenses, drug delivery devices, separations and scaffolds for tissue engineering [34, 39, 79]. Hydrogels have also been researched to replace damaged articular cartilage [34-37, 78, 80]. The motivation is twofold; first, due to their biphasic nature, hydrogels may maintain natural joint lubrication [35, 38]. Second, their structure can be tailored so that their mechanical properties mimic those of articular cartilage and reduce contact stresses [35, 40]. Increasing crosslinking density, creating a double network with a stronger material, and increasing molecular weight of the polymers were considered to improve the mechanical strength of hydrogels for load bearing applications [34, 40, 79]. Polyvinyl alcohol (PVA) [32, 36, 40, 80-84], Poly-acrylamide (AAm) and poly-dimethylacrylamide (DMAA) [85], gellan and poly(2-acrylomido-2-methylpropanesulfonic) (PAMPS) [82], poly vinyl alcohol and poly(vinyl pyrolidone) (PVA/PVP) [35, 79, 86], poly (2-hydroxyethyl methacrylate) (pHEMA) [37, 39], full interpenetrating network (FIPN) methacrylate [38] and double network hydrogels [34] were among the hydrogels evaluated for this purpose.

Mechanical Behavior of Hydrogels

Hydrogels have been characterized by various testing configurations, such as confined and unconfined compression creep tests and indentation tests [37, 86, 87]. Yet,

modeling the mechanical response of hydrogels using biphasic cartilage models will enable direct comparisons to articular cartilage [86].

The biphasic cartilage model successfully explained how interstitial fluid pressurization supports the collagen-proteoglycan network in withstanding high contact loads by taking into account an incompressible fluid phase and a solid matrix phase [41, 42, 49, 88]. Mow et al. modeled the collagen-proteoglycan network as a linear elastic matrix in the biphasic model (KLM) where the time dependent response of cartilage was only due to interstitial fluid flow [41, 89]. Since collagen fibrils and proteoglycan gel are known to be viscoelastic [90], Mak expanded on the linear biphasic model by introducing relaxation of the solid matrix as a second source of time dependent response, which resulted in the biphasic poroviscoelastic (BPVE) cartilage model [49, 88]. Although these models were successful in predicting cartilage response in confined compression configuration, peak to equilibrium load intensity ratio observed in unconfined compression experiments was not possible to account for using isotropic matrix assumptions [91, 92]. Most recently, anisotropy was introduced to the solid matrix phase of the linear biphasic model where differences in stiffness in compression and tension enabled better prediction of mechanical response of articular cartilage [91, 92].

Comparing the mechanical response of hydrogels with the biphasic cartilage models will indicate if the viscoelasticity of the hydrogel is caused by drag forces due to interstitial fluid flow, inherent matrix viscoelasticity or by anisotropy in the polymer matrix, similar to cartilage. Based on this approach, Spiller et al. utilized a linear biphasic cartilage model to compare the mechanical properties of their hydrogel with articular cartilage in terms of aggregate modulus and permeability [86].

Lubrication Theory

It was Osborne Reynolds who reported that the unique combination of properties of articular cartilage gives rise to specific lubrication mechanisms and that hydrodynamic lubrication is fundamental to animal joints [93]. Hydrodynamic lubrication is generation of a fluid film caused by sliding action. The fluid film can separate the surfaces depending on the velocity and loading conditions and it can reduce wear to insignificant amounts [94]. However, velocities and loads in human joints do not fulfill the stipulations of hydrodynamic lubrication whereas, a newer approach, namely micro-elastohydrodynamic lubrication (micro-EHL), predicted generation of fluid films that are closer to the experimental findings [93, 94]. According to micro-EHL, a pool of lubricant is trapped on the surface because of elastic deformation, while asperities experience higher pressures and flatten [94]. The combination of these effects causes the film to be thicker than the height of asperities and makes fluid film lubrication possible. Nevertheless, recent experimental studies showed that articular cartilage would not operate in fluid film lubrication and that lubrication of cartilage could not precisely be simulated by the current models [25, 95]. Most recently, the lubrication phenomenon of cartilage was attributed to the interstitial fluid pressurization [44, 55, 96, 97]. The interstitial fluid is now known to contribute significantly to cartilage lubrication mechanisms [41, 42, 45, 49, 88]. According to this theory, drag forces produced by interstitial fluid flow through pores in the extracellular matrix separate articulating surfaces by hydrostatic load support and minimize friction forces by fluid film [44]. The fluid film, which is dictated by the bulk properties of the lubricant, produces a low coefficient of friction [45, 62, 98, 99]. Once the interstitial fluid is exuded out as a result

of extended static loading, the articulating cartilage surfaces come into contact and the coefficient of friction in boundary lubrication is then determined by substances adsorbed on the surfaces [25, 62, 99]. Components of synovial fluid, such as hyaluronic acid, lubricin and glycosaminoglycans, aid in lubricating the articulating surfaces [62, 98].

For hydrogel lubrication, Gong developed Repulsion-Adsorption theory to model the friction of PVA hydrogels [100]. According to "Repulsion-Adsorption model", there are 2 friction regimes for adhesive gels: elastic friction and hydrodynamic friction [82, 83, 100]. At low speeds and high loads, the elastic friction properties are determined by the adsorption of polymer chains to the counterface or by their repulsion. In elastic friction regime, coefficient of friction increases with decreasing speed. At high speeds and low loads, hydrodynamic lubrication regime is active; friction is determined by the viscosity of the lubricant. Increasing velocity or decreasing load results in increasing coefficient of friction [82, 83, 100]. Assuming a repulsive gel, on the other hand, the model predicts increasing frictional response with increasing load or velocity [82].

In order to assess the tribological response of articular cartilage and biphasic materials under varying velocity and load conditions, Stribeck analysis, which was originally developed for hard bearings, can be used [25, 95, 101]. In Stribeck analysis, coefficient of friction is a function of lubricant viscosity, velocity and load [95, 101, 102]. In boundary lubrication regime, the coefficient of friction is invariant to changes in viscosity, load or velocity. Boundary lubrication is usually attained at high load and low speed where the surface asperities come into contact without lubricant. In this mode of lubrication, surface chemistry determines the friction force [93, 95]. In mixed lubrication, the coefficient of friction correlates positively with load and negatively with speed. In

this lubrication regime, both surface chemistry and fluid mechanics contribute to the friction force. In hydrodynamic lubrication regime, on the other hand, coefficient of friction increases with increasing velocity and decreasing load and a fluid film separates the surfaces. The friction force is determined by fluid dynamics; increasing velocity results in higher friction due to viscous forces [93, 95].

Wear

Wear is the removal of material from the contact surfaces due to mechanical action. For monophasic, homogeneous materials, wear rate obeys Archard's law and depends on load and sliding distance only [103]. According to Archard's law [103], volume of wear debris generated is proportional to load and sliding distance by a wear factor [104-106], which is assumed to be constant independent of magnitude of load [8]. Mazzucco and Spector showed on a Pin-on-disk tester that Archard's law did not apply to UHMWPE and polyethylene wear was proportional to contact area but not to the magnitude of load [107]. Furthermore, in order to facilitate in vivo wear mechanisms and wear rates, clinically relevant loading profiles were not sufficient; serum lubrication [8] and multidirectional sliding [108] were also required.

Wear mechanisms can be broadly categorized into three groups. Adhesive wear is when the adhesion between the polymer and the counterface is sufficiently high that the junction ruptures and is deposited on the counterface [109]. Abrasive wear is the removal of material in relative motion due to hard protuberances or hard particles embedded on the articulating surfaces [110]. Fatigue wear, on the other hand, describes the generation of particles when surface or subsurface cracks due to cyclic loading coalesce [1]. For

instance, adhesive and abrasive wear mechanisms are observed in acetabular liners whereas retrieved knee inserts display signs of fatigue wear [1].

For articular cartilage, Lipshitz and Glimcher excluded a fatigue wear mechanism and emphasized constant crack formation and wear particle generation by chain scission when cartilage pins articulated against stainless steel [111]. Mow et al., on the other hand, described the cartilage wear mechanism as fatigue micro-cracks coalescing and eventually causing delamination [42]. In another study, a proteoglycan-deficient wear layer was reported to accumulate on the surface of the cartilage pins as cartilage wear progressed [27].

For hydrogels, adhesive wear mechanism was reported when PVA hydrogel articulated against stainless steel ball without lubricant and fatigue wear was reported when articulating surfaces were lubricated [39]. In another study, compliant formulations of pHEMA hydrogel facilitated adhesive wear when articulating against stainless steel and abrasive wear when the crosslinking of the hydrogel was increased [37].

The primary objective of this research was to devise a methodology to predict the performance of biphasic materials as articular cartilage replacement based on their tribological properties. Three criteria regarding the tribology of a biphasic cartilage replacement material were assessed: (1) the lubrication mechanisms of biphasic material should be evaluated and compared to those of articular cartilage [38, 39, 112]; (2) the degradation and wear of articular cartilage opposing the biomaterial should be characterized [30, 31, 38, 39]; and, (3) the wear properties of the biomaterial under clinically relevant conditions should be quantified [24, 31, 34, 38].

Understanding the relationship between the mechanical response and the active lubrication modes of articular cartilage is useful for the design of implants [112]. Therefore, identifying material properties of hydrogels using biphasic cartilage model is a necessary step in evaluating the cause of similarities and differences in active lubrication modes of cartilage and hydrogels. Design guidelines produced by this approach to mimic the behavior of articular cartilage may improve tribological properties of hydrogels.

Cartilage wear comprises chemical and mechanical degradation and can manifest itself as a loss of proteoglycans, changes in collagen structure or even changes in the ionic equilibrium [51]. Since quantification of cartilage wear with conventional gravimetric measurements or by direct wear debris analysis is not possible [30, 51, 113], various methods including biochemical characterization by hydroxyproline and glycosaminoglycan contents in lubricant, optical profilometry, and staining with india ink were employed [111, 114]. However, a single parameter as obtained by these methods cannot sufficiently model wear mechanisms of articular cartilage because of its heterogeneous and zone-dependent composition [31].

Quantifying the wear rate of biphasic materials is problematic [24, 34, 39, 84]. Since monitoring the wet weight of the biphasic material does not allow differentiation between the mass change caused by fluid movement as opposed to worn mass, it is not accurate [84, 115]. No established, standardized methods for characterizing the wear behavior of biphasic material articulations have yet been developed [34].

In this research, hydrogel material properties were obtained using biphasic cartilage models, and the relationship between the lubrication properties and the material properties of hydrogels was evaluated. *In vitro* wear of articular cartilage was

characterized using Fourier Transform Infrared Spectroscopy (FTIRS) and histology, and the effects of wear of cartilage against cartilage as control, and against CoCr and a hydrogel as hemiarthroplasty materials were compared. Finally, the performance of submerged measurements in quantifying hydrogel wear was assessed and the wear characteristics of hydrogel on hydrogel articulation were characterized.

In summary, a methodology for screening biphasic materials for replacing damaged articular cartilage was established. With this methodology, the lubrication mechanisms that the biphasic material will facilitate, its potential effect on the opposing cartilage surface and its wear resistance may be characterized.

References

[1] Kurtz SM. UHMWPE biomaterials handbook: ultra high molecular weight polyethylene in total joint replacement and medical devices: Academic Press; 2009.
[2] Wang A. A unified theory of wear for ultra-high molecular weight polyethylene in multi-directional sliding. Wear. 2001;248:38-47.
[3] Bragdon CR, O'Connor DO, Lowenstein JD, Jasty M, Biggs SA, Harris WH. A new pin-on-disk wear testing method for simulating wear of polyethylene on cobalt-chrome alloy in total hip arthroplasty. The Journal of Arthroplasty. 2001;16:658-65.
[4] Bozic KJ, Kurtz SM, Lau E, Ong K, Chiu V, Vail TP, et al. The epidemiology of revision total knee arthroplasty in the United States. Clinical Orthopaedics and Related Research®. 2010;468:45-51.
[5] Kurtz SM, Medel FJ, MacDonald DW, Parvizi J, Kraay MJ, Rimnac CM. Reasons for revision of first-generation highly cross-linked polyethylenes. The Journal of Arthroplasty. 2010;25:67-74.
[6] Muratoglu OK, Bragdon CR, O'Connor DO, Jasty M, Harris WH, Gul R, et al. Unified wear model for highly crosslinked ultra-high molecular weight polyethylenes (UHMWPE). Biomaterials. 1999;20:1463-70.
[7] Bragdon C, O'Connor D, Lowenstein J, Jasty M, Syniuta W. The importance of multidirectional motion on the wear of polyethylene. Proceedings of the Institution of Mechanical Engineers, Part H: Journal of Engineering in Medicine. 1996;210:157-65.
[8] McKellop H, Clarke I, Markolf K, Amstutz H. Wear characteristics of UHMW polyethylene: a method for accurately measuring extremely low wear rates. Journal of biomedical materials research. 1978;12:895-927.
[9] Muratoglu OK, Merrill EW, Bragdon CR, O'Connor D, Hoeffel D, Burroughs B, et al. Effect of radiation, heat, and aging on in vitro wear resistance of polyethylene. Clinical orthopaedics and related research. 2003;417:253.
[10] Sathasivam S, Walker PS, Campbell PA, Rayner K. The effect of contact area on wear in relation to fixed bearing and mobile bearing knee replacements. Journal of biomedical materials research. 2001;58:282-90.
[11] Kurtz SM, Muratoglu OK, Evans M, Edidin AA. Advances in the processing, sterilization, and crosslinking of ultra-high molecular weight polyethylene for total joint arthroplasty. Biomaterials. 1999;20:1659-88.
[12] Barbour P, Stone M, Fisher J. A study of the wear resistance of three types of clinically applied UHMWPE for total replacement hip prostheses. Biomaterials. 1999;20:2101-6.
[13] Gul RM, McGarry FJ, Bragdon CR, Muratoglu OK, Harris WH. Effect of consolidation on adhesive and abrasive wear of ultra high molecular weight polyethylene. Biomaterials. 2003;24:3193-9.
[14] Oral E, Ghali BW, Rowell SL, Micheli BR, Lozynsky AJ, Muratoglu OK. A surface crosslinked UHMWPE stabilized by vitamin E with low wear and high fatigue strength. Biomaterials. 2010;31:7051-60.

[15] Oral E, Wannomae KK, Hawkins N, Harris WH, Muratoglu OK. α-Tocopherol-doped irradiated UHMWPE for high fatigue resistance and low wear. Biomaterials. 2004;25:5515-22.
[16] Deng M, Shalaby SW. Properties of self-reinforced ultra-high-molecular-weight polyethylene composites. Biomaterials. 1997;18:645-55.
[17] Dowson D, Harding R. The wear characteristics of ultrahigh molecular weight polyethylene against a high density alumina ceramic under wet (distilled water) and dry conditions. Wear. 1982;75:313-31.
[18] Miller D, Ainsworth R, Dumbleton J, Page D, Miller E. A comparative evaluation of the wear of ultra-high molecular weight polyethylene abraded by Ti-6Al-4V. Wear. 1974;28:207-16.
[19] Saikko V, Ahlroos T. Type of motion and lubricant in wear simulation of polyethylene acetabular cup. Proceedings of the Institution of Mechanical Engineers, Part H: Journal of Engineering in Medicine. 1999;213:301-10.
[20] Shen C, Dumbleton J. The friction and wear behavior of irradiated very high molecular weight polyethylene. Wear. 1974;30:349-64.
[21] Hill MR, Catledge SA, Konovalov V, Clem WC, Chowdhury SA, Etheridge BS, et al. Preliminary tribological evaluation of nanostructured diamond coatings against ultra-high molecular weight polyethylene. Journal of Biomedical Materials Research Part B: Applied Biomaterials. 2008;85:140-8.
[22] Pavoor PV, Gearing BP, Muratoglu O, Cohen RE, Bellare A. Wear reduction of orthopaedic bearing surfaces using polyelectrolyte multilayer nanocoatings. Biomaterials. 2006;27:1527-33.
[23] Caravia L, Dowson D, Fisher J, Corkhill P, Tighe B. A comparison of friction in hydrogel and polyurethane materials for cushion-form joints. Journal of Materials Science: Materials in Medicine. 1993;4:515-20.
[24] Bigsby R, Auger D, Jin Z, Dowson D, Hardaker C, Fisher J. A comparative tribological study of the wear of composite cushion cups in a physiological hip joint simulator. Journal of biomechanics. 1998;31:363-9.
[25] Gleghorn JP, Doty SB, Warren RF, Wright TM, Maher SA, Bonassar LJ. Analysis of frictional behavior and changes in morphology resulting from cartilage articulation with porous polyurethane foams. Journal of orthopaedic research. 2010;28:1292-9.
[26] Schwartz CJ, Bahadur S. Development and testing of a novel joint wear simulator and investigation of the viability of an elastomeric polyurethane for total-joint arthroplasty devices. Wear. 2007;262:331-9.
[27] Patel A, Spector M. Tribological evaluation of oxidized zirconium using an articular cartilage counterface: a novel material for potential use in hemiarthroplasty. Biomaterials. 1997;18:441-7.
[28] Lizhang J, Fisher J, Jin Z, Burton A, Williams S. The effect of contact stress on cartilage friction, deformation and wear. Proceedings of the Institution of Mechanical Engineers, Part H: Journal of Engineering in Medicine. 2011;225:461-75.
[29] Chan S, Neu C, Komvopoulos K, Reddi A, Di Cesare P. Friction and Wear of Hemiarthroplasty Biomaterials in Reciprocating Sliding Contact With Articular Cartilage. Journal of tribology. 2011;133.

[30] McGann ME, Vahdati A, Wagner DR. Methods to assess in vitro wear of articular cartilage. Proceedings of the Institution of Mechanical Engineers, Part H: Journal of Engineering in Medicine. 2012;226:612-22.
[31] Northwood E, Fisher J, Kowalski R. Investigation of the friction and surface degradation of innovative chondroplasty materials against articular cartilage. Proceedings of the Institution of Mechanical Engineers, Part H: Journal of Engineering in Medicine. 2007;221:263-79.
[32] Oka M, Ushio K, Kumar P, Ikeuchi K, Hyon S, Nakamura T, et al. Development of artificial articular cartilage. Proceedings of the Institution of Mechanical Engineers, Part H: Journal of Engineering in Medicine. 2000;214:59-68.
[33] Chang YS, Oka M, Gu HO, Kobayashi M, Toguchida J, Nakamura T, et al. Histologic comparison of tibial articular surfaces against rigid materials and artificial articular cartilage. Journal of Biomedical Materials Research. 1997;37:51-9.
[34] Yasuda K, Ping Gong J, Katsuyama Y, Nakayama A, Tanabe Y, Kondo E, et al. Biomechanical properties of high-toughness double network hydrogels. Biomaterials. 2005;26:4468-75.
[35] Katta JK, Marcolongo M, Lowman A, Mansmann KA. Friction and wear behavior of poly (vinyl alcohol)/poly (vinyl pyrrolidone) hydrogels for articular cartilage replacement. Journal of Biomedical Materials Research Part A. 2007;83:471-9.
[36] Bodugoz-Senturk H, Macias CE, Kung JH, Muratoglu OK. Poly (vinyl alcohol)-acrylamide hydrogels as load-bearing cartilage substitute. Biomaterials. 2009;30:589-96.
[37] Bavaresco V, Zavaglia C, Reis M, Gomes J. Study on the tribological properties of pHEMA hydrogels for use in artificial articular cartilage. Wear. 2008;265:269-77.
[38] Northwood E, Fisher J. A multi-directional in vitro investigation into friction, damage and wear of innovative chondroplasty materials against articular cartilage. Clinical Biomechanics. 2007;22:834-42.
[39] Freeman ME, Furey MJ, Love BJ, Hampton JM. Friction, wear, and lubrication of hydrogels as synthetic articular cartilage. Wear. 2000;241:129-35.
[40] Stammen JA, Williams S, Ku DN, Guldberg RE. Mechanical properties of a novel PVA hydrogel in shear and unconfined compression. Biomaterials. 2001;22:799-806.
[41] Mow V, Kuei S, Lai W, Armstrong C. Biphasic Creep and Stress Relaxation of Articular Cartilage in Compression: Theory and Experiments. Journal of biomechanical engineering. 1980;102:73.
[42] Mow VC, Ateshian GA, Spilker RL. Biomechanics of diarthrodial joints: a review of twenty years of progress. Journal of biomechanical engineering. 1993;115:460.
[43] Forster H, Fisher J. The influence of loading time and lubricant on the friction of articular cartilage. Proceedings of the Institution of Mechanical Engineers, Part H: Journal of Engineering in Medicine. 1996;210:109-19.
[44] Ateshian GA. The role of interstitial fluid pressurization in articular cartilage lubrication. Journal of biomechanics. 2009;42:1163-76.
[45] Caligaris M, Ateshian GA. Effects of sustained interstitial fluid pressurization under migrating contact area, and boundary lubrication by synovial fluid, on cartilage friction. Osteoarthritis and Cartilage. 2008;16:1220-7.
[46] Mow VC, Lai WM. Recent developments in synovial joint biomechanics. Siam Review. 1980;22:275-317.

[47] Yuehuei HA, Kylie L. Handbook of histology methods for bone and cartilage: Humana Press; 2003.
[48] Boskey A, Pleshko Camacho N. FT-IR imaging of native and tissue-engineered bone and cartilage. Biomaterials. 2007;28:2465-78.
[49] Mak A. Unconfined compression of hydrated viscoelastic tissues: a biphasic poroviscoelastic analysis. Biorheology. 1986;23:371.
[50] Cohen N, Foster R, Mow V. Composition and dynamics of articular cartilage: structure, function, and maintaining healthy state. The Journal of orthopaedic and sports physical therapy. 1998;28:203.
[51] Katta J, Jin Z, Ingham E, Fisher J. Biotribology of articular cartilage—A review of the recent advances. Medical engineering & physics. 2008;30:1349-63.
[52] Setton LA, Zhu W, Mow VC. The biphasic poroviscoelastic behavior of articular cartilage: role of the surface zone in governing the compressive behavior. Journal of biomechanics. 1993;26:581-92.
[53] Cooke A, Dowson D, Wright V. The rheology of synovial fluid and some potential synthetic lubricants for degenerate synovial joints. Engineering in Medicine. 1978;7:66-72.
[54] Mavraki A, Cann P. Lubricating film thickness measurements with bovine serum. Tribology International. 2011;44:550-6.
[55] Forster H, Fisher J. The influence of continuous sliding and subsequent surface wear on the friction of articular cartilage. Proceedings of the Institution of Mechanical Engineers, Part H: Journal of Engineering in Medicine. 1999;213:329-45.
[56] Lipshitz H, Etheredge 3rd R, Glimcher M. In vitro wear of articular cartilage. The Journal of bone and joint surgery American volume. 1975;57:527.
[57] Naji L, Kaufmann J, Huster D, Schiller J, Arnold K. 13C NMR relaxation studies on cartilage and cartilage components. Carbohydrate research. 2000;327:439.
[58] Pawaskar S, Jin Z, Fisher J. Modelling of fluid support inside articular cartilage during sliding. Proceedings of the Institution of Mechanical Engineers, Part J: Journal of Engineering Tribology. 2007;221:165-74.
[59] Saarakkala S, Julkunen P, Kiviranta P, Makitalo J, Jurvelin J, Korhonen R. Depth-wise progression of osteoarthritis in human articular cartilage: investigation of composition, structure and biomechanics. Osteoarthritis and Cartilage. 2009;18:73-81.
[60] West P, Bostrom M, Torzilli P, Camacho N. Fourier transform infrared spectral analysis of degenerative cartilage: an infrared fiber optic probe and imaging study. Applied spectroscopy. 2004;58:376-81.
[61] Bonnevie E, Baro V, Wang L, Burris DL. In situ studies of cartilage microtribology: roles of speed and contact area. Tribology Letters. 2011;41:83-95.
[62] Caligaris M, Canal CE, Ahmad CS, Gardner TR, Ateshian GA. Investigation of the frictional response of osteoarthritic human tibiofemoral joints and the potential beneficial tribological effect of healthy synovial fluid. Osteoarthritis and Cartilage. 2009;17:1327-32.
[63] Cabanela M. Bipolar versus total hip arthroplasty for avascular necrosis of the femoral head. A comparison. Clin Orthop Relat Res. 1990;261:59-62.
[64] Majithia V, Geraci SA. Rheumatoid arthritis: diagnosis and management. The American journal of medicine. 2007;120:936-9.

[65] Camacho N, West P, Torzilli P, Mendelsohn R. FTIR microscopic imaging of collagen and proteoglycan in bovine cartilage. Biopolymers. 2001;62:1.
[66] Potter K, Kidder L, Levin I, Lewis E, Spencer R. Imaging of collagen and proteoglycan in cartilage sections using Fourier transform infrared spectral imaging. Arthritis Care & Research. 2001;44:846-55.
[67] David-Vaudey E, Burghardt A, Keshari K, Brouchet A, Ries M, Majumdar S. Fourier Transform Infrared Imaging of focal lesions in human osteoarthritic cartilage. Eur Cell Mater. 2005;10:51-60.
[68] Xia Y, Ramakrishnan N, Bidthanapally A. The depth-dependent anisotropy of articular cartilage by Fourier-transform infrared imaging (FTIRI). Osteoarthritis and Cartilage. 2007;15:780-8.
[69] Saarakkala S, Julkunen P, Kiviranta P, M‰kitalo J, Jurvelin J, Korhonen R. Depth-wise progression of osteoarthritis in human articular cartilage: investigation of composition, structure and biomechanics. Osteoarthritis and Cartilage. 2009.
[70] Baykal D, Irrechukwu O, Lin PC, Fritton K, Spencer RG, Pleshko N. Nondestructive assessment of engineered cartilage constructs using near-infrared spectroscopy. Applied spectroscopy. 2010;64:1160-6.
[71] Li G, Thomson M, Dicarlo E, Yang X, Nestor B, Bostrom M, et al. A chemometric analysis for evaluation of early-stage cartilage degradation by infrared fiber-optic probe spectroscopy. Applied Spectroscopy. 2005;59:1527-33.
[72] Kim M, Bi X, Horton Jr W, Spencer R, Camacho N. Fourier transform infrared imaging spectroscopic analysis of tissue engineered cartilage: histologic and biochemical correlations. Journal of Biomedical Optics. 2005;10:031105.
[73] Potter K, Kidder LH, Levin IW, Lewis EN, Spencer RGS. Imaging of collagen and proteoglycan in cartilage sections using Fourier transform infrared spectral imaging. Arthritis & Rheumatism. 2001;44:846-55.
[74] Camacho NP, West P, Torzilli PA, Mendelsohn R. FTIR microscopic imaging of collagen and proteoglycan in bovine cartilage. Biopolymers. 2000;62:1-8.
[75] Bi X, Yang X, Bostrom MPG, Camacho NP. Fourier transform infrared imaging spectroscopy investigations in the pathogenesis and repair of cartilage. Biochimica et Biophysica Acta (BBA)-Biomembranes. 2006;1758:934-41.
[76] Farlay D, Duclos M-E, Gineyts E, Bertholon C, Viguet-Carrin S, Nallala J, et al. The Ratio 1660/1690 cm− 1 Measured by Infrared Microspectroscopy Is Not Specific of Enzymatic Collagen Cross-Links in Bone Tissue. PLoS ONE. 2011;6.
[77] West PA, Torzilli P, Chen C, Lin P, Camacho NP. Fourier transform infrared imaging spectroscopy analysis of collagenase-induced cartilage degradation. Journal of biomedical optics. 2005;10:014015--6.
[78] Peppas NA, Merrill EW. Development of semicrystalline poly (vinyl alcohol) hydrogels for biomedical applications. Journal of Biomedical Materials Research. 1977;11:423-34.
[79] Thomas BH, Craig Fryman J, Liu K, Mason J. Hydrophilic, hydrophobic hydrogels for cartilage replacement. Journal of the mechanical behavior of biomedical materials. 2009;2:588-95.
[80] Bray JC, Merrill EW. Poly (vinyl alcohol) hydrogels for synthetic articular cartilage material. Journal of Biomedical Materials Research. 1973;7:431-43.

[81] Covert RJ, Ott R, Ku DN. Friction characteristics of a potential articular cartilage biomaterial. Wear. 2003;255:1064-8.
[82] Gong JP. Friction and lubrication of hydrogels—its richness and complexity. Soft Matter. 2006;2:544-52.
[83] Mamada K, Fridrici V, Kosukegawa H, Kapsa P, Ohta M. Friction Properties of Poly (vinyl alcohol) Hydrogel: Effects of Degree of Polymerization and Saponification Value. Tribology Letters. 2011;42:241-51.
[84] Suciu AN, Iwatsubo T, Matsuda M, Nishino T. A study upon durability of the artificial knee joint with PVA hydrogel cartilage. JSME International Journal Series C. 2004;47:199-208.
[85] Ishikawa Y, Hiratsuka K, Sasada T. Role of water in the lubrication of hydrogel. Wear. 2006;261:500-4.
[86] Spiller KL, Laurencin SJ, Charlton D, Maher SA, Lowman AM. Superporous hydrogels for cartilage repair: evaluation of the morphological and mechanical properties. Acta biomaterialia. 2008;4:17-25.
[87] Bodugoz-Senturk H, Macias CE, Kung JH, Muratoglu OK. Poly (vinyl alcohol)–acrylamide hydrogels as load-bearing cartilage substitute. Biomaterials. 2009;30:589-96.
[88] Mak A. The apparent viscoelastic behavior of articular cartilage--the contributions from the intrinsic matrix viscoelasticity and interstitial fluid flows. Journal of biomechanical engineering. 1986;108:123.
[89] Armstrong C, Lai W, Mow V. An analysis of the unconfined compression of articular cartilage. Journal of biomechanical engineering. 1984;106:165.
[90] Suh JK, Bai S. Finite element formulation of biphasic poroviscoelastic model for articular cartilage. Journal of biomechanical engineering. 1998;120:195.
[91] Cohen B, Lai W, Mow V. A transversely isotropic biphasic model for unconfined compression of growth plate and chondroepiphysis. Journal of biomechanical engineering. 1998;120:491.
[92] Soltz MA, Ateshian GA. A conewise linear elasticity mixture model for the analysis of tension-compression nonlinearity in articular cartilage. Journal of biomechanical engineering. 2000;122:576.
[93] Unsworth A. Tribology of human and artificial joints. ARCHIVE: Proceedings of the Institution of Mechanical Engineers, Part H: Journal of Engineering in Medicine 1989-1996 (vols 203-210). 1991;205:163-72.
[94] Dowson D, Jin Z. Micro-elastohydrodynamic lubrication of synovial joints. Engineering in medicine. 1986;15:63.
[95] Gleghorn JP, Bonassar LJ. Lubrication mode analysis of articular cartilage using Stribeck surfaces. Journal of biomechanics. 2008;41:1910-8.
[96] Ateshian GA, Soltz MA, Mauck RL, Basalo IM, Hung CT, Michael Lai W. The role of osmotic pressure and tension-compression nonlinearity in the frictional response of articular cartilage. Transport in porous media. 2003;50:5-33.
[97] Soltz MA, Ateshian GA. A conewise linear elasticity mixture model for the analysis of tension-compression nonlinearity in articular cartilage. Journal of Biomechanical Engineering. 2000;122:576.

[98] Accardi MA, Dini D, Cann PM. Experimental and numerical investigation of the behaviour of articular cartilage under shear loading - Interstitial fluid pressurisation and lubrication mechanisms. Tribology International. 2011;44:565-78.
[99] Katta J, Jin Z, Ingham E, Fisher J. Biotribology of articular cartilage, A review of the recent advances. Medical engineering & physics. 2008;30:1349-63.
[100] Gong J, Osada Y. Gel friction: a model based on surface repulsion and adsorption. The Journal of chemical physics. 1998;109:8062.
[101] Unsworth A. Tribology of human and artificial joints. Proceedings of the Institution of Mechanical Engineers, Part H: Journal of Engineering in Medicine. 1991;205:163-72.
[102] Shi L, Sikavitsas VI, Striolo A. Experimental friction coefficients for bovine cartilage measured with a pin-on-disk tribometer: Testing configuration and lubricant effects. Annals of biomedical engineering. 2011;39:132-46.
[103] Archard J. Contact and rubbing of flat surfaces. Journal of applied physics. 1953;24:981-8.
[104] Dumbleton J, Shen C, Miller E. A study of the wear of some materials in connection with total hip replacement. Wear. 1974;29:163-71.
[105] Seedhom B, Dowson D, Wright V. Wear of solid phase formed high density polyethylene in relation to the life of artificial hips and knees. Wear. 1973;24:35-51.
[106] Brown K, Atkinson J, Dowson D, Wright V. The wear of ultrahigh molecular weight polyethylene and a preliminary study of its relation to the in vivo behaviour of replacement hip joints. Wear. 1976;40:255-64.
[107] Mazzucco D, Spector M. Contact Area as a Critical Determinant in the Tribology of Metal-on-Polyethylene Total Joint Arthroplasty. ASME; 2004.
[108] Wang A, Polineni V, Essner A, Sokol M, Sun D, Stark C, et al. The significance of nonlinear motion in the wear screening of orthopaedic implant materials. Journal of testing and evaluation. 1997;25:239-45.
[109] Briscoe B. Wear of polymers: an essay on fundamental aspects. Tribology International. 1981;14:231-43.
[110] Lancaster J. Abrasive wear of polymers. Wear. 1969;14:223-39.
[111] Lipshitz H, Glimcher MJ. In vitro studies of the wear of articular cartilage II. Characteristics of the wear of articular cartilage when worn against stainless steel plates having characterized surfaces. Wear. 1979;52:297-339.
[112] Accardi MA, Dini D, Cann PM. Experimental and numerical investigation of the behaviour of articular cartilage under shear loading—Interstitial fluid pressurisation and lubrication mechanisms. Tribology International. 2011;44:565-78.
[113] Verberne G, Merkher Y, Halperin G, Maroudas A, Etsion I. Techniques for assessment of wear between human cartilage surfaces. Wear. 2009;266:1216-23.
[114] Schwartz CJ, Bahadur S. Investigation of articular cartilage and counterface compliance in multi-directional sliding as in orthopedic implants. Wear. 2007;262:1315-20.
[115] Covert RJ. Durability evaluation of articular cartilage prostheses [Ph.D. Dissertation]: Georgia Institute of Technology; 2003.

1. Evaluation of friction properties of hydrogels based on a biphasic cartilage model

Abstract

Characterizing hydrogels using a biphasic cartilage model, which can predict their behavior based on structural properties, such as permeability and aggregate modulus, may be useful for comparing active lubrication modes of cartilage and hydrogels for the design of articular cartilage implants. A biphasic poroviscoelastic model yielded the lowest RMSE and highest R^2 compared to a linear biphasic cartilage model and a linear biphasic model with cubic symmetry when predicting confined and unconfined compression stress-relaxation response of hydrogels (n=15): 0.220 ± 0.316 MPa and 0.93 ± 0.08; and 0.017 ± 0.008 MPa and 0.98 ± 0.01 respectively. However, the differences in error between models were not statistically significant. The coefficient of friction (COF) of a hydrogel-ceramic articulation was measured at varying loads and pressures. Material parameters obtained by biphasic models correlated with COF. Based on the linear biphasic model, COF correlated positively with aggregate modulus (spearman's rho=0.5; $p<0.001$) and velocity (rho=0.3; $p<0.001$), and negatively with permeability (rho=-0.4; $p<0.001$) and load (rho=-0.6; $p<0.001$). This study supports a linear biphasic model as sufficient for predicting the mechanical response of hydrogels in compression tests. Hydrogels with low aggregate modulus and high permeability produced low COFs. Hydrogels were also shown to result lower COFs at low velocities and high loads.

Introduction

Researchers have investigated the structure-function relationship of articular cartilage in order to understand causes and effects of pathologies such as osteoarthritis, which is thought to be mechanically induced [1, 2]. The interstitial fluid, which constitutes 65-75% of articular cartilage [3, 4], is now known to contribute significantly to its viscoelastic mechanical response and lubrication mechanisms [3-7]. By taking into account an incompressible fluid phase and a solid matrix phase, a biphasic cartilage model has been shown to successfully explain how interstitial fluid pressurization supports the collagen-proteoglycan network in withstanding high contact loads [3-5, 7]. Mow et al. idealized the collagen-proteoglycan network as a linear elastic matrix in the biphasic model (KLM) in which the time-dependent response of cartilage was only due to interstitial fluid flow [4, 8]. Because collagen fibrils and proteoglycan gel are known to be viscoelastic [9], Mak expanded on the linear biphasic model by introducing relaxation of the solid matrix as a second source of time-dependent response, which resulted in the biphasic poroviscoelastic (BPVE) cartilage model [3, 7]. Although these models were successful in predicting cartilage response in confined compression configuration, peak to equilibrium load intensity ratio observed in unconfined compression experiments was not possible to account for using isotropic matrix assumptions [10, 11]. More recently, anisotropy was introduced to the solid matrix phase of the linear biphasic model in which differences in stiffness in compression and tension enabled better prediction of mechanical response of articular cartilage [10, 11].

According to the biphasic cartilage model, drag forces produced by interstitial fluid flow through pores in the extracellular matrix separate articulating surfaces by hydrostatic load support and facilitate fluid film lubrication. The fluid film lubrication,

which is dictated by the bulk properties of the lubricant, produces a low coefficient of friction [1, 2, 6, 12]. Once the interstitial fluid is exuded out as a result of extended static loading, the articulating cartilage surfaces come into contact and the coefficient of friction in boundary lubrication is then determined by substances adsorbed on the surfaces [2, 12, 13]. Components of synovial fluid, such as hyaluronic acid, lubricin and glycosaminoglycans, aid in lubricating the articulating surfaces [1, 2]. Because multiple lubrication modes may occur within the joint, researchers employed methods to assess the tribological response of articular cartilage under varying velocity and load conditions. For instance, Stribeck analysis, which was originally developed to explain lubrication mode transitions of hard bearings by displaying coefficient of friction on a "Stribeck curve", was used in studying lubrication of articular cartilage [13, 14].

Hydrogels are complex hydrophilic polymers that are swollen with water [15, 16]. Due to their structural similarity to articular cartilage, hydrogels have been considered for replacing damaged articular cartilage in the joints [17-20]. Hydrogels have been characterized by various testing configurations, such as confined and unconfined compression creep tests and indentation tests [18, 21, 22]. However, correlating the mechanical behavior of hydrogels to their structural properties, such as water content and stiffness, will be useful during the material design phase. Furthermore, employing the articular cartilage-modeling framework for this purpose will also enable direct comparisons to articular cartilage [22]. Based on this approach, Spiller et al. utilized a linear biphasic cartilage model to compare the mechanical properties of their hydrogel with articular cartilage in terms of aggregate modulus and permeability [22].

Understanding the relationship between active lubrication modes of articular cartilage and its mechanical response is useful for the design of articular cartilage implants [1]. Therefore, identifying material properties of hydrogels using biphasic cartilage model is a necessary step in evaluating the cause of similarities and differences in active lubrication modes of cartilage and hydrogels. Design guidelines produced by this approach to mimic the behavior of articular cartilage may improve tribological properties of hydrogels. The objectives of this study were to obtain hydrogel material properties using a biphasic cartilage model, and to investigate the relationship between the frictional properties and the material properties of hydrogels. Because hydrogels display cartilage-like viscoelastic behavior [16, 18, 22], we hypothesized that the solid phase of hydrogels would be intrinsically viscoelastic to complement the viscoelasticity caused by interstitial fluid pressurization. In addition, we assumed isotropic matrix properties for simplicity in this study. Our hypotheses were: (1) the BPVE model would yield a lower error than KLM or a linear biphasic with anisotropy (ANISOTROPIC) cartilage model when predicting mechanical response of hydrogels in confined and unconfined stress-relaxation tests; and (2) coefficient of friction of hydrogel articulation at various speeds and loads that covered the clinically relevant range would correlate more strongly with material parameters obtained by BPVE model compared to parameters obtained by KLM and ANISOTROPIC models.

Methods

Biphasic Modeling Framework

Confined Compression Stress Relaxation

The biphasic model equations for confined compression configuration were derived by complementing the momentum and continuity equations of continuum mechanics with Darcy's law, which couples interstitial fluid flow with the pressure gradient, to arrive at the general governing equation (eq. 1) [4, 7, 11, 23]. The governing equation for the linear elastic matrix assumption depends on permeability (k) and aggregate modulus (H_A) (eq. 2) [4, 11]. In the biphasic poroviscoelastic model (BPVE), inherent viscoelasticity of the solid matrix as modeled by a relaxation function yields the governing equation that depends on permeability, aggregate modulus and g(t), which is a function of a relaxation constant and two time constants: c,τ_1 and τ_2 (eq. 3) [7, 23].

$$\frac{\partial u}{\partial t} - k\nabla \cdot \sigma^e = 0 \qquad (1)$$

$$\frac{\partial u}{\partial t} - kH_A \frac{\partial^2 u}{\partial z^2} = 0 \qquad (2)$$

$$\frac{\partial u}{\partial t} - kH_A \int_{-\infty}^{t} g(t-\tau) \frac{\partial \frac{\partial^2 u}{\partial z^2}}{\partial \tau} \partial \tau = 0 \qquad (3)$$

Since the chamber allowed for movement only in the vertical direction, confined compression models reduced to a single dimension in the vertical direction. Displacement, u(z) was normalized with respect to height, h, and time was normalized with respect to H_Ak/h^2 before the governing equations were transformed to Laplace domain with respect to time. The boundary conditions were (1) $u(1,s) = 0$ since the bottom part of the specimen was not allowed to move by the base of the chamber; (2) $u(0,s) = \frac{\bar{v_0}}{s^2}\left(1 - e^{-\bar{t}_0 s}\right)$ since the filter was ramped at velocity, v_0 until time, t_0 and dwelled at that position; and (3) $u(z,0) = 0$ since there was no deformation in the specimen initially at

t=0. Solution of the differential equation in Laplace domain with the boundary conditions yielded equation 4 for both models. In the linear biphasic model (KLM), f(s) is simply s (eq. 5) whereas in BPVE model, f(s) depends on relaxation terms: c, τ_1 and τ_2 (eq. 6).

$$F(s) = \left(H_A \pi r_0^2\right) \frac{v_0 \sqrt{f(s)}}{s^2} \left(1 - e^{-t_0 s}\right) \coth\left(\sqrt{f(s)}\right) \quad (4)$$

$$f(s) = s \quad (5)$$

$$f(s) = \frac{s}{1 + c \ln \frac{1 + s\tau_2}{1 + s\tau_1}} \quad (6)$$

Full derivation of the stress relaxation response of the BPVE model in confined compression is detailed in Appendix 1.1.

Unconfined Compression Stress Relaxation

The biphasic model equations for unconfined compression configuration were based on the assumptions that interstitial fluid and the solid matrix did not move relative to each other since the platens were impermeable and that the friction between the top and bottom surfaces of the specimens and the platens was negligible [3, 8]. Based on these assumptions, the axial strain was independent from spatial location and the equations reduced to a single dimension in the radial direction. Velocity of interstitial fluid, which was expressed using the continuity equation in the radial direction, was plugged into the equilibrium equation of continuum mechanics to obtain the governing equation (eq. 7) [3, 8, 10, 11].

$$\frac{\partial u^2}{\partial r^2} + \frac{1}{r}\frac{\partial u}{\partial r} - \frac{u}{r^2} = \frac{1}{kH_A}\left(\frac{\partial u}{\partial t} + \frac{r}{2}\frac{\partial \varepsilon}{\partial t}\right) \quad (7)$$

Displacement, radius and velocity were normalized with respect to radius, a. Time was normalized with respect to $H_A k/a^2$ and force was normalized with respect to $\mu\pi a^2$, where

μ is the second Lame constant of elastic matrix, before the governing equations were transformed to Laplace domain with respect to time. The boundary conditions were (1) $u(0,s)=0$ since the specimen was axisymmetric; (2) $H_A\frac{\partial u}{\partial r}+\lambda u+\lambda\epsilon=0$ at r=a, since there was no load at the outer rim of specimen in unconfined compression, where λ and ϵ are the first Lame constant of elastic matrix and axial strain respectively; (3) $u(r,0)=0$ since there was no deformation in the specimen initially at t=0. The differential equation in Laplace domain was solved as a modified Bessel equation of order 1 with the above boundary conditions and yields equation 8. Similar to confined compression model, f(s) is simply s for KLM model (eq. 9). For BPVE model, f(s) is given in equation (10).

$$\hat{F}=\varepsilon\frac{3I_0(\sqrt{f(s)})-\frac{8\mu_s}{H_A}\frac{I_1(\sqrt{f(s)})}{\sqrt{f(s)}}}{I_0(\sqrt{f(s)})-\frac{2\mu_s}{H_A}\frac{I_1(\sqrt{f(s)})}{\sqrt{f(s)}}},\ \text{where}\ \varepsilon=\frac{\bar{v}_0}{s^2}\left(1-e^{-\bar{t}_0 s}\right) \quad (8)$$

$$f(s)=s \quad (9)$$

$$f(s)=\frac{s}{1+c\ln\frac{1+s\tau_2}{1+s\tau_1}} \quad (10)$$

For linear biphasic model with anisotropy (ANISOTROPIC), cubic symmetry was considered. Cubic symmetry requires only four material parameters while allowing different moduli in tension and compression [11]. The elastic constants used in this model are $H_{+A}, H_{-A}, \lambda_2\ and\ \mu$, which are aggregate modulus in tension, aggregate modulus in compression, the first and second Lame constants respectively. The solution for linear biphasic model with anisotropy is given in equation (11), which is the same equation as the transversely isotropic biphasic model with a higher degree of symmetry [10].

$$\hat{F} = \varepsilon \frac{C_1 I_0(\sqrt{s}) - C_2 \dfrac{I_1(\sqrt{s})}{\sqrt{s}}}{I_0(\sqrt{s}) - C_0 \dfrac{I_1(\sqrt{s})}{\sqrt{s}}}, \text{ where } \varepsilon = \frac{\overline{v}_0}{s^2}\left(1 - e^{-\overline{t}_0 s}\right) \quad (11)$$

$$C_1 = \frac{2H_{-A} + H_{+A} - 3\lambda_2}{H_{+A} - \lambda_2}$$

$$C_2 = \frac{2\left(H_{-A}\left(H_{+A} - \lambda_2\right) + H_{+A}\left(H_{+A} - 3\lambda_2\right) + 2\lambda_2^2\right)}{H_{+A}\left(H_{+A} - \lambda_2\right)}$$

$$C_0 = \frac{H_{+A} - \lambda_2}{H_{+A}}$$

Sample Preparation

A proprietary hydrogel (CyborGel, Formae Inc, Paoli, PA) was used in this study. Two rods of the same formulation (material #1 and #2) with 44% water content, which were produced under different manufacturing conditions, and one rod of %55 water content formulation (material #3) were cut into disks of height ~4.5 mm. The disks were then lathed to ensure flat surfaces. A 3/16" core punch was used to produce 5 specimens of each material type from the larger disks. These size-1 specimens (n=15) were 4.66 ± 0.17 mm in diameter and 4.45 ± 0.22 mm in height. These specimens were soaked in PBS before testing.

Mechanical Testing

Confined Stress Relaxation

In confined compression testing, the hydrogel size-1 specimen was compressed by a sintered stainless steel, free-draining porous filter (Mott Corporation, Farmington, CT) inside a cylindrical stainless steel chamber (diameter=4.7 mm) with impermeable walls and base. A preload of 2N was applied and testing started when the load dropped to 1N to ensure radial confinement. The porous filter was ramped using a load frame (Instron,

Norwood, MA) at a constant velocity of 1.3 microns/s until 10% strain was achieved. The filter was maintained at this position for 3000s while load was recorded at 1 Hz by a 500 N load cell. The testing was performed in PBS at room temperature.

The theoretical response in time domain was calculated by inverting equation (4) to time domain (with equation (5) for linear biphasic model and with equation (6) for poroviscoelastic biphasic models) for $\tilde{z} = 0$ using a Matlab script (Hollenbeck, K. J. (1998) invlap.m) based on a numerical inverse Laplace transform algorithm [24]. Matlab (Mathworks, Natick, MA) optimization function, FMINSEARCH, based on the Nelder-Mead simplex algorithm was then used to minimize the root mean square error between the measured transient reaction force for each of 15 specimens and the theoretical response by finding best-fit parameters: H_A and k for KLM model; H_A, k, c, τ_1 and τ_2 for BPVE model. Code for Matlab scripts used in the current study for parameter optimization and error calculation of BPVE model in confined compression is detailed in Appendix 1.2. Curve-fits between theoretical and experimental responses were further assessed by a nonlinear coefficient of determination, r^2. Following confined compression testing, specimens were soaked in PBS for 48 hours before unconfined compression testing.

Unconfined Stress Relaxation

In unconfined compression testing, the hydrogel size-1 specimen was compressed between two impermeable flat platens in a bath filled with PBS at room temperature. A preload of 2N was applied. Similar to confined compression tests, the top platen was ramped at a constant velocity of 1.3 microns/s until 10% strain was achieved. The platen

was maintained at this position for 3000s while load was recorded at 1 Hz by a 500 N load cell.

The theoretical response in time domain was calculated by inverting equation (8) to time domain with equation (9) for KLM and with equation (10) for BPVE models and by inverting equation (11) for linear biphasic with anisotropy model for $\tilde{z} = 0$ based on a numerical inverse Laplace transform algorithm. Matlab optimization function, FMINSEARCH, was used to minimize the root mean square error between the measured transient reaction force for each of the 15 specimens and the theoretical response by finding best-fit parameters: μ, H_A and k for linear biphasic models; μ, H_A, k, c, τ_1 and τ_2 for BPVE; and $H_{+A}, H_{-A}, \lambda_2$ and k_z for ANISOTROPIC models. Curve-fits between theoretical and experimental responses were further assessed by a nonlinear coefficient of determination, r^2. Following unconfined compression testing, specimens were soaked in PBS for 48 hours before coefficient of friction measurements.

Coefficient of Friction Measurements

For coefficient of friction measurements, two sets of specimens were tested. For the first set, size-1 specimens (n=15), which were already tested in confined and unconfined compression tests, were epoxied (8276- JB Weld, Sulfur Springs, TX) onto the tip of Ultra-high-Molecular-Weight Polyethylene cylinders for easy mounting on pin-on-disk tester. For the second set, three size-2 specimens (diameter = 9.525 mm and height = 22.0 ± 1.6 mm) were lathed from rods of each of the three materials used in producing size-1 specimens.

The specimens were articulated against ceramic disks (Biolox Delta, Ceramtec AG, Plochingen, Germany) with an initial average roughness (R_a) of 9 ± 1 nm using an

OrthoPOD Pin-on-Disk machine (AMTI, Watertown, MA). The lubricant used was Hyclone Wear Testing fluid (HyClone, Logan, UT) with a protein concentration of 20 g/L to simulate synovial fluid [25]. The samples were presoaked in bovine serum for 48 h prior to testing. The lubricant was maintained at 37 ± 0.1^0C during the test. For coefficient of friction tests, a linear track of 10 mm was programmed. In order to investigate changes in coefficient of friction, measurements were performed at various load and speed combinations [13, 14]. Different speeds were attained by changing the frequency of the waveform while maintaining the same track. Sliding speeds used were 1,5,10,20 and 40 mm/s. Loads used were 1,5,15 and 50 N for size-1 specimens and 4, 22.5, 67.5 and 225 N for size-2 specimens, which resulted in 0.05, 0.3, 0.9 and 3.1 MPa of contact stress for both sets of specimens.

Data acquisition rate was 200 Hz and acquisition lasted at least 1s or long enough to cover one cycle at lower speeds. The mean of the coefficient of friction measurements for each specimen was calculated for the corresponding load and velocity condition.

Results

Mechanical Testing

Confined Stress Relaxation

The biphasic poroviscoelastic (BPVE) and linear biphasic (KLM) models performed equally well in predicting the results of the confined stress-relaxation behavior of the hydrogels. The root-mean-squared error (RMSE) and coefficient of determination yielded by BPVE model were 0.220 ± 0.316 MPa (mean ± st. dev.) and 0.93 ± 0.08 (mean ± st. dev.) respectively whereas KLM yielded 0.225 ± 0.307 MPa and 0.85 ± 0.12. However, the difference in error between the models was not statistically significant. In order to

discard toe region in the data, which was caused by lack of confinement of specimens in the chamber, only the relaxation portion of the curves were used for modeling purposes. An example parameter fit is shown in figure 1. Two samples exhibited chamber confinement problems even in the relaxation regime and were excluded as outliers. Both KLM and BPVE models yielded similar aggregate moduli (p=0.9; Related samples Wilcoxon signed rank test) whereas the KLM model yielded higher permeability estimates compared to the BPVE model (p=0.0003; Related samples Wilcoxon signed rank test) as shown in table 1.

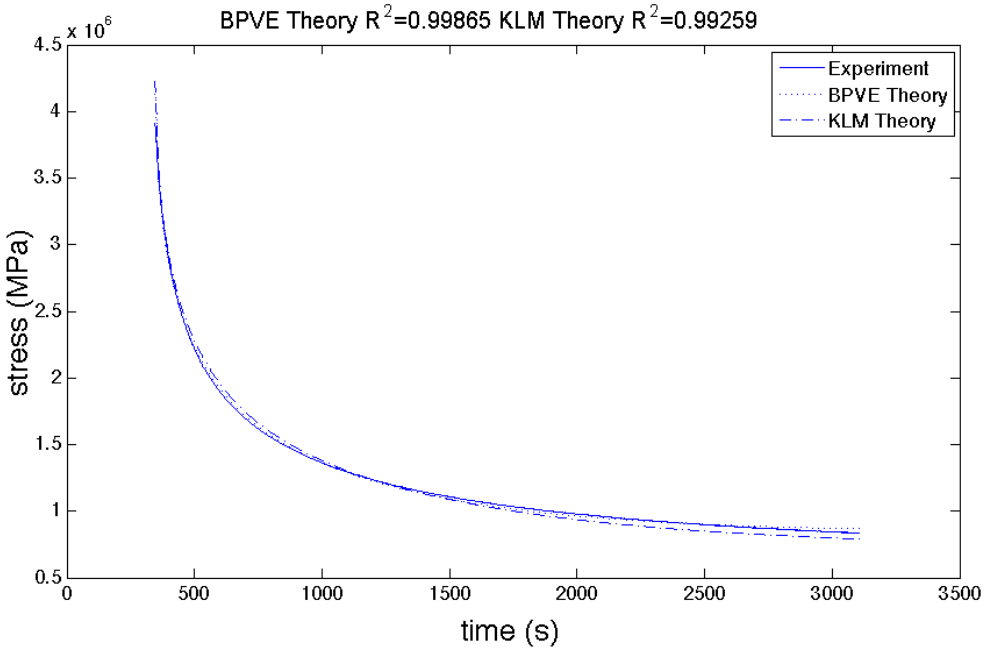

Figure 1-1) Force response predicted by BPVE and KLM models were shown along with the experimental response in confined compression testing.

Table 1-1) Material Parameters obtained by biphasic models in confined compression testing. *Specimens #1-1 and #2-4 were removed as outliers.

	R^2		BPVE						KLM		
Mat.-Spec.	BPVE	KLM	RMSE (Pa)	H_a (10^6 Pa)	k (10^{-16} mm^4/N.s)	c	τ_1	τ_2	RMSE (Pa)	H_a (10^6 Pa)	k (10^{-16} mm^4/N.s)
1-2	0.99	0.99	54308	10.51	2.13	0.60	11.98	62.95	40668	10.48	3.82
1-3	0.86	0.87	59711	6.05	4.03	0.82	4.67	43.10	56503	6.12	11.28
1-4	0.82	0.83	640788	7.54	0.23	1.38	13.03	154.92	631477	1.70	0.23
1-5	0.80	0.80	939551	2.86	0.20	0.01	0.10	2.51	938115	2.87	0.21
2-1	0.89	0.93	286455	4.02	0.16	2.32	1.02	5.90	237641	4.78	1.14
2-2	0.92	0.93	213931	6.13	0.14	2.86	0.49	10.64	211532	5.26	1.14
2-3	1.00	1.00	17620	8.15	0.36	2.69	0.32	8.90	34128	7.58	3.17
2-5	0.83	0.83	632508	8.81	0.16	2.02	10.70	99.13	631475	7.73	0.80
3-1	1.00	0.95	4962	2.89	14.46	0.38	0.03	0.34	23426	3.41	21.40
3-2	1.00	0.79	1062	2.21	18.46	1.34	0.02	0.13	26245	2.63	26.67
3-3	1.00	0.78	1308	2.49	19.35	1.33	0.00	0.12	31476	2.94	25.75
3-4	1.00	0.56	2407	2.68	23.29	3.60	0.03	0.10	32186	3.16	41.21
3-5	0.99	0.81	5393	2.45	27.36	2.82	0.01	0.07	25606	2.68	26.88
Average	0.93	0.85	220000	5.14	8.49	1.71	3.26	29.91	224652	4.72	12.59
Standard deviation	0.08	0.12	316088	2.88	10.41	1.10	5.10	48.52	307224	2.60	13.99

Unconfined Stress Relaxation

The BPVE, KLM and linear biphasic with cubic symmetry (ANISOTROPIC) models performed equally well in predicting the results of unconfined stress-relaxation of hydrogels in this study. RMSE yielded by the BPVE model was 17048 ± 8360 Pa (mean ± st. dev.). It was 17112 ± 8215 by KLM model and 17092 ± 8394 Pa by ANISOTROPIC model. Coefficient of determination of the models were 0.98 ± 0.01, 0.98 ± 0.01 and 0.98 ± 0.01 respectively. Yet, the differences in error between the models were not statistically significant. An example parameter fit is shown in figure 2. KLM and ANISOTROPIC models yielded similar aggregate modulus estimates (p=1) whereas BPVE model yielded different aggregate moduli compared to KLM and ANISOTROPIC

models (p=0.006 and p=0.002 respectively; Related samples Friedman's two-way ANOVA by ranks) as shown in table 2. In terms of permeability, BPVE and ANISOTROPIC models yielded similar estimates (p=1) while KLM model produced higher permeability estimates than BPVE and ANISOTROPIC (p=0.01 and p=0.032 respectively; Related samples Friedman's two-way ANOVA by ranks), also shown in table 2. Finally, ANISOTROPIC predicted higher aggregate moduli in tension compared to compression (p=0.012; Related samples Wilcoxon signed rank test).

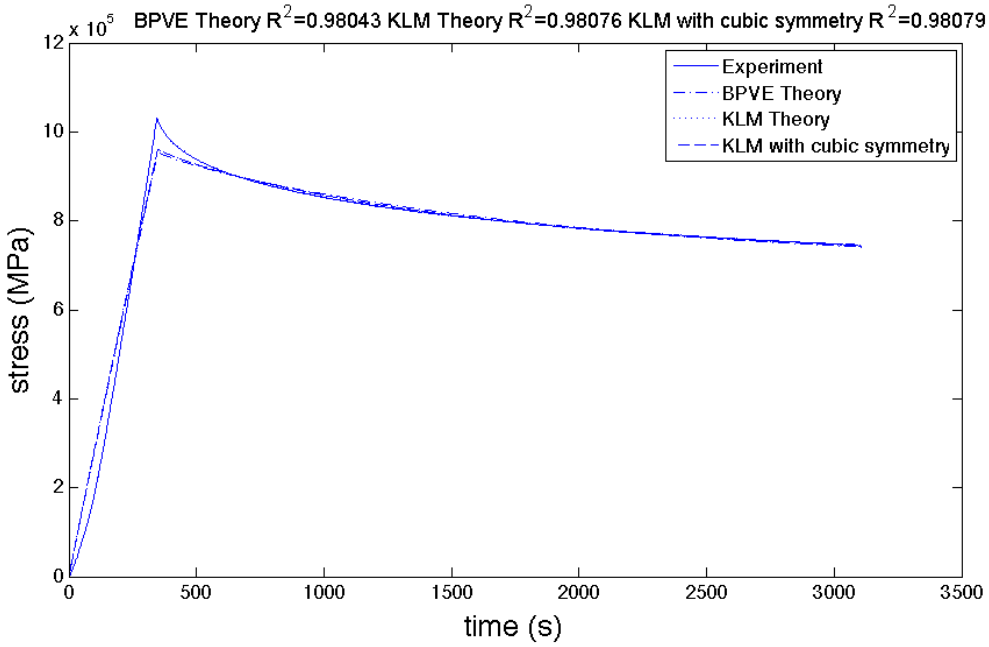

Figure 1-2) Force response predicted by BPVE, KLM and ANISOTROPIC models were shown along with the experimental response in unconfined compression testing.

Table 1-2) Material parameters obtained by biphasic models in unconfined compression testing

	R^2			BPVE						
Mat. - Spec.	BPVE	KLM	ANISOTROPIC	RMSE (Pa)	μ (10^6 Pa)	H_a (10^6 Pa)	k (10^{-16} mm^4/N.s)	c	τ_1	τ_2
1-1	0.98	0.98	0.98	35421	3.09	5.50	1.24	0.003	11.82	39.86
1-2	0.99	0.99	0.99	16231	3.75	7.85	1.32	0.136	8.34	39.49
1-3	0.99	0.99	0.99	17050	3.59	7.47	1.34	0.538	15.43	31.98
1-4	0.99	0.99	0.99	18627	3.59	7.51	1.20	0.376	10.66	26.60
1-5	0.99	0.99	0.99	19893	3.46	7.32	1.38	0.399	12.72	20.99
2-1	0.99	0.99	0.99	23198	3.76	7.77	1.37	0.371	14.07	35.08
2-2	0.99	0.99	0.99	20324	3.74	7.80	1.28	0.904	12.54	19.38
2-3	0.98	0.98	0.98	22890	3.45	7.20	1.16	0.443	9.84	32.49
2-4	0.97	0.97	0.97	26546	3.14	6.60	1.22	0.335	11.64	33.20
2-5	0.99	0.99	0.99	17308	3.76	7.77	1.26	0.548	9.64	32.06
3-1	0.99	0.98	0.99	7548	1.56	3.10	1.97	0.825	13.55	42.98
3-2	0.97	0.97	0.97	9864	1.20	2.33	1.31	0.800	0.81	30.08
3-3	0.99	0.99	0.99	5824	1.35	2.62	1.67	0.759	1.15	28.76
3-4	0.96	0.96	0.96	9273	1.00	1.96	2.68	0.392	2.67	29.22
3-5	0.99	0.99	0.99	5717	1.42	2.74	2.82	0.367	2.59	28.34
Average	0.98	0.98	0.98	17048	2.79	5.70	1.55	0.480	9.16	31.37
Std. Dev.	0.01	0.01	0.01	8360	1.11	2.39	0.53	0.254	4.95	6.48

KLM				ANISOTROPIC				
RMSE (Pa)	μ (10^6 Pa)	H_a (10^6 Pa)	k (10^{-16} mm^4/N.s)	RMSE (Pa)	H+a (10^6 Pa)	H-a (10^6 Pa)	λ_2 (10^6 Pa)	k (10^{-16} mm^4/N.s)
35123	3.09	3.95	0.80	35699	11.168	6.766	2.012	0.670
16231	3.75	7.86	1.60	16305	11.392	8.309	1.813	0.989
17051	3.59	7.47	1.85	17116	12.927	8.335	2.652	0.921
18626	3.60	7.53	1.61	18609	6.871	7.490	0.100	1.802
19896	3.46	7.33	1.66	19964	10.765	7.809	1.846	1.008
23192	3.76	7.79	1.86	23243	9.789	7.939	1.026	1.354
20324	3.74	7.81	1.79	20386	11.364	8.255	1.787	1.104
22891	3.45	7.21	1.77	22874	6.578	7.200	0.100	2.015
26546	3.14	6.60	1.64	26524	5.948	6.596	0.100	1.906
17301	3.76	7.79	2.10	17273	7.562	7.776	0.187	2.152
8816	1.63	3.27	5.97	7572	4.307	3.173	0.420	2.502
9860	1.19	2.34	5.05	9877	2.797	2.338	0.100	3.936
5827	1.35	2.63	5.71	5832	3.137	2.634	0.100	4.564
9272	1.00	1.97	5.24	9358	7.437	3.381	2.709	0.940
5723	1.42	2.74	5.14	5751	7.276	3.526	1.904	1.539
17112	2.80	5.62	2.92	17092	7.95	6.10	1.12	1.83
8215	1.11	2.43	1.86	8394	3.17	2.33	1.01	1.12

Coefficient of Friction Measurements

Aggregate modulus estimates of each of the three models correlated equally strongly with coefficient of friction at each load and velocity condition. In addition, permeability values obtained by KLM model correlated more strongly with coefficient of friction compared to values obtained by BPVE or ANISOTROPIC models, which also correlated significantly with coefficient of friction. Based on size-1 specimens, coefficient of friction increased with increasing aggregate modulus as obtained by each of the three biphasic models (spearman's rho=0.5; $p<0.001$ for each of the models). However, coefficient of friction decreased with increasing permeability as obtained by BPVE, KLM and ANISOTROPIC models (spearman's rho=-0.3, $p<0.001$; rho=-0.4, $p<0.001$; rho=-0.2, $p<0.001$ respectively).

For size-2 specimens, on the other hand, material parameters obtained by each of the three models correlated equally strongly with coefficient of friction measurements. Similar to size-1 specimens, coefficient of friction of size-2 specimens increased with increasing aggregate modulus as obtained by the biphasic models (spearman's rho=0.3; $p<0.001$ for each of the models) whereas coefficient friction decreased with increasing permeability (spearman's rho=-0.3; $p<0.001$ for each of the models). Range of coefficient of friction measurements was 0.04 – 0.57 and 0.03 – 0.48 for size-1 and size-2 specimens respectively.

For the range of velocities and loads used in this study, coefficient of friction increased with increasing velocity (spearman's rho=0.3; $p<0.001$) and decreased with increasing load (spearman's rho=-0.6; $p<0.001$) for size-1 specimens as shown in representative plots (Fig. 3-a and b). Similarly, coefficient of friction increased with

increasing velocity (spearman's rho=0.3; p<0.001) and decreased with increasing load (spearman's rho=-0.8; p<0.001) for size-2 specimens as shown in figures 3-c and d.

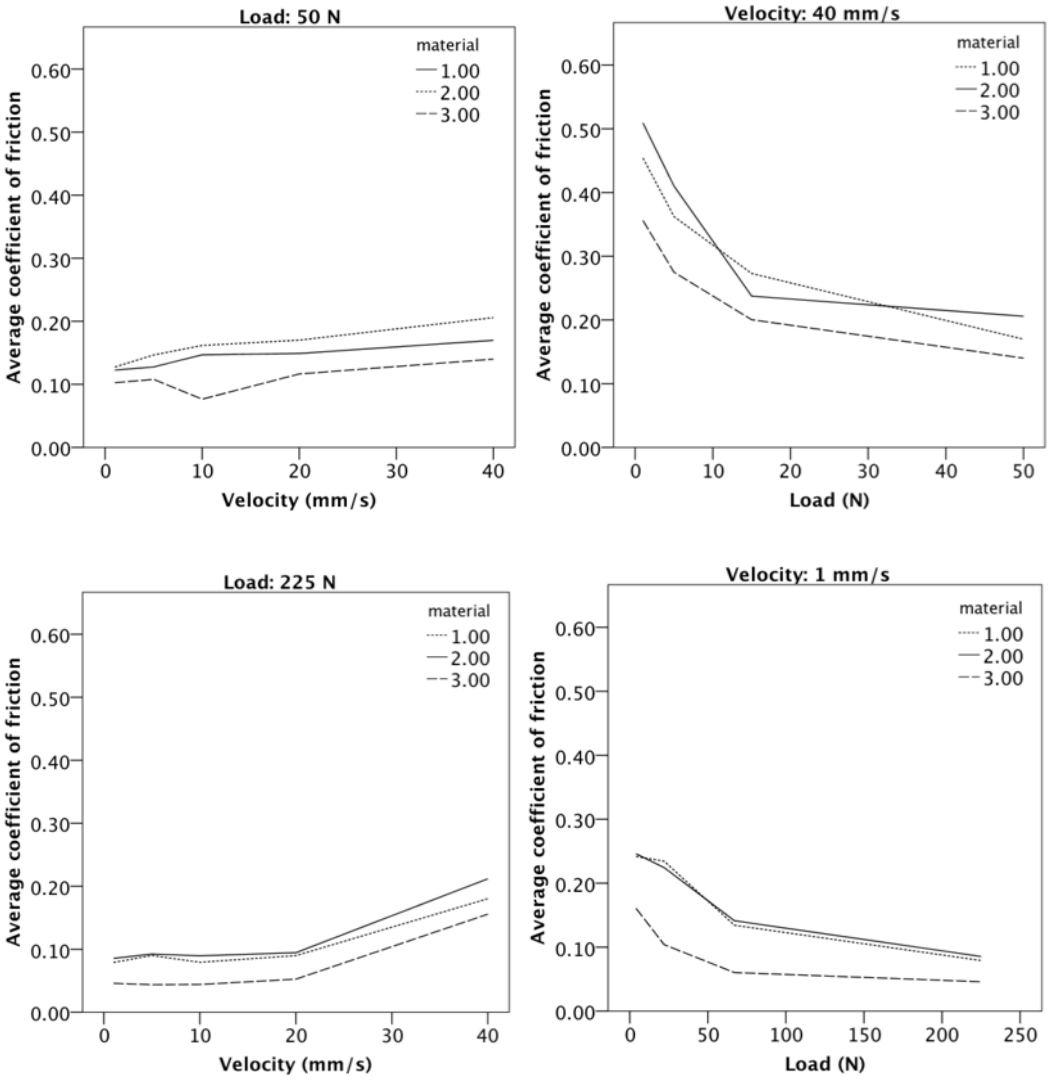

Figure 1-3) Change in coefficient of friction with respect to varying velocities and loads. Figures 3-a and b show data from size-1 specimens (average of 15 specimens). Figures 3-c and d show data from size-2 specimens (average of 9 samples).

DISCUSSION

A material model linking physical behavior to structural properties would be useful for the design of tissue replacements [9]. As hydrogels have been proposed for replacing damaged articular cartilage, characterizing hydrogels based on cartilage modeling

framework is a valuable step in tailoring their tribological behavior. The objectives of this study were to obtain hydrogel material properties using biphasic cartilage model, and to investigate the relationship between the tribological properties and the material properties of hydrogels. Our hypotheses were: (1) the BPVE model would yield a smaller error than KLM or ANISOTROPIC cartilage model when predicting mechanical response of hydrogels in stress relaxation tests; and (2) coefficient of friction of hydrogel articulation at various speeds and loads would correlate more strongly with material parameters obtained by BPVE model compared to parameters obtained by KLM and ANISOTROPIC models.

This study did not support the hypothesis that BPVE model would yield a lower error compared to KLM and ANISOTROPIC cartilage models in stress relaxation tests. The results of this study indicate that the simplest model we considered, i.e., the biphasic model with linear-elastic solid matrix (KLM), is sufficient to describe the material behavior of this family of hydrogels. Setton et al. showed that for articular cartilage, the effects of drag forces caused by fluid flow were more dominant in the viscoelastic response of the material compared to the viscoelasticity of the intrinsic solid matrix if the permeability was smaller than 10^{-14} m^4/Ns [23]. Our results were consistent with this conclusion since hydrogel permeability values were equal or smaller than 10^{-15} m^4/Ns in this study. Stammen et al. also reported that the viscoelastic behavior of their hydrogel depended primarily on interstitial fluid flow [26], which was in agreement with our conclusion that the linear biphasic model should predict the mechanical response of the hydrogels as successfully as biphasic poroviscoelastic cartilage model (BPVE). Although ANISOTROPIC cartilage model predicted a higher aggregate modulus in tension

compared to compression for the hydrogels, similar to the tension-compression nonlinearity of articular cartilage [10], the KLM model predicted the mechanical response with a comparable error and invalidated the assumption that the hydrogel solid matrix is anisotropic.

This study did not support the hypothesis that coefficient of friction of hydrogel correlated more strongly with material parameters obtained by BPVE model compared to KLM and ANISOTROPIC models in unconfined compression testing. The results of this study indicate that the material properties obtained by the simplest model we considered, i.e., the biphasic model with linear-elastic solid matrix (KLM), correlated with coefficient of friction of hydrogels at all the tested speed and load combinations as strongly as parameters obtained by the BPVE and ANISOTROPIC models. These correlations suggested that in order to obtain smaller coefficients of friction, hydrogels with small aggregate modulus and large permeability values are required.

Comparison of mechanical properties of hydrogel obtained in this study with properties of articular cartilage from literature, which were obtained by biphasic models, showed that the aggregate modulus of the hydrogel was an order of magnitude larger than aggregate modulus of cartilage while the permeability of hydrogel was within the range of reported values of articular cartilage permeability (table 3). In vitro coefficient of friction of articular cartilage was reported as low as 0.014 for initial coefficient of friction, and up to 0.3 for equilibrium coefficient of friction [1, 14], which is attained when fluid pressurization effects subside [1, 13, 14]. The range of coefficients of friction in our study were 0.03 – 0.57.

Table 1-3) Mechanical Properties of hydrogel obtained by linear biphasic cartilage model was compared to material properties of articular cartilage obtained by biphasic cartilage models. *Aggregate modulus in compression and radial permeability of cartilage was reported from Soltz et al.

		Aggregate Modulus (MPa)	Permeability (× 10^{-14} m^4/Ns)
Cartilage	Setton et al.[23]	0.54	0.5
	Soltz et al.[11]*	0.64	0.006
	Mow et al.[4]	0.7	0.76
Hydrogel	Baykal et al.	5.6	0.029

The results of this study showed a positive correlation between coefficient of friction and material stiffness similar to the results by Covert et al., who reported a positive correlation between coefficient of friction and material stiffness [19]. Thomas et al., on the other hand, found no correlation between coefficient of friction and compressive modulus [27]. Based on the correlations between material parameters and coefficient of friction reported in this study, designing hydrogels that match the smaller aggregate moduli of cartilage while maintaining or increasing their permeability would result in lower coefficients of friction, which are also closer to those of articular cartilage. It should be noted that although the correlations between material properties and coefficient of friction reported in this study should pertain to different types of hydrogels with similar aggregate moduli and permeability, different chemical properties of a hydrogel, such as surface fixed charge density, could cause deviations from the behavior reported in this study.

Identifying the active lubrication mode of the hydrogel articulation in this study will enable further evaluation of its tribological properties. In order to assess which lubrication mode was active, the relationship between coefficient of friction, load and

velocity was analyzed. The frictional behavior of hydrogel based on speed and load observed in this study was in agreement with Mamada et al., who utilized the "Repulsion-Adsorption model" for poly(vinyl alcohol) hydrogels [28]. According to this theory, there are 2 friction regimes for adhesive gels: elastic friction and hydrodynamic friction [16, 28, 29]. In elastic friction regime, coefficient of friction increased with decreasing speed. This was similar to results from Covert et al. and Pan et al., who reported that coefficient of friction of hydrogels increased with decreasing speed [19, 30] and increasing load [30]. In the hydrodynamic lubrication regime, on the other hand, increased velocity or decreased load resulted in increased coefficient of friction similar to the results in our study [16, 28, 29]. In order to investigate whether the hydrogel articulation was always in hydrodynamic lubrication for the range of speed and load combinations in this study, the average coefficient of friction at the lowest contact stress and the average coefficient of friction at the highest contact stress were plotted against velocity/pressure, similar to Stribeck analysis, for size-1 and size-2 specimens (Figures 4 and 5). The existence of a positive slope and the linearity of friction against the range of V/P values suggested that the specimens were always in hydrodynamic lubrication regime of the "Repulsion-Adsorption model" for an adhesive gel [16]. Given the correlations between friction, load and velocity reported in this study, Stribeck theory also predicts hydrodynamic lubrication where coefficient of friction increases with increasing velocity and decreasing load [13, 14]. Furthermore, the traditional elastohydrodynamic lubrication theory (EHL) for hard bearings predicts film thickness to correlate positively with velocity and negatively with load if there is no asperity contact [31]. The effect of increasing bovine serum film thickness is an increase in coefficient of friction since thicker film results in

lower shear rates and higher viscosity [32, 33]. Finally, De Vicente et al. developed a theory for compliant and lubricated ball-on-flat contacts and showed that coefficient of friction correlated positively with velocity and negatively with load [34]. Because our results showed a positive correlation between velocity and coefficient of friction, and the correlation between friction and load was negative, these theories suggested that the hydrogel articulation in this study was separated by fluid film.

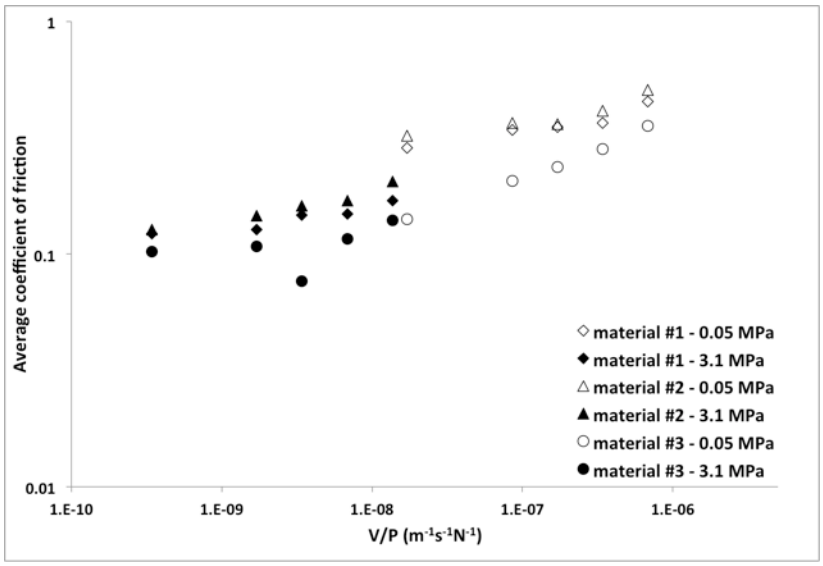

Figure 1-4) Average coefficient of friction of size-1 specimens (n=15) was plotted in a double-log scale against V/P, similar to Stribeck theory.

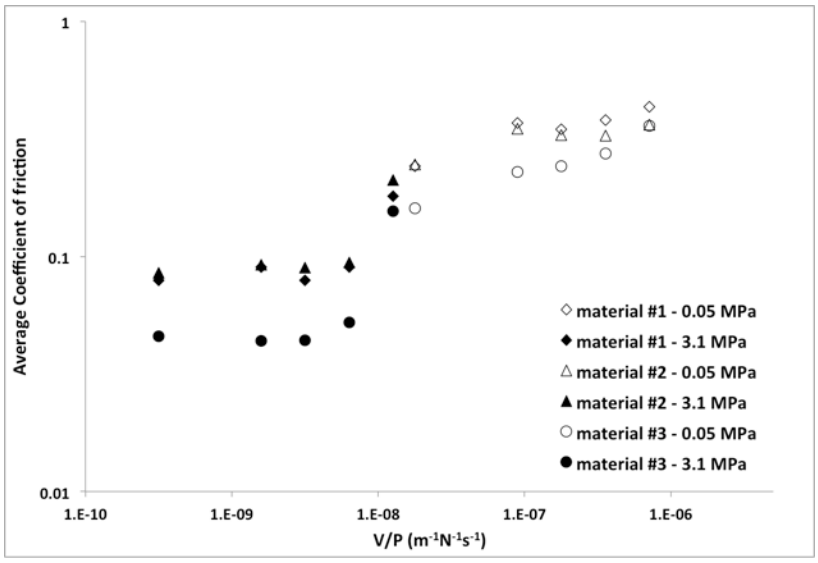

Figure 1-5) Average coefficient of friction of size-2 specimens (n=9) was plotted in a double-log scale against V/P, similar to Stribeck theory.

In order to assess the lubricating effect of bovine serum, another set of coefficient of friction measurements was performed at 3.1 MPa pressure and 5 mm/s velocity with both size-1 (n=5) and size-2 (n=9) specimens with distilled water as lubricant. For both types of specimens, coefficient of friction was smaller in bovine serum than in water (Figure 6). The dependence of coefficient of friction on the type of lubricant further supported our findings that the surfaces were separated by fluid film. Fluid film theory suggests that friction would be dominated by bulk fluid properties and not affected by lubricant proteins [31]. However, lower coefficient of friction with bovine serum, in this study, suggested that increased viscosity of serum due to molecules such as hyaluronic acid [14] did not increase the friction as expected whereas the lubricant proteins might have played a role in decreasing the friction. We postulated that lubricant proteins might have blocked the pores of hydrogel affecting interstitial fluid pressurization or the charge density of he hydrogel [16] caused it to interact with lubricant proteins and resulted in a lower coefficient of friction than in water. In conclusion, the inhomogeneous and non-

Newtonian properties of bovine serum [33] combined with the low modulus and permeability of hydrogels might have led to complications and deviations from classical fluid film theory. It should also be noted that EHL and Stribeck theories assume a Newtonian lubricant whereas bovine serum is non-Newtonian due to the lubricant proteins [32, 33]. Furthermore, these theories, except for Repulsion-Adsorption theory, are not developed for flat-on-flat contacts.

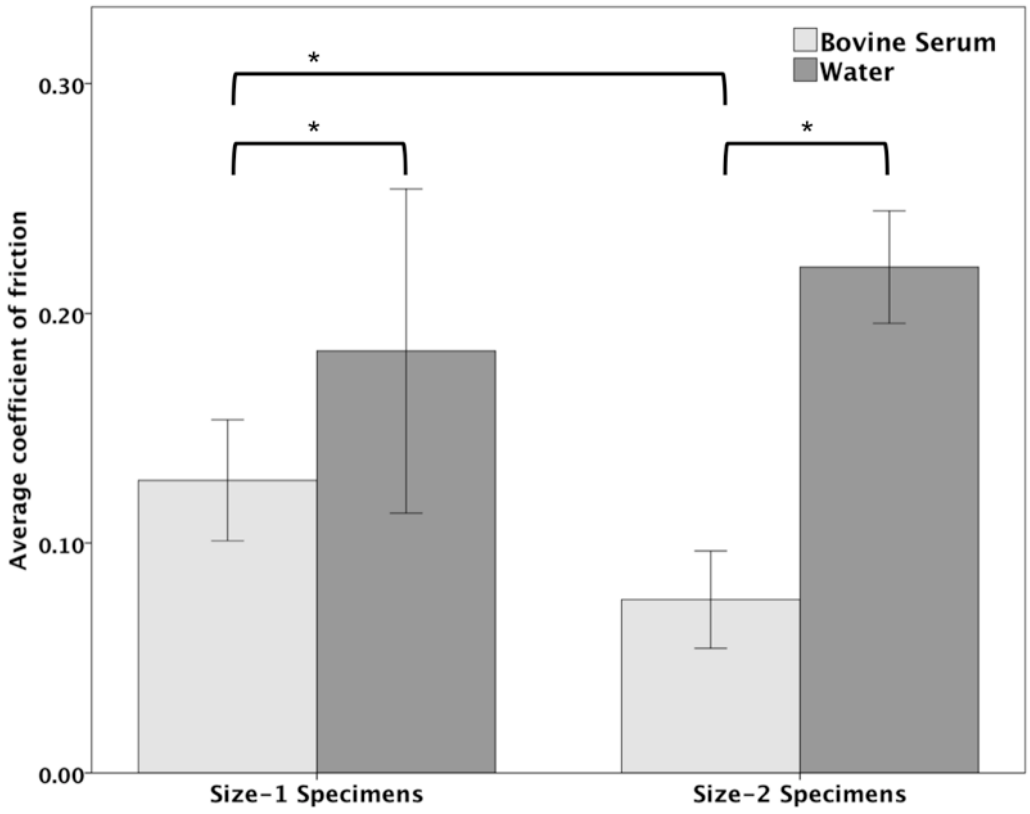

Figure 1-6) Average coefficient of friction of size-1 (n=5) and size-2 (n=9) specimens were shown with a 95% confidence interval. The coefficient of friction of hydrogel in bovine serum was smaller than in water ($p=0.03$ and $p<0.001$ for size-1 and size-2 specimens respectively; two samples t-test). The coefficients of friction of size-2 specimens were smaller than those of size-1 specimens in bovine serum ($p=0.003$; two samples t-test), and similar in water ($p=0.14$).

We acknowledge the limitations of our study: 1) startup coefficient of friction was used; 2) the coring process. The rationale behind using startup coefficient of friction instead of the equilibrium coefficient of friction was that initial coefficient of friction,

which was determined by interstitial fluid pressurization [1, 13], was sufficient to investigate the relationship between the mechanical properties and the biphasic lubrication capacity of the hydrogel tested in this study. Similarly, Gleghorn et al. measured the coefficient of friction of polyurethane foam only briefly and predicted the equilibrium coefficient of friction based on the biphasic model [13]. The coring process resulted in hydrogel specimens that were not precisely cylindrical. The lateral surfaces of cylinders were slightly concave since the hydrogel deformed while being cut. Deviations from a perfect cylinder resulted in confinement issues during confined compression testing. In order to discard the toe region, curve fitting in confined compression was performed only for the relaxation portion of the data. High coefficients of determination reported in the confined stress-relaxation section of this study showed that the artifacts caused by confinement issues were successfully removed by discarding the toe region.

In most studies, coefficient of friction of hydrogel was measured by articulating a metal ball on a hydrogel disk or sheet [20, 27, 28, 35]. The novel approach used in this study was that hydrogels that were shaped as pins were articulated against hard counterface. The advantage of this configuration was that the hydrogel specimen was always in compression during the coefficient of friction measurement, which enabled monitoring of the effects of velocity on friction while eliminating effects of rehydration. Another advantage was that both mechanical tests and friction measurements could be performed on the same individual specimens, which had similar dimensions to articular cartilage specimens used in mechanical tests. This allowed for the direct investigation of correlations between the material parameters and coefficient of friction of each specimen. However, mounting size-1 hydrogel specimen as the pin posed a complication: epoxy

that held the hydrogel on the UHMWPE pin broke for several specimens during tests with high loads. Size-2 specimens, which were large enough to be mounted on the pin-on-disk tester by themselves, were also produced to verify the friction measurements of specimens that were held with epoxy.

This study showed that linear biphasic cartilage model could be used to predict the mechanical response of hydrogels in compression tests. Furthermore, it was shown that hydrogels with low aggregate modulus and high permeability produced lower coefficient of friction. Finally, hydrogels were shown to produce lower coefficients of friction at low velocities and high loads.

References

[1] Accardi MA, Dini D, Cann PM. Experimental and numerical investigation of the behaviour of articular cartilage under shear loading - Interstitial fluid pressurisation and lubrication mechanisms. Tribology International. 2011;44:565-78.
[2] Caligaris M, Canal CE, Ahmad CS, Gardner TR, Ateshian GA. Investigation of the frictional response of osteoarthritic human tibiofemoral joints and the potential beneficial tribological effect of healthy synovial fluid. Osteoarthritis and Cartilage. 2009;17:1327-32.
[3] Mak A. Unconfined compression of hydrated viscoelastic tissues: a biphasic poroviscoelastic analysis. Biorheology. 1986;23:371.
[4] Mow V, Kuei S, Lai W, Armstrong C. Biphasic Creep and Stress Relaxation of Articular Cartilage in Compression: Theory and Experiments. Journal of biomechanical engineering. 1980;102:73.
[5] Mow VC, Ateshian GA, Spilker RL. Biomechanics of diarthrodial joints: a review of twenty years of progress. Journal of biomechanical engineering. 1993;115:460.
[6] Caligaris M, Ateshian GA. Effects of sustained interstitial fluid pressurization under migrating contact area, and boundary lubrication by synovial fluid, on cartilage friction. Osteoarthritis and Cartilage. 2008;16:1220-7.
[7] Mak A. The apparent viscoelastic behavior of articular cartilage--the contributions from the intrinsic matrix viscoelasticity and interstitial fluid flows. Journal of biomechanical engineering. 1986;108:123.
[8] Armstrong C, Lai W, Mow V. An analysis of the unconfined compression of articular cartilage. Journal of biomechanical engineering. 1984;106:165.
[9] Suh JK, Bai S. Finite element formulation of biphasic poroviscoelastic model for articular cartilage. Journal of biomechanical engineering. 1998;120:195.

[10] Cohen B, Lai W, Mow V. A transversely isotropic biphasic model for unconfined compression of growth plate and chondroepiphysis. Journal of biomechanical engineering. 1998;120:491.
[11] Soltz MA, Ateshian GA. A conewise linear elasticity mixture model for the analysis of tension-compression nonlinearity in articular cartilage. Journal of biomechanical engineering. 2000;122:576.
[12] Katta J, Jin Z, Ingham E, Fisher J. Biotribology of articular cartilage, A review of the recent advances. Medical engineering & physics. 2008;30:1349-63.
[13] Gleghorn JP, Doty SB, Warren RF, Wright TM, Maher SA, Bonassar LJ. Analysis of frictional behavior and changes in morphology resulting from cartilage articulation with porous polyurethane foams. Journal of orthopaedic research. 2010;28:1292-9.
[14] Gleghorn JP, Bonassar LJ. Lubrication mode analysis of articular cartilage using Stribeck surfaces. Journal of biomechanics. 2008;41:1910-8.
[15] Peppas NA, Merrill EW. Development of semicrystalline poly (vinyl alcohol) hydrogels for biomedical applications. Journal of biomedical materials research. 1977;11:423-34.
[16] Gong JP. Friction and lubrication of hydrogels—its richness and complexity. Soft Matter. 2006;2:544-52.
[17] Baykal D, Day J, Jaekel D, Katta J, Mansmann K, Kurtz S. Tribological evaluation of hydrogel articulations for joint arthroplasty applications. Journal of the Mechanical Behavior of Biomedical Materials. 2012;14:39.
[18] Bodugoz-Senturk H, Macias CE, Kung JH, Muratoglu OK. Poly (vinyl alcohol)–acrylamide hydrogels as load-bearing cartilage substitute. Biomaterials. 2009;30:589-96.
[19] Covert RJ, Ott R, Ku DN. Friction characteristics of a potential articular cartilage biomaterial. Wear. 2003;255:1064-8.
[20] Katta JK, Marcolongo M, Lowman A, Mansmann KA. Friction and wear behavior of poly (vinyl alcohol)/poly (vinyl pyrrolidone) hydrogels for articular cartilage replacement. Journal of Biomedical Materials Research Part A. 2007;83:471-9.
[21] Bavaresco V, Zavaglia C, Reis M, Gomes J. Study on the tribological properties of pHEMA hydrogels for use in artificial articular cartilage. Wear. 2008;265:269-77.
[22] Spiller KL, Laurencin SJ, Charlton D, Maher SA, Lowman AM. Superporous hydrogels for cartilage repair: evaluation of the morphological and mechanical properties. Acta biomaterialia. 2008;4:17-25.
[23] Setton LA, Zhu W, Mow VC. The biphasic poroviscoelastic behavior of articular cartilage: role of the surface zone in governing the compressive behavior. Journal of biomechanics. 1993;26:581-92.
[24] de Hoog FR, Knight J, Stokes A. An improved method for numerical inversion of Laplace transforms. SIAM Journal on Scientific and Statistical Computing. 1982;3:357-66.
[25] ASTM International PA U. F732 - Standard Test Method for Wear Testing of Polymeric Materials Used in Total Joint Prostheses. 2011.
[26] Stammen JA, Williams S, Ku DN, Guldberg RE. Mechanical properties of a novel PVA hydrogel in shear and unconfined compression. Biomaterials. 2001;22:799-806.
[27] Thomas BH, Craig Fryman J, Liu K, Mason J. Hydrophilic–hydrophobic hydrogels for cartilage replacement. Journal of the Mechanical Behavior of Biomedical Materials. 2009;2:588-95.

[28] Mamada K, Fridrici V, Kosukegawa H, Kapsa P, Ohta M. Friction Properties of Poly (vinyl alcohol) Hydrogel: Effects of Degree of Polymerization and Saponification Value. Tribology Letters. 2011;42:241-51.
[29] Gong J, Osada Y. Gel friction: a model based on surface repulsion and adsorption. The Journal of chemical physics. 1998;109:8062.
[30] Pan YS, Xiong DS, Ma RY. A study on the friction properties of poly (vinyl alcohol) hydrogel as articular cartilage against titanium alloy. Wear. 2007;262:1021-5.
[31] Dowson D. Elastohydrodynamic and micro-elastohydrodynamic lubrication. Wear. 1995;190:125-38.
[32] Cooke A, Dowson D, Wright V. The rheology of synovial fluid and some potential synthetic lubricants for degenerate synovial joints. Engineering in Medicine. 1978;7:66-72.
[33] Mavraki A, Cann P. Lubricating film thickness measurements with bovine serum. Tribology International. 2011;44:550-6.
[34] De Vicente J, Stokes J, Spikes H. Rolling and sliding friction in compliant, lubricated contact. Proceedings of the Institution of Mechanical Engineers, Part J: Journal of Engineering Tribology. 2006;220:55-63.
[35] Yasuda K, Ping Gong J, Katsuyama Y, Nakayama A, Tanabe Y, Kondo E, et al. Biomechanical properties of high-toughness double network hydrogels. Biomaterials. 2005;26:4468-75.

2. Microscopic Characterization of in vitro Wear of Articular Cartilage based on Fourier Transform Infrared Analysis and Histology

Abstract

Biphasic materials, i.e., hydrogels, which could facilitate biphasic lubrication, were proposed to replace damaged articular cartilage tissue. In order to improve the performance of hemiarthroplasty materials, wear of articular cartilage against cartilage replacement material should be evaluated. Histology and Fourier transfer infrared (FTIR) spectroscopy were used to microscopically characterize *in vitro* wear of cartilage. Cartilage-on-cartilage (n=6), cartilage-on-hydrogel (n=3) and cartilage-on-CoCr articulations (n=3) were characterized on a Pin-on-disk tester. Histology results showed that cartilage pins that articulated against cartilage had the thinnest proteoglycan deficient layer close to the surface compared cartilage-on-hydrogel articulation, followed by cartilage-on-CoCr articulation. Mechanical damage to the collagen ultrastructure due to wear was not visible on the surfaces or in the deeper zones. FTIR analysis, on the other hand, yielded higher collagen maturity for cartilage pins that articulated against cartilage and pins that articulated against hydrogel compared to cartilage-on-CoCr articulation ($p=0.004$; $p=0.01$ respectively). In terms of proteoglycan content however, only cartilage-on-cartilage was higher than cartilage-on-CoCr articulation ($p=0.008$). We concluded that at the onset of articular cartilage wear, both collagen maturity and proteoglycan content decreased before surface damage occurred.

Introduction

Hemiarthroplasty is advantageous over total joint arthroplasty in conditions such as femoral neck fracture, localized chondral defects and trauma damage [1-3]. However, cartilage articulation against the hemiarthroplasty material may lead to pain and cartilage

erosion [3-5]. Researchers have therefore investigated materials that could perform better than CoCr [3, 4], the primary material used for this procedure. Recently, biphasic materials, i.e., hydrogels, were proposed to replace damaged articular cartilage tissue [2, 6, 7] and facilitate biphasic lubrication while articulating against the opposing cartilage surface [2]. In order to ultimately assess and improve the performance of hemiarthroplasty materials, characterizing wear of articular cartilage against the hemiarthroplasty material is required [1-3].

Cartilage wear comprises chemical and mechanical degradation and can manifest itself as a loss of proteoglycans, changes in collagen structure or even changes in the ionic equilibrium [8]. Lipshitz and Glimcher excluded a fatigue wear mechanism and emphasized constant crack formation and wear particle generation by chain scission when cartilage pins articulated against stainless steel [9]. Mow et al., on the other hand, described the cartilage wear mechanism as fatigue micro-cracks coalescing and eventually causing delamination [10]. Patel and Spector reported a proteoglycan-deficient wear layer accumulating on the surface of the cartilage pins as cartilage wear progressed [4]. Quantification of cartilage wear is not possible using conventional gravimetric measurements or direct wear debris analysis [1, 8, 11], hence alternative methods such as biochemical characterization by hydroxyproline and glycosaminoglycan contents in lubricant, optical profilometry, and staining with india ink have been used [9, 12]. However, a single parameter as obtained by these methods will not sufficiently model wear mechanisms of articular cartilage because of its heterogeneous and zone-dependent composition [2]. Histology allows spatial analysis and has been widely utilized for

cartilage characterization [3-5, 13]. Yet, histology is hard to quantify and requires separate staining for each parameter [14].

Fourier transfer infrared (FTIR) microspectroscopy is quantitative and capable of spatially resolving multiple parameters simultaneously [13-18]. FTIR has been used to detect biochemical degradation of cartilage matrix and thereby differentiate between healthy and early osteoarthritic cartilage before surface damage, such as clefts, fissures and fibrillations were apparent. [13, 15]. As the early stages of degenerative joint disease have been attributed to cartilage wear [10, 19] and involve changes in collagen structure and loss of proteoglycans [13], FTIR analysis can be employed for the study of articular cartilage wear. The objectives of this study were to microscopically characterize *in vitro* wear of articular cartilage using FTIR and histology, and to compare the effects of wear of cartilage against cartilage, and against CoCr and a hydrogel as hemiarthroplasty materials. We hypothesized that early stages of wear of articular cartilage can be detected by utilizing FTIR parameters related to collagen maturity [15] and proteoglycan content [13, 17]. Specifically, our hypotheses were: (1) the onset of wear of articular cartilage involved a decrease in collagen maturity and loss of proteoglycans; and (2) cartilage pins that articulated against a CoCr counterface would result in reduced collagen maturity and reduced proteoglycan concentration, compared to articulation against either articular cartilage or a biphasic material.

Methods

Specimen Preparation

Healthy adult bovine femurs were obtained from a local abattoir. While frozen, femoral heads, patella and condyles were positioned under the coring axis of a drill press using an

any-angle precision vise in order to produce approximately planar surfaces. Phosphate buffered saline was used to keep cartilage surfaces wet. The specimens were cored with one of two drill press wood plug cutters to obtain osteochondral pins (n=14) of 9.5 mm in diameter from the femoral head and osteochondral disks (n=6) of 15.9 mm in diameter from the patella and both of the medial and distal condyles. The pins and disks had subchondral bone (~ 10 mm) bonded to the cartilage. The test pin (n=12) and disk specimens (n=6) were submerged in protease-inhibitor cocktail (#S8820, Sigma-Aldrich, St. Louis, MO, USA) at 4°C for 24 hours before testing. The non-tested control pins (n=2) were frozen at -20°C immediately following harvest.

A sheet shaped proprietary hydrogel (CyborGel, Formae Inc, Paoli, PA) with 44% water content was used to produce disks of 15.9 mm in diameter and 10 mm in height (n=3). Finally, CoCr disks (n=3) with a surface roughness of 8 ± 3 nm were also used as counterface.

Wear Testing of Cartilage Specimens

Cartilage-on-cartilage (n=6), cartilage-on-hydrogel (n=3) and cartilage-on-CoCr articulations (n=3) were characterized using an OrthoPOD Pin-on-Disk machine (AMTI, Watertown, MA). Cartilage pin samples were mounted on the tester using collet pin holders while cartilage and hydrogel disk samples were press-fit into the center holes of ultra-high-molecular-weight-polyethylene disks. CoCr disks were mounted on the tester using dowel pins. All disk samples had their individual chambers filled with 20 g/L bovine serum (Wear testing fluid, Hyclone, Logan, UT) as lubricant that was kept at 37°C. A constant load of 40 N corresponding to a nominal contact stress of 0.56 MPa, which represented the low end of the physiological range [4], was applied. Pins

reciprocated linearly at a velocity of 6.58 mm/s with a stroke length of 3.29 mm while they rotated ± 30° per cycle around their axes of symmetry to facilitate cross-shear. Testing lasted 25000 cycles. Articular cartilage was expected to operate in a mixed or boundary lubrication regime with these contact stress and sliding velocity parameters [2, 20] and avoid non-physiological hydrodynamic lubrication [8, 20]. The rationale for selecting these parameters was to generate sufficient cartilage wear for monitoring of the ultrastructural changes without severe surface damage. Immediately after the wear tests, pin specimens were photo-documented. Subchondral bone was removed from pins using a scalpel before cartilage was submerged in a universal molecular fixative (Tissue-Tek Xpress Molecular Fixative; Sakura Finetek, California, USA) for 24 hours.

Tissue Processing

The center region of cartilage specimens were cored along their height using a 6 mm biopsy punch. The specimens were then dehydrated and fixed in paraffin. Eighteen histological sections for each of the tested cartilage pins (n=12) and for each of the non-tested control pins (n=2) were cut at 6 μm thickness perpendicular to the articular surface. Histological sections were mounted on low-e slides (MirrIR, Kevley Technologies, OH, USA) and histology slides for FTIR (n=9 for each pin) and histologic (n=9 for each pin) analyses respectively. All slides were deparaffinized before histological and FTIR analysis.

Histological Evaluation

Slides for histologic analysis were stained with Hematoxylin and Eosin (H&E), and Alcian blue stains simultaneously. On stained slides, red corresponded to nuclei whereas tissue structures including collagen were pink to red and proteoglycan was stained blue

[13]. Microscopic images were acquired using a Jenoptik ProgRes (Jenoptik AG, Germany) digital camera.

FTIR Data Acquisition and Analysis

A Nicolet Continuum FT-IR Microscope (Thermo Fisher Scientific Inc., Waltham, MA) was used to acquire IR data in reflectance mode with a resolution of 4 cm^{-1} over the spectral region of 800–6000 cm^{-1}. Each spectrum comprised 64 co-added scans, and spectra were baselined by straight-line subtraction before analysis. Spectral outliers were visually identified and removed; spectral outliers were a consequence of scattering artifacts and increased water content relative to other sampling sites. To characterize wear induced changes to the ultrastructure of cartilage throughout its depth, 6 spectra per histological section were recorded along the centerline of each specimen using an aperture of 100 x 100 μm. These spectra spanned ~ 0.5 mm in thickness. Spectra of sections were grouped together based on articulation couple, i.e., non-tested, cartilage, biphasic material and CoCr.

The infrared absorbance regions evaluated in this study were 1595-1710 and 985-1140 cm^{-1}. The amide I absorbance (1595-1710 cm^{-1}) arises from the amide I carbonyl (C=O) stretch [15, 21, 22]. The infrared absorbance area between 985-1140 cm^{-1} is due to the proteoglycan sugar ring C-O absorbance [13, 15, 23].

The ratio of infrared absorbances at 1660 and 1690 cm^{-1} [15, 21] have been shown to decrease as collagen degrades, or, in less mature collagen. Thus, the ratio of infrared absorbance sub-bands (i.e. peak heights) at 1660 and 1690 cm^{-1} was used as the collagen maturity parameter. The ratio of infrared absorbance area of the proteoglycan and amide I bands was calculated to evaluate the relative proteoglycan content [15, 23]. FTIR data

analysis was performed by Grams 8.0 software (Thermo Fisher Scientific, Waltham, MA). Representative spectra from non-tested control, tested control (cartilage on cartilage articulation), cartilage on biphasic articulation and cartilage on CoCr articulation, along with infrared absorbance regions used in characterizing cartilage matrix constituents, are shown in Figure 1.

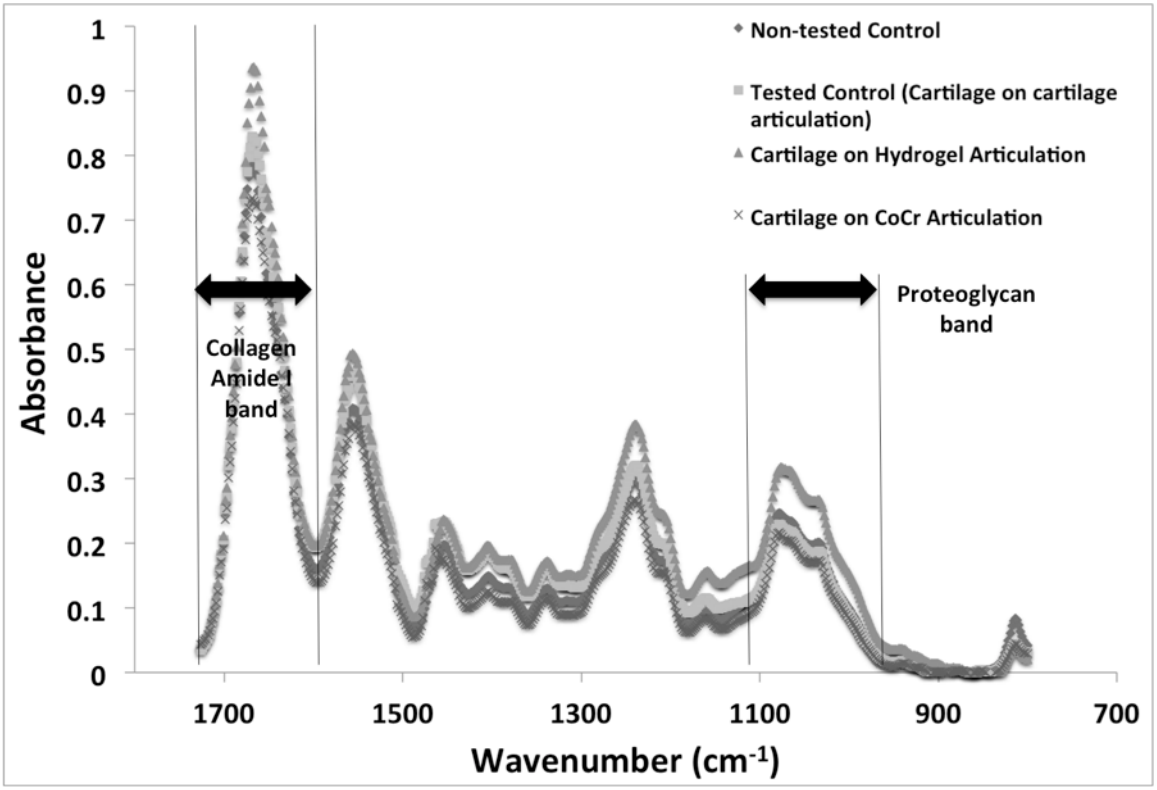

Figure 2-1) Representative spectra of articular cartilage pins from non-tested control, tested control (cartilage on cartilage articulation), cartilage on hydrogel articulation and cartilage on CoCr articulation groups. Spectral features used in this study to characterize cartilage properties are indicated.

The FTIR data from the non-tested control and 3 test groups (cartilage-on-cartilage as tested control, cartilage-on-CoCr and cartilage-on-hydrogel articulations) were not normally distributed (Shapiro-Wilk test). A non-parametric one-way analysis of variance (ANOVA) statistical test (Independent Samples Kruskal Wallis Test) with a post

hoc Dunn test was performed to compare the non-tested control and 3 test groups. Statistical significance was determined at the $p<0.05$ level.

Results

Cartilage Characterization based on Histological Evaluation

The effect of *in vitro* wear testing on the distribution of proteoglycans was visible in the histological sections of cartilage pins. Tested control specimens (cartilage on cartilage articulation) had an approximately 15 μm thick proteoglycan deficient layer close to the articulating surface (Figure 2a). Tested control specimens had the thinnest proteoglycan deficient layer close to the surface compared to cartilage pins that articulated against biphasic material, followed by cartilage pins that articulated against CoCr disks (Figure 2b-c). However, non-tested control specimens (Figure 2d) also had a thicker proteoglycan deficient layer compared to tested control specimens. Mechanical damage to the collagen ultrastructure due to wear, i.e. fissures and clefts, was not visible on the surfaces or in the deeper zones of cartilage pins.

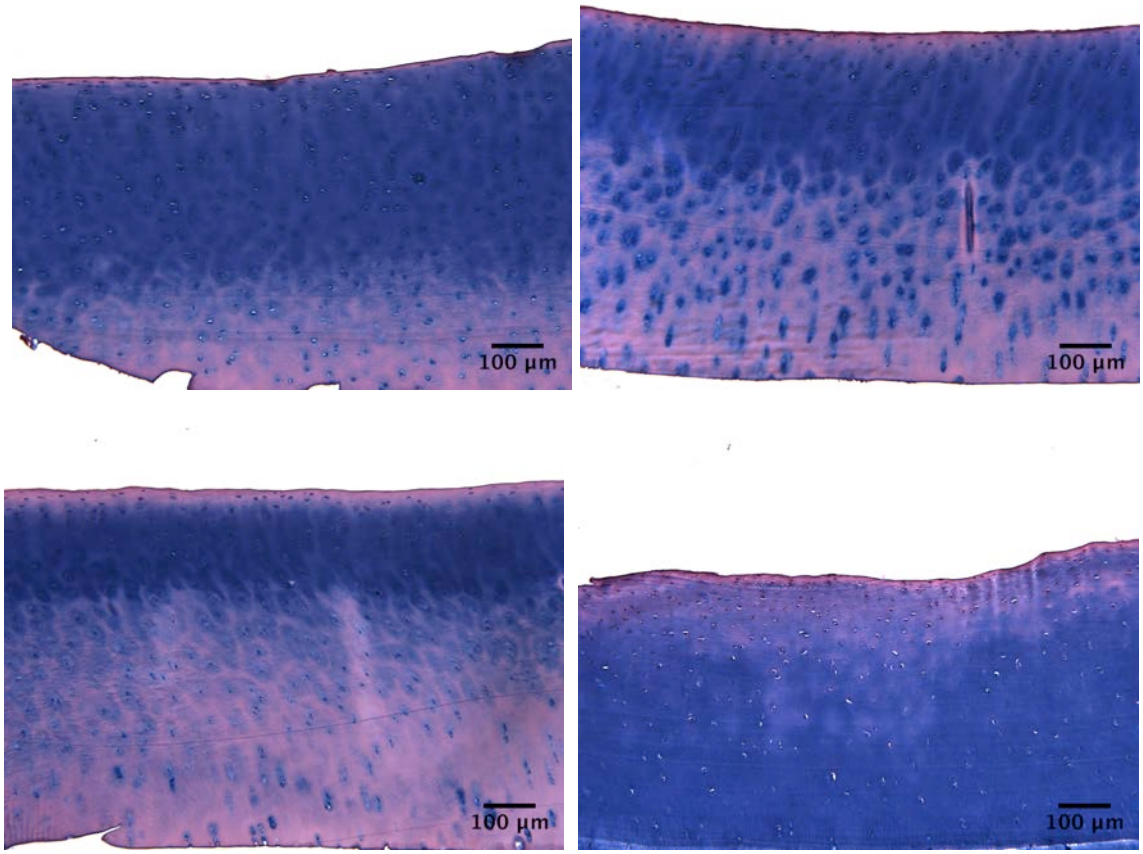

Figure 2-2) H&E and Alcian blue stained sections of a- Tested control specimen (cartilage on cartilage articulation), b- Cartilage on hydrogel articulation specimen, c- Cartilage on CoCr articulation specimen, d- Non-tested control specimen are shown.

Cartilage characterization by FTIR spectroscopy

Collagen Maturity

In vitro wear testing affected the collagen maturity of articular cartilage ($p<0.001$) as shown in figure 3. Cartilage pins that articulated against CoCr disks yielded lower collagen maturity compared to pins that articulated against biphasic material ($p=0.004$) or cartilage ($p=0.01$) and compared to non-tested controls ($p=0.01$). However, there was no significant difference in the collagen maturity of non-tested controls and cartilage pins that articulated against cartilage or biphasic materials.

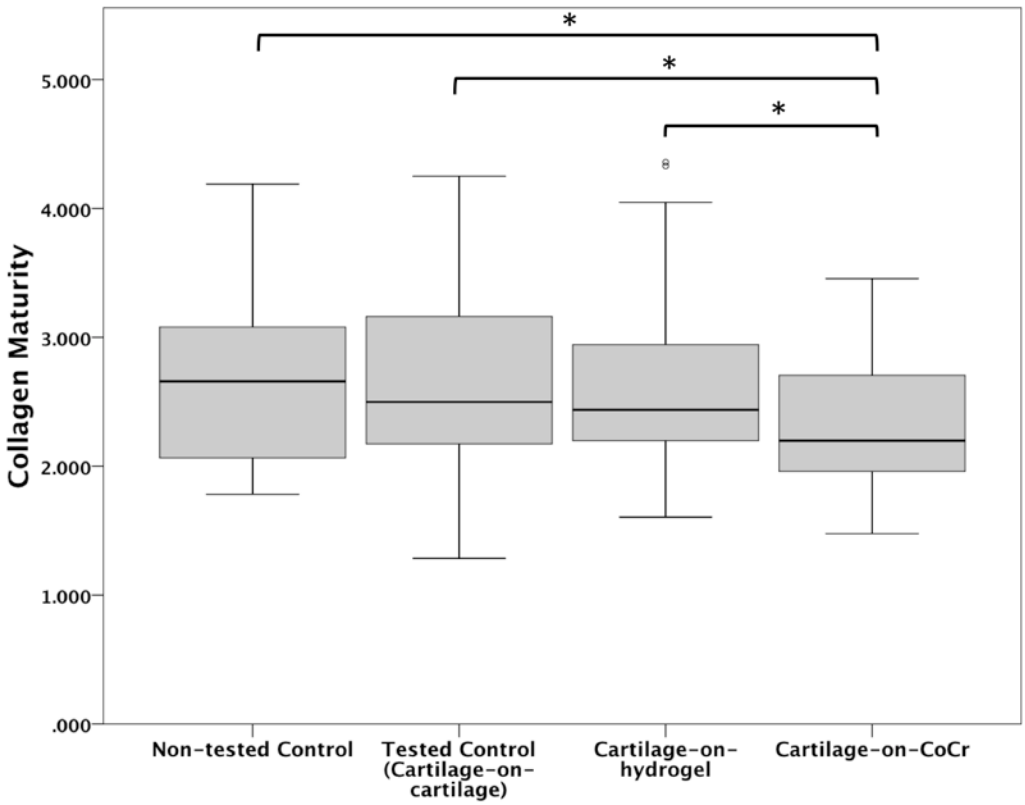

Figure 2-3) Box plots of collagen maturity (ratio of peak heights at 1660 and 1690 cm-1) for cartilage specimens from non-tested control, tested control (cartilage on cartilage articulation), cartilage on hydrogel articulation and cartilage on CoCr articulation groups. In figures 3 and 4, non-tested control group (n=2) was based on 58 scans. Tested control (cartilage on cartilage articulation) group (n=6) was based on 227 scans. Cartilage on hydrogel articulation group (n=3) was based on 79 scans. Cartilage on CoCr articulation group (n=3) was based on 81 scans.

Proteoglycan Content

In vitro wear testing affected the proteoglycan content of articular cartilage ($p<0.001$). Cartilage pins that articulated against cartilage had higher proteoglycan content than cartilage pins that articulated against CoCr disks ($p=0.008$). However, non-tested control specimens had lower proteoglycan content compared to cartilage pins that articulated against cartilage ($p=0.001$). The proteoglycan content of pins that articulated against biphasic material and CoCr disks were similar to non-tested control pins (Figure 4).

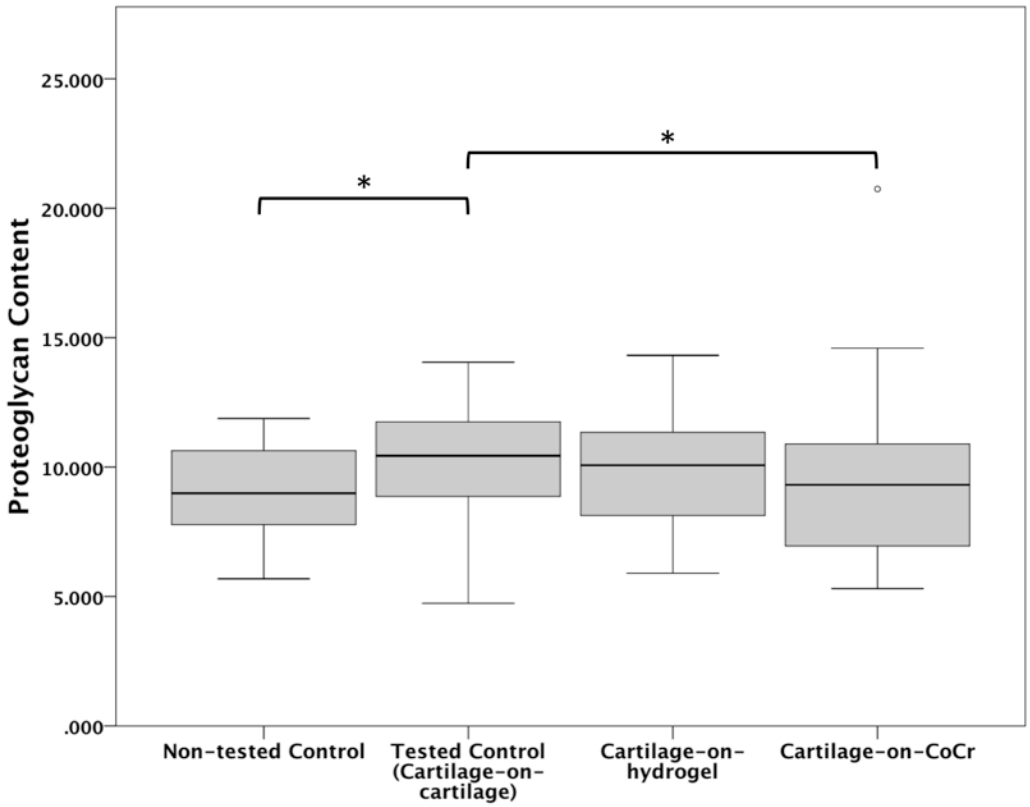

Figure 2-4) Box plots of proteoglycan content (ratio of proteoglycan and amide I peak areas) of cartilage specimens from non-tested control, tested control (cartilage on cartilage articulation), cartilage on hydrogel articulation and cartilage on CoCr articulation groups.

Discussion

Microscopically characterizing wear of articular cartilage is important for screening hemiarthroplasty materials [2, 8]. Monitoring the effect of wear on multiple parameters relevant to the ultrastructure of articular cartilage simultaneously will be useful in determining wear mechanisms. The objectives of this study were to characterize *in vitro* wear of articular cartilage using FTIR and histology, and to compare the effects of wear of cartilage against cartilage, and against CoCr and a hydrogel as hemiarthroplasty materials.

This study supported the hypothesis that the onset of articular cartilage wear involved a decrease in collagen maturity and loss of proteoglycans. The collagen maturity parameter was suggested to depend on collagen crosslinking because it was shown to decrease as collagen crosslinks were photolysed [15, 21]. However, it was recently reported in another study that the collagen maturity FTIR parameter was unchanged between control and lathyritic rat bones whereas high performance liquid chromatography detected the difference in the ratios of mature pyridinium crosslinks and immature dehydro-dihydrox-ylysinonorleucine crosslinks between the two groups of rats [21]. Farlay et al. concluded that the collagen maturity parameter reflected a modification to the secondary structure of collagen due to changes in packing of triple helices between new and old bone [21]. Our results showed that *in vitro* wear testing of articular cartilage could have affected the secondary structure of cartilage by disrupting the packing of triple helices. The combined effect of disrupting the secondary structure of collagen and compression due to creep under compressive loads could have caused unbound glycosaminoglycans to diffuse out of the matrix [24], hence the loss of proteoglycans in the tested cartilage pins. The non-tested control pins may have exhibited a larger PG deficient layer than tested specimens because compression and creep might have resulted in thinner zones within the cartilage transect. Although changes to the secondary structure of collagen could be detected by FTIR, *in vitro* wear testing did not result in visible damage to the collagen network that could be detected by histological evaluation with H&E stain, in this study. Disruptions to the proteoglycan distribution, on the other hand, could be detected by both FTIR analysis and histological evaluation.

This study supported our hypothesis that cartilage pins that articulated against a biphasic material would yield higher collagen maturity. However, there was no difference in proteoglycan content between cartilage pins that articulated against CoCr disks and pins that articulated against the biphasic material. The difference in both collagen maturity and proteoglycan content between tested controls and pins that articulated against CoCr disks were statistically significant whereas only the difference in collagen maturity was statistically significant between pins that articulated against biphasic material and those that articulated against CoCr disks. Cartilage articulation against cartilage, biphasic material and CoCr, in this study, might have represented three distinct stages of *in vitro* wear of articular cartilage. Thus, we postulated that *in vitro* wear testing of cartilage first disrupted the collagen maturity followed by proteoglycan loss from the matrix before surface fibrillation and clefts occurred.

Comparison with literature confirmed our findings that loss of proteoglycans due to wear precedes surface damage [25]. Furthermore, cartilage articulating against CoCr disks resulted in collagen degeneration and proteoglycan loss in rabbit [26] and canine models [25, 27] similar to our *in vitro* testing results. *In vitro* studies reported collagen [1, 9, 11] and proteoglycan loss [9, 11] due to wear. A major difference between *in vitro* studies in literature and this study was that we could detect changes in the molecular structure of matrix constituents using FTIR before gross damage that could be detected by histological evaluation occurred. Previous studies have focused on quantifying debris related to collagen content [9, 11] or on surface damage, such as fibrillation, using india ink [1] or by monitoring changes to surface morphology [2, 11]. For these methods to detect wear, it has to exceed a certain threshold to initiate material removal.

We acknowledge the limitations of our study: 1) non-tested controls were not loaded and 2) H&E stain used in this study cannot detect unraveling of collagen fibers. Non-tested controls were chosen not to be loaded in order to avoid losing proteoglycans due to mechanical loading [25]. Although unloaded thickness of non-tested controls might have differed from tested specimens and have affected the proteoglycan concentration, histological evaluation enabled comparisons between non-tested controls and tested specimens in terms of proteoglycan distribution. FTIR analyses based on collagen parameters, on the other hand, were not affected by compression of the cartilage pins. Finally, H&E stain was used to evaluate collagen structure [4, 13, 28] to allow for comparisons with the structure of healthy cartilage reported in literature.

In this study, we evaluated *in vitro* wear mechanisms of articular cartilage using Fourier transform infrared microspectroscopy. We concluded that at the onset of articular cartilage wear, both collagen maturity and proteoglycan content decreased before surface damage, such as clefts and fibrillations, occurred. Cartilage on cartilage and cartilage on biphasic material articulation yielded higher collagen maturity than cartilage on CoCr articulation. In terms of proteoglycan content however, only cartilage on cartilage was higher than cartilage on CoCr articulation. We suggest that FTIR-derived collagen and proteoglycan parameters could be used to quantitatively characterize *in vitro* wear of articular cartilage in screening hemiarthroplasy materials.

References

[1] McGann ME, Vahdati A, Wagner DR. Methods to assess in vitro wear of articular cartilage. Proceedings of the Institution of Mechanical Engineers, Part H: Journal of Engineering in Medicine. 2012;226:612-22.
[2] Northwood E, Fisher J, Kowalski R. Investigation of the friction and surface degradation of innovative chondroplasty materials against articular cartilage.

Proceedings of the Institution of Mechanical Engineers, Part H: Journal of Engineering in Medicine. 2007;221:263-79.
[3] Chan S, Neu C, Komvopoulos K, Reddi A, Di Cesare P. Friction and Wear of Hemiarthroplasty Biomaterials in Reciprocating Sliding Contact With Articular Cartilage. Journal of tribology. 2011;133.
[4] Patel A, Spector M. Tribological evaluation of oxidized zirconium using an articular cartilage counterface: a novel material for potential use in hemiarthroplasty. Biomaterials. 1997;18:441-7.
[5] Chang YS, Oka M, Gu HO, Kobayashi M, Toguchida J, Nakamura T, et al. Histologic comparison of tibial articular surfaces against rigid materials and artificial articular cartilage. Journal of biomedical materials research. 1997;37:51-9.
[6] Yasuda K, Ping Gong J, Katsuyama Y, Nakayama A, Tanabe Y, Kondo E, et al. Biomechanical properties of high-toughness double network hydrogels. Biomaterials. 2005;26:4468-75.
[7] Katta JK, Marcolongo M, Lowman A, Mansmann KA. Friction and wear behavior of poly (vinyl alcohol)/poly (vinyl pyrrolidone) hydrogels for articular cartilage replacement. Journal of Biomedical Materials Research Part A. 2007;83:471-9.
[8] Katta J, Jin Z, Ingham E, Fisher J. Biotribology of articular cartilage—A review of the recent advances. Medical engineering & physics. 2008;30:1349-63.
[9] Lipshitz H, Glimcher MJ. In vitro studies of the wear of articular cartilage II. Characteristics of the wear of articular cartilage when worn against stainless steel plates having characterized surfaces. Wear. 1979;52:297-339.
[10] Mow VC, Ateshian GA, Spilker RL. Biomechanics of diarthrodial joints: a review of twenty years of progress. Journal of biomechanical engineering. 1993;115:460.
[11] Verberne G, Merkher Y, Halperin G, Maroudas A, Etsion I. Techniques for assessment of wear between human cartilage surfaces. Wear. 2009;266:1216-23.
[12] Schwartz CJ, Bahadur S. Investigation of articular cartilage and counterface compliance in multi-directional sliding as in orthopedic implants. Wear. 2007;262:1315-20.
[13] Bi X, Yang X, Bostrom MPG, Camacho NP. Fourier transform infrared imaging spectroscopy investigations in the pathogenesis and repair of cartilage. Biochimica et Biophysica Acta (BBA)-Biomembranes. 2006;1758:934-41.
[14] David-Vaudey E, Burghardt A, Keshari K, Brouchet A, Ries M, Majumdar S. Fourier Transform Infrared Imaging of focal lesions in human osteoarthritic cartilage. Eur Cell Mater. 2005;10:51-60.
[15] Boskey A, Pleshko Camacho N. FT-IR imaging of native and tissue-engineered bone and cartilage. Biomaterials. 2007;28:2465-78.
[16] Potter K, Kidder LH, Levin IW, Lewis EN, Spencer RGS. Imaging of collagen and proteoglycan in cartilage sections using Fourier transform infrared spectral imaging. Arthritis & Rheumatism. 2001;44:846-55.
[17] Camacho NP, West P, Torzilli PA, Mendelsohn R. FTIR microscopic imaging of collagen and proteoglycan in bovine cartilage. Biopolymers. 2000;62:1-8.
[18] West P, Bostrom M, Torzilli P, Camacho N. Fourier transform infrared spectral analysis of degenerative cartilage: an infrared fiber optic probe and imaging study. Applied spectroscopy. 2004;58:376-81.

[19] Graindorge SL, Stachowiak GW. Changes occurring in the surface morphology of articular cartilage during wear. Wear. 2000;241:143-50.
[20] Forster H, Fisher J. The influence of loading time and lubricant on the friction of articular cartilage. Proceedings of the Institution of Mechanical Engineers, Part H: Journal of Engineering in Medicine. 1996;210:109-19.
[21] Farlay D, Duclos M-E, Gineyts E, Bertholon C, Viguet-Carrin S, Nallala J, et al. The Ratio 1660/1690 cm− 1 Measured by Infrared Microspectroscopy Is Not Specific of Enzymatic Collagen Cross-Links in Bone Tissue. PLoS ONE. 2011;6.
[22] West PA, Torzilli P, Chen C, Lin P, Camacho NP. Fourier transform infrared imaging spectroscopy analysis of collagenase-induced cartilage degradation. Journal of biomedical optics. 2005;10:014015--6.
[23] Baykal D, Irrechukwu O, Lin PC, Fritton K, Spencer RG, Pleshko N. Nondestructive assessment of engineered cartilage constructs using near-infrared spectroscopy. Applied spectroscopy. 2010;64:1160-6.
[24] Thibault M, Robin Poole A, Buschmann MD. Cyclic compression of cartilage/bone explants in vitro leads to physical weakening, mechanical breakdown of collagen and release of matrix fragments. Journal of orthopaedic research. 2006;20:1265-73.
[25] Cruess RL, Kwok DC, Duc PN, Lecavalier M, Dang G. The response of articular cartilage to weight-bearing against metal. The Journal of Bone and Joint Surgery. 1984:592-7.
[26] Jung M, Wieloch P, Lorenz H, Gotterbarm T, Veyel K, Daniels M, et al. Comparison of cobalt chromium, ceramic and pyrocarbon hemiprostheses in a rabbit model: Ceramic leads to more cartilage damage than cobalt chromium. Journal of Biomedical Materials Research Part B: Applied Biomaterials. 2008;85:427-34.
[27] Laberge M, Dennis Bobyn J, Drouin G, Rivard CH. Evaluation of metallic personalized hemiarthroplasty: a canine patellofemoral model. Journal of biomedical materials research. 1992;26:239-54.
[28] Kyomoto M, Moro T, Saiga K-i, Miyaji F, Kawaguchi H, Takatori Y, et al. Lubricity and stability of poly (2-methacryloyloxyethyl phosphorylcholine) polymer layer on Co–Cr–Mo surface for hemi-arthroplasty to prevent degeneration of articular cartilage. Biomaterials. 2010;31:658-68.

3. Tribological Evaluation of Hydrogel Articulations for Joint Arthroplasty Applications

Abstract

Characterizing the wear behavior of hydrogel articulations is problematic and a standardized method has not yet been developed. The aims of this study were to evaluate the wear resistance of hydrogel-on-hydrogel articulations and to assess the suitability of a submerged measurement technique as a practical and non-destructive method in quantifying their wear rates. Five hydrogel bearings were tested for 5 million cycles using a pin-on-disk tester. As the test progressed, the coefficient of friction increased (Spearman's rho = 0.76; $p < 0.001$) while the surfaces of the pins were burnished (Spearman's rho = -0.31; $p < 0.001$) and those of the disks got rougher (Spearman's rho = 0.19; $p < 0.01$). Environmental scanning electron microscopy analysis showed no evidence of gross wear and revealed similar surface morphology between contacting and non-contacting regions of specimens. These results support the finding of low wear, which were -1.4 ± 8.3 mm^3 / MC and 6.6 ± 35.3 mm^3 / MC based on submerged and wet weights respectively. Pins displayed higher wear than disks based on submerged weights. This was anticipated since surfaces of pins were constantly under load and cross-shear while only a portion of the disk in contact with the pin was loaded at a given time. Wet weights, on the other hand, indicated higher wear for disks than pins. In addition, submerged weights yielded a lower standard error of the mean in wear rates than wet weights, 3.7 and 14.6 mm^3 / MC respectively. These results indicated that submerged weights were more suitable than wet weights in quantifying wear of hydrogels in spite of unwanted effects of swelling.

Introduction

Hydrogels are complex hydrophilic polymer networks that are swollen with water [1-3], which have been researched to replace damaged articular cartilage [1, 4-8]. The motivation is twofold; first, due to their biphasic nature, hydrogels may maintain natural joint lubrication [7, 9]. Second, their structure can be tailored so that their mechanical properties mimic those of articular cartilage and reduce contact stresses [7, 10]. Various studies have assessed tribological properties of hydrogels since Bray and Merrill first proposed hydrogels as artificial cartilage materials [4]. Although earlier studies focused primarily on the coefficient of friction associated with hydrogel articulations, the current consensus is that the ability to maintain a low coefficient of friction alone does not imply adequate wear resistance [2, 7, 8]. Nevertheless, quantifying the wear rate of swellable materials is problematic [2, 8, 11, 12] and no established, standardized methods for characterizing the wear behavior of hydrogel articulations have yet been developed [8].

Gravimetric measurement, which is widely used to quantify polymer wear loss, has been utilized in some studies to characterize the wear properties of swellable materials based on wet weights [6, 12]. Suciu et al. monitored the progression of wear of PVA hydrogels for up to 0.1 million cycles and reported fluctuating wear factors [12]. Since wet weighing does not allow differentiation between the mass change caused by fluid movement as opposed to worn mass, it is not accurate when testing swellable materials [12, 13]. Bavaresco et al. utilized a static sample to compensate for effects of fluid absorption when testing pHEMA hydrogels but reported only a final wear rate which does not make it possible to observe whether the calculated wear rate was influenced by the effects of swelling [6]. While implementing a soak control could

compensate for changes in equilibrium water content, possible increase in swelling capacity due to degradation and mechanical breakdown of crosslinks would prevent precise wear rate calculations [14-16]. Katta et al. desiccated PVA/PVP hydrogels for 25 days following pin-on-disk testing and compared the dry weight before and after the wear test to calculate wear [7]. Although measurements based on dehydrated hydrogels should be impervious to changes in swelling and should successfully detect low magnitudes of wear, this method is destructive and not practical. Fully dehydrated hydrogels cannot revert to their initial volume, geometry and stiffness upon rehydration [17]. In addition, dehydrating hydrogels for weighing is not practical since desiccation may take up to a month without elevated temperatures [7] and drying in an oven, in an attempt to expedite this process, induces crosslinking [18]. Since complete dehydration of hydrogels results in irreversible changes, employing dry weights before testing and at intervals during the test to characterize wear properties is not possible without altering the material. The capability to examine evolution of hydrogel wear, however, is valuable since the duration of wear testing should be kept long enough to ensure that wear rate is stable and the wear generated is linear.

Weighing in fluid, which have been used to calculate volume of trabecular bone [19, 20] and density of porous ceramics [21], has the potential to overcome the complications inherent in wear measurement of swellable materials. The objectives of this study were to characterize hydrogel-on-hydrogel articulation and to assess the suitability of submerged measurement technique as a practical and non-destructive method in quantifying wear rates of hydrogels. Our hypotheses are: (1) Changes in

magnitude of swelling will not affect the submerged weights; and (2) Submerged weights will be more precise than wet weights in characterizing volumetric wear of hydrogels.

Methods

Materials Preparation

A proprietary hydrogel (CyborGel, Formae Inc, Paoli, PA) was used in this study. Sheet and rod shaped hydrogel (Fig. 1) was used to produce disks in validating the submerged measurement technique. The material was also available in pin cap (n=7) and disk (n=7) forms for the wear test. Hemispherical hydrogel pin caps were 0.6 inches in diameter and had slightly convex articulating surfaces. Stainless steel backing pins with the same surface profiles were manufactured to mount the pins on the pin-on-disk tester. Hydrogel disks were ~1.6 inches in diameter and housed hoops within them around their perimeter. These hoops had three protrusions that extended out to fix the hydrogel disks onto backing disks, which made mounting on the pin-on-disk tester possible.

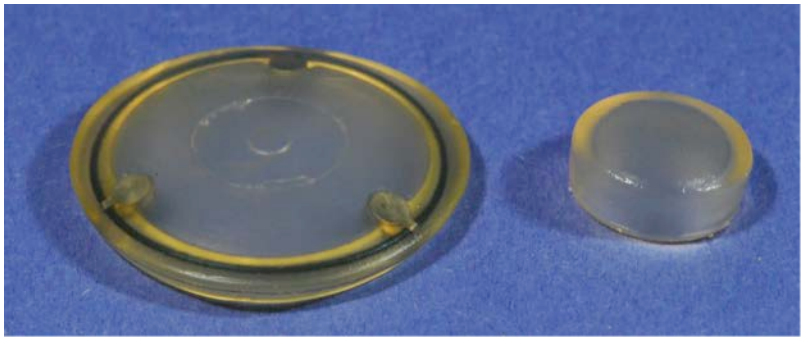

Figure 3-1) Pin cap and disk shaped hydrogel used in wear testing

Rationale for Submerged Measurements

Submerged measurements were conducted under a controlled temperature in distilled water, Phosphate buffered saline and bovine serum (HyClone, Logan, UT) at 20.8 ± 0.1^0C on an Archimedes' basket setup (YDK01 Density kit, Sartorius Inc., Germany)

using a 0.01 mg precision balance as shown in figure 2a. The advantage of this setup is that the buoyancy force exerted by the fluid, which submerges the hydrogel, counteracts the weight of fluid contained within the hydrogel. When the hydrogel is soaked with the same fluid that fills the cup, these forces negate each other, and forces applying to the specimen based on Archimedes' Principle are reduced to those shown in equation 1, equation 2 and figure 2b. Δ represents the submerged weight and $V_{hydrogelnetwork}$ represents the volume of the polymer, excluding the fluid within the hydrogel. $\rho_{hydrogelnetwork}$ is the density of hydrogel whereas ρ_{fluid} is the density of the submerging fluid. This equation shows that submerged mass of a sample is proportional only to the polymer volume, independent of fluid fraction, as long as it is measured in the same fluid at the same temperature. Our assumption was that densities of fluid molecules remain constant whether the molecules are free or entrapped within the hydrogel. This equation also shows that the submerged mass is not affected by the amount of fluid uptake or exudation since fluid is neutrally buoyant in this setup. This is our motivation for using submerged mass in quantifying wear rates of swellable materials.

$$\Delta = F_{weight} - F_{buoyancy} = V_{hydrogelnetwork} \times \rho_{hydrogelnetwork} - V_{hydrogelnetwork} \times \rho_{fluid} \quad (1)$$

$$\Delta = V_{hydrogelnetwork} \times \underbrace{(\rho_{hydrogelnetwork} - \rho_{fluid})}_{\text{constant}} \quad (2)$$

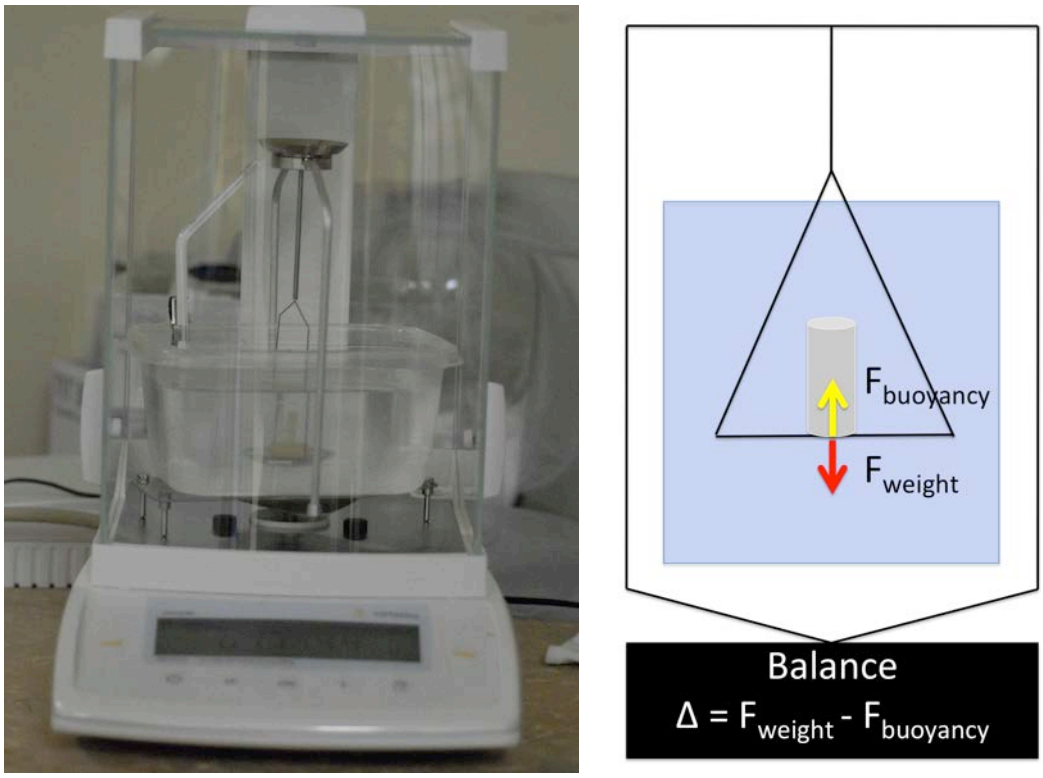

Figure 3-2) a- Archimedes' basket was placed on precision balance for submerged measurements. b- Forces acting on a sample during submerged measurement are shown.

Validation of Submerged Measurement Technique

Sensitivity Test

The relationship between submerged and dry weights of hydrogel discs was analyzed to assess the threshold of detectable change in submerged weights. Cylinders were stamped from sheets using a 3 mm diameter biopsy punch. They were then sliced at various thicknesses using a microtome on a cryostage (BFS-30MP, Physitemp Inc., NJ) to create discs (n=25) of varying volume. Following three submerged measurements in distilled water, each disc was dried in an oven at 95^0C overnight and weighed in air three times. A linear regression model based on dry weights, which represent the amount of polymer, predicted submerged weights to evaluate the standard error in estimated submerged measurements as the limit of sensitivity.

The density of the hydrogel network was calculated in order to normalize the standard error in submerged weight to error in hydrogel volume. Larger samples were chosen for this calculation to decrease the effects of measurement noise. A razor blade was used to create samples that were in the range of 50-130 mm^3 (n=3). Following three submerged measurements at 20.8 ± 0.1^0C, samples were oven dried and weighed three times in air. Density was calculated using Archimedes' principle.

Soaking Test

The relationship between submerged weights and wet weights after stabilizing in various fluids was also evaluated in order to further validate submerged weight as a parameter for polymer quantification. A razor blade was used to create nine disc samples. Discs were stabilized in distilled water (n=3), PBS (n=3) and bovine serum (n=3). Bovine serum used in this study was Hyclone Wear Testing fluid (HyClone, Logan, UT) with a protein concentration of 20 g/L. Along with submerged measurements in their respective fluids at 20.8 ± 0.1^0C, samples were blotted dry and their wet weights were recorded three times. These measurements were repeated every 48 hours until the weights stabilized. Data reported in this paper belongs to day 13 when weights were stable. For each of the three fluids used, a regression model was built based on wet weights and submerged weights as dependent and independent variables respectively.

Pin-on-Disk Testing

Hydrogel-on-hydrogel articulation was characterized using an OrthoPOD Pin-on-Disk machine (AMTI, Watertown, MA) for 5 million cycles in accordance with ASTM F732 [22]. Five hydrogel bearings (Fig. 1) were evaluated. A static load of 100 N, which corresponded to an average contact stress of 2.3 ± 0.39 MPa as determined using pressure

film, was applied with a lift off at the end of each cycle. The lubricant used in the wear test was Hyclone Wear Testing fluid (HyClone, Logan, UT) with a protein concentration of 20 g/L. The lubricant was maintained at 37 ± 0.1^0C during the test. An elliptical wear pattern (59 mm) was employed to induce multidirectional wear at a velocity of 59 mm/s. The samples were presoaked in bovine serum for 48 hours prior to testing.

Each 0.25 million cycles, the specimens were stabilized for 2 hours in distilled water and then submerged measurements were recorded three times. Following the submerged measurements, the specimens were blotted dry and their wet weights were recorded. At the end of 5 million cycles, the wear rate was calculated as the slope of best-fit line for each specimen. ANOVA analysis of the regression line was utilized to test for statistical significance. Two surface roughness measurements of the articulating surfaces were recorded using a white-light profilometer (Zygo, Middlefield, CT, USA) with a depth resolution of 300 microns on an area of 719 x 539 microns. Surfaces of samples were visually observed and photo documented. Coefficient of friction for each station was also measured before dismounting the specimens for gravimetric measurements. During coefficient of friction measurements, samples were reciprocated in a linear track at a velocity of 20 mm/s under 100 N of static load. In one cycle, 200 coefficient of friction measurements were obtained for each station.

In an attempt to compensate for fluid uptake during the wear test, static and dynamic soak control stations were employed. In the static soak control station, a pin and disk couple soaked in bovine serum for the duration of the test whereas in the dynamic soak control station, another pin and disk couple underwent the same motion as the test

samples without contact while soaking in bovine serum. Either of soak control stations was used exclusively in quantifying wear.

Paired samples t-test was utilized to compare the wear rates based on wet weights with wear rates based on submerged weights of each specimen and also each station. The wear rates of pins, disks and stations were also compared to 0 mm^3 / million cycles, indicative of undetectable wear, using t-test.

Environmental Scanning Electron Microscopy

The surfaces of hydrogel were examined by environmental scanning electron microscopy (XL-30, FEI, USA) after the wear test. Two sets of tested pins and disks along with two sets of soak control pins and disks were air dried for 72 hours prior to examination.

Energy-dispersive X-ray Spectroscopy (EDS) was also utilized to determine whether the elemental content of hydrogels was changed during the wear test in bovine serum. Small sections were obtained from tested and non-tested disks, which were being kept in distilled water. The sections were air dried for 72 hours. The data was analyzed using the EDAX Genesis software.

Results

The correlation between submerged weights and dry weights in the sensitivity test as shown in figure 3 (R^2=0.9) demonstrated that submerged weights were reliable in quantifying amount of hydrogel. The standard error in submerged measurements was 0.05 mg as estimated by the linear regression model (Fig. 3). Based on hydrogel density of 1.26 mg/mm^3 and water content of 39%, this standard error corresponded to 0.3 mm^3 when normalized to volume. Submerged measurement was also validated by the soaking test; submerged mass was capable of quantifying amount of hydrogel in distilled water,

PBS and bovine serum on day 13, after stabilizing in different fluids, as evidenced by the correlation with wet weight (Table 1). All three of the regression models, which had submerged weight as the predictor and wet weight as the estimate, yielded statistically significant correlations and low standard errors of the estimate. The standard errors in wet weights as predicted by submerged weights, along with R^2 and p values, are provided in table 1.

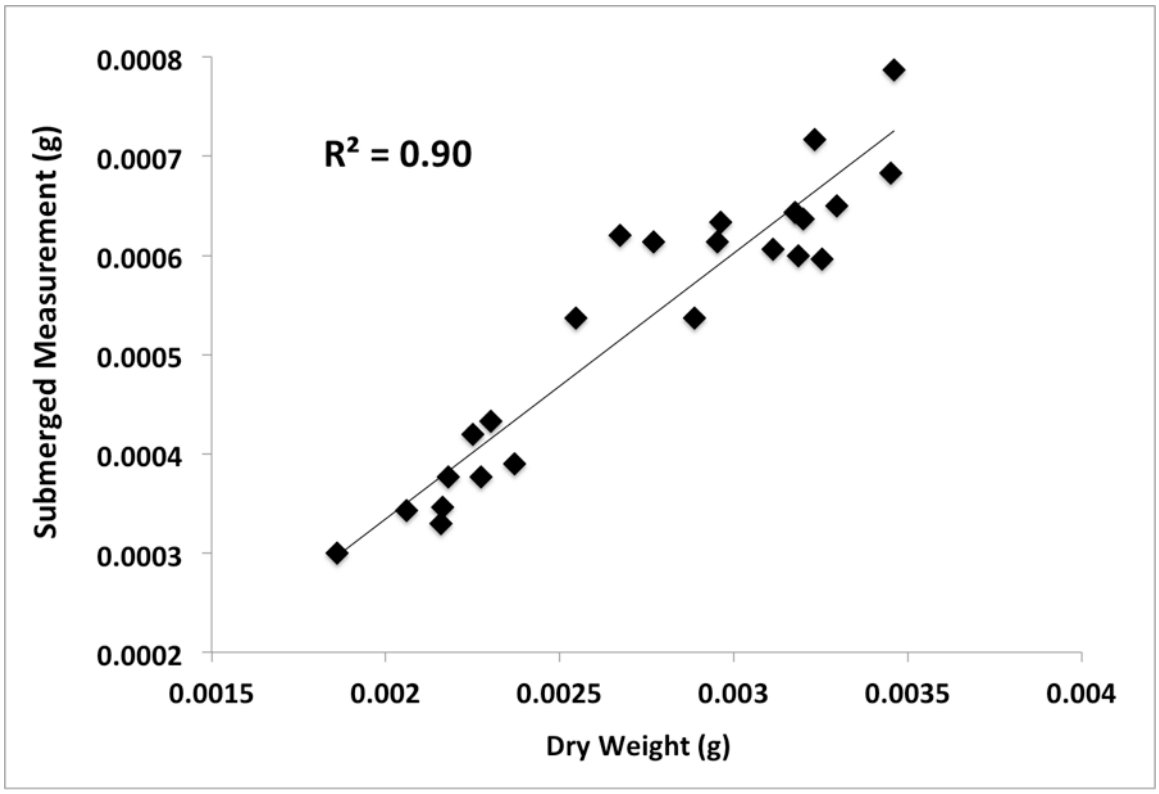

Figure 3-3) Linear regression model, which predicted the submerged measurements from dry weights was based on 24 samples.

Table 3-1) Standard error in predicted wet weights is shown. Submerged and wet weights on day 13 were used. The standard error was normalized using the average of wet weights of three samples in each group to obtain percentage standard error.

Fluid	R^2	Significance	Standard Error (mg)	Standard Error (%)
Distilled Water	1	0.04	9	0.8%
PBS	1	0.001	1	0.1%
Bovine Serum	1	0.006	5	0.3%

At the end of the wear test, submerged weights of tested specimens and soak control specimens, which were monitored for the duration of 5 million cycles of wear testing, increased as shown in figures 4 and 5. Increases in submerged weight indicate increased magnitudes of swelling. Regression lines yielded positive slopes for submerged weights of tested specimens as well as soak control specimens ($p < 0.001$). Comparison of submerged weights and wet weights of soak control pins and disks showed that wet weights of soak control samples (n=4) increased 1.2% ± 1.9% per million cycles (Mean ± SD) whereas submerged weights of the same soak control samples increased 0.5% ± 0.4% per million cycles. Although there was no difference in the average gain of soak control specimens based on wet weights and submerged weights ($p=0.47$), submerged weights displayed a more uniform gain across soak control specimens than wet weights as evidenced by a smaller variation. The standard error of the mean for wet weights and submerged weights were 1% and 0.2% respectively.

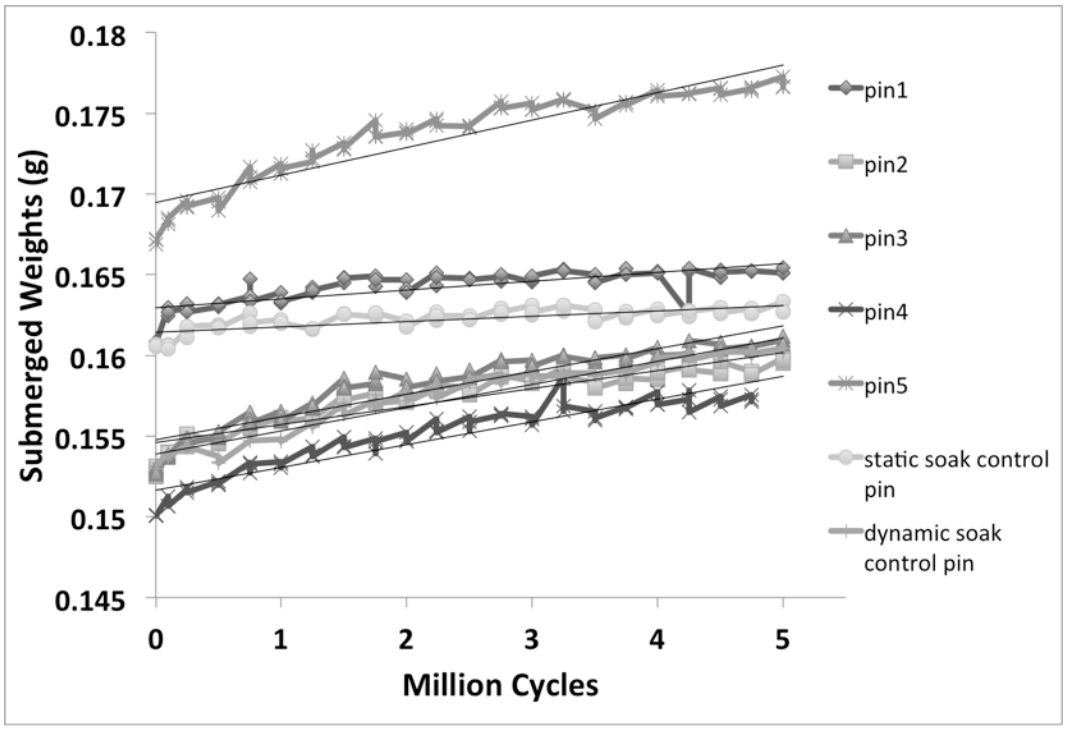

Figure 3-4) Submerged weights of pins

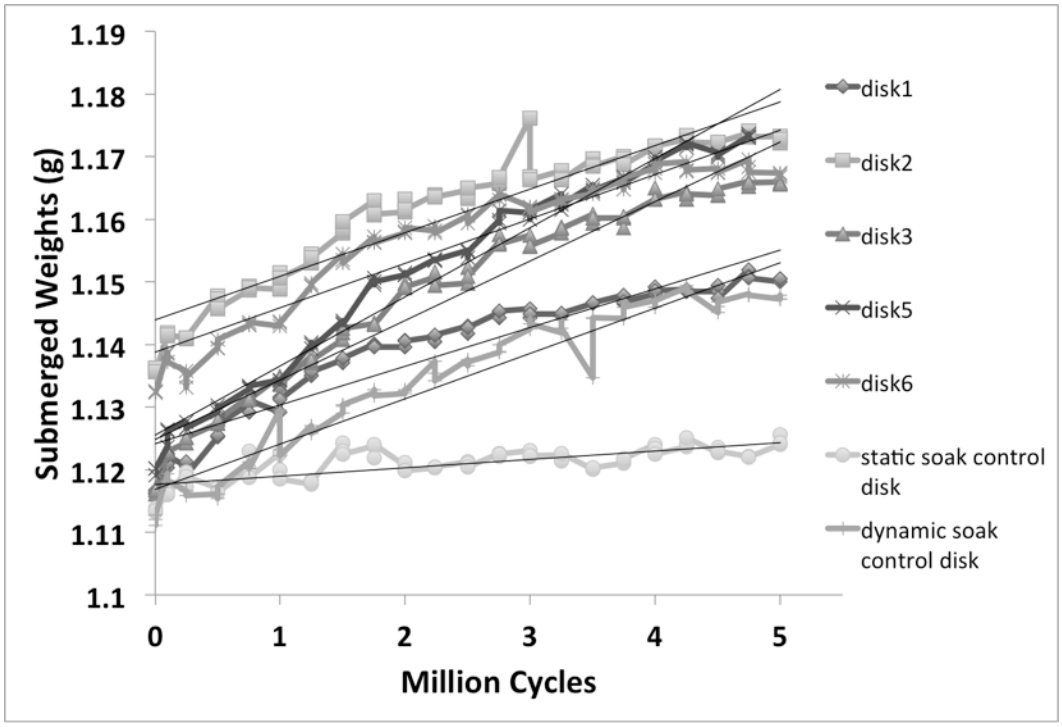

Figure 3-5) Submerged weights of disks

Wet weights of specimens also increased with respect to test duration as shown in figures 6 and 7. The increase in wet weights of tested pins and disks were evident in the positive slopes of best-fit lines ($p < 0.001$). Although the wet weight of static control disk increased similarly ($p < 0.001$), the static control pin slightly lost weight without displaying a linear trend ($p = 0.3$). The combined wear rate of the pin and the corresponding disk in each station, which is representative of total joint wear rate, indicated undetectable wear with static soak compensation (-146.3 ± 35.3 mm^3 / million cycles). While the wet weight of dynamic soak control disk increased ($p < 0.001$), the dynamic soak control pin slightly increased in wet weight but did not display a linear trend ($p = 0.2$). When wet weights of tested samples were compensated by dynamic soak specimens, detectable wear was calculated. The combined wear rate of pin and disk of each bearing was 6.6 ± 35.3 mm^3 / million cycles with dynamic soak compensation as measured by wet weights. Similarly to wet weights, the increase in submerged weights of both static soak control specimens ($p < 0.001$) was not as great as the increase for tested samples ($p < 0.001$). Submerged weights of dynamic control specimens, on the other hand, displayed similar trends ($p < 0.001$) to those of tested samples. As with wet weights, no wear could be detected for hydrogel-on-hydrogel articulations with static soak compensation based on submerged weights (-27.1 ± 8.3 mm^3 / million cycles). Submerged weights compensated with dynamic soak controls, on the other hand, yielded detectable wear for pin and disk couples, -1.4 ± 8.3 mm^3 / million cycles. In order to examine the contribution of pins and disks to the combined wear, their wear rates based on both wet weights and submerged weights are shown in table 2. The wear rates of pins based on wet weights suggested that they significantly gained in weight ($p < 0.05$)

whereas submerged weights of the same pins displayed changes that were not different from undetectable wear ($p>0.05$). The wear rates of individual disks and combined stations, which include the disk and the pin of each bearing, were not different than undetectable wear ($p>0.05$) based on either submerged or wet weights. Although there was no difference in average wear rate of hydrogel-on-hydrogel articulation calculated by wet and submerged weights ($p>0.05$), the standard deviation in wear rates of the same specimens was four times smaller based on submerged weights than wet weights

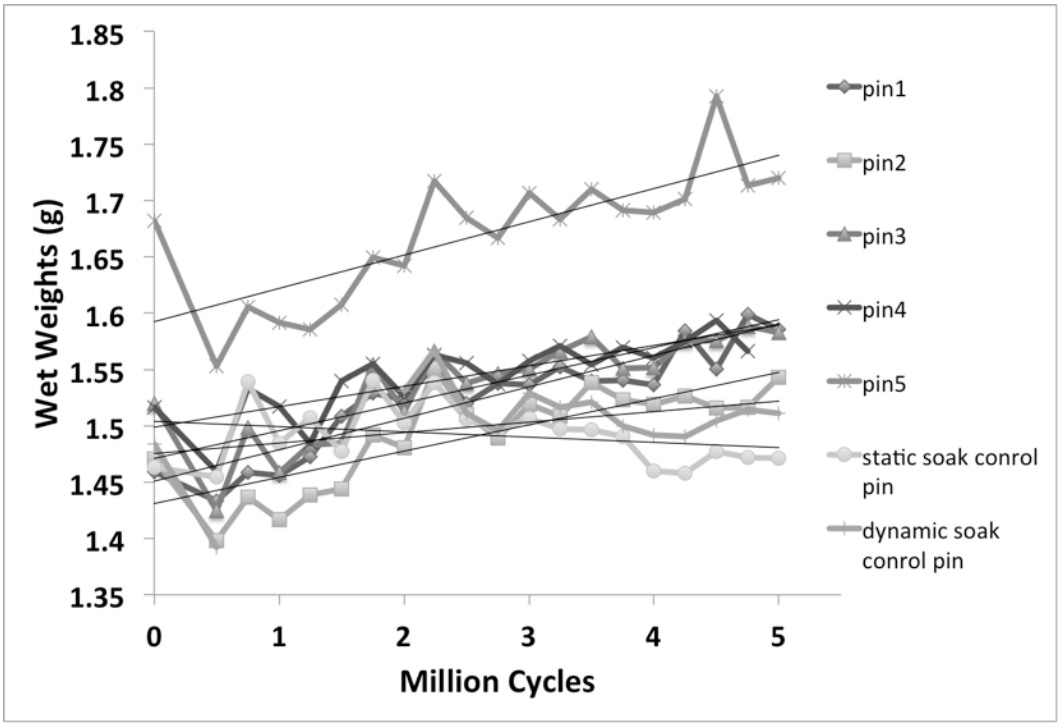

Figure 3-6) Wet weights of pins

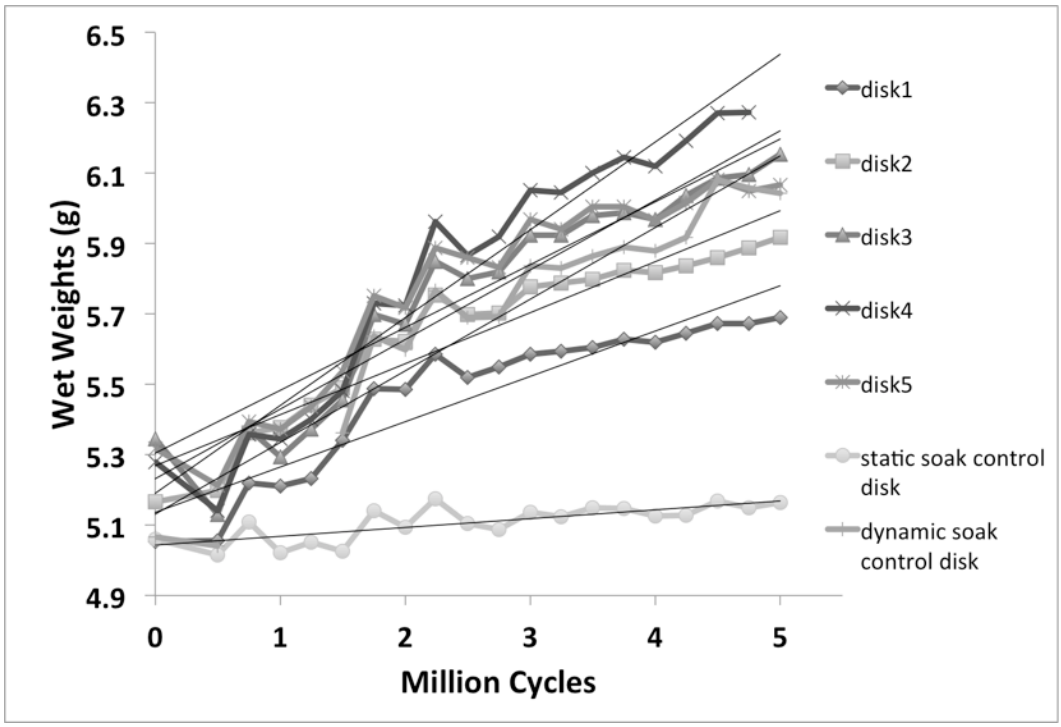

Figure 3-7) Wet weights of disks

Table 3-2) Wear rate of pins and disks (Average ±SD) are shown. * $p < 0.05$ based on paired samples t test shows difference between measurement methods; + $p < 0.05$ based on one sample t test checks if wear rate is different than undetectable wear.

Wear Rate (mm^3 / million cycles)	Disks	Pins	Combined
Wet Weights	18.8 ± 37.7	-12.2 ± 3.5*+	6.6 ± 35.3
Submerged Weights	-2.8 ± 6.4	1.3 ± 2.8	-1.4 ± 8.3

Although no changes on articulating surfaces of pins and disks were visible at the end of the test, both white light interferometry and coefficient of friction measurements indicated minor changes on articulating surfaces. White light interferometry showed that the surfaces of pins were smoother and burnished while the surfaces of disks got rougher (Fig. 8). These trends were statistically significant for both pins (Spearman's rho = -0.31;

$p < 0.001$) and disks (Spearman's rho = 0.19; $p < 0.01$). The average coefficient of friction data of wear test stations decreased for the first half million cycles and then increased and stabilized around 0.06 after 3 million cycles (Fig. 9). The coefficient of friction had a positive correlation with time (Spearman's rho = 0.76; $p < 0.001$). ESEM examination of hydrogels revealed variations in surface morphology from specimen to specimen. Comparisons of articulating and non-articulating surfaces of individual specimens, however, revealed that grainy surfaces present in non-articulating regions were also present in articulating regions after 5 million cycles of testing (Figure 10). Surface damage such as scratches, burnished regions, or pitting was not observed and thus provided no visual evidence of gross wear. EDS revealed sodium on the surfaces of the tested hydrogel specimens (Fig. 11a), however, it could not be detected on non-tested samples (Fig.11b). NaCl is an abundant molecule in the bovine serum, which the tested samples were exposed to during wear testing.

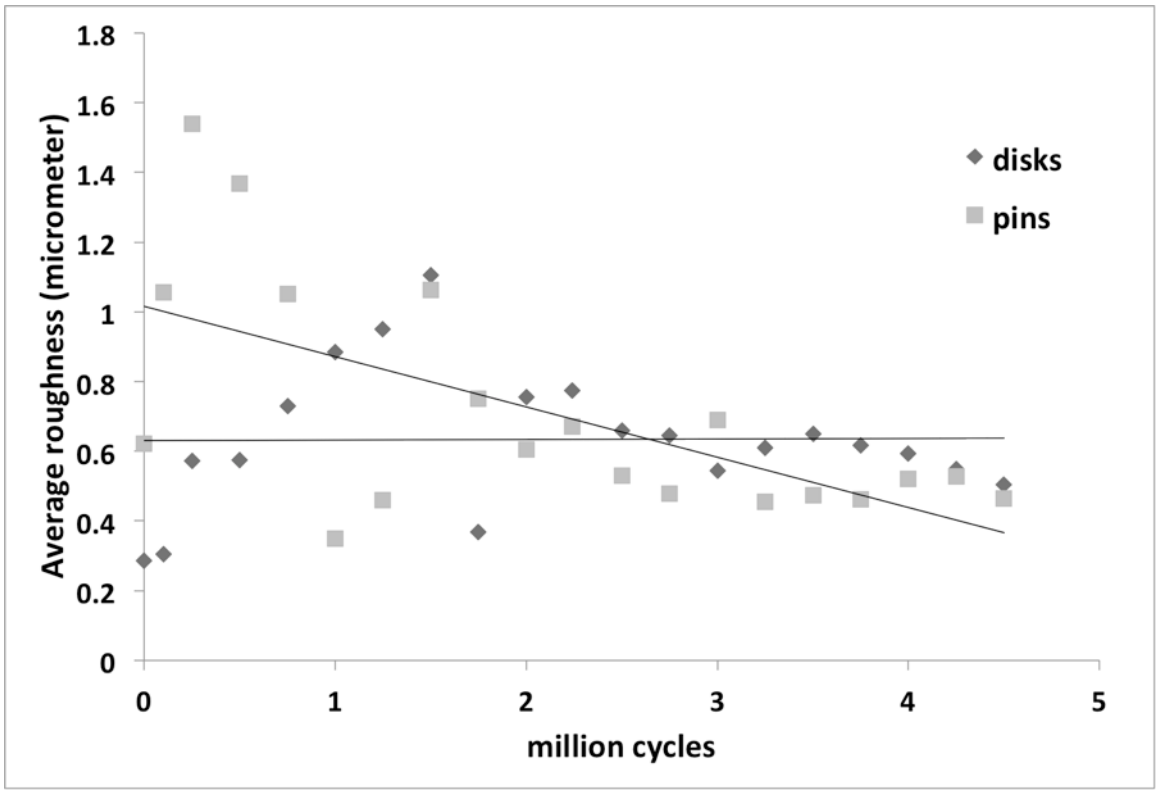

Figure 3-8) Changes in surface roughness of pins and disks are shown.

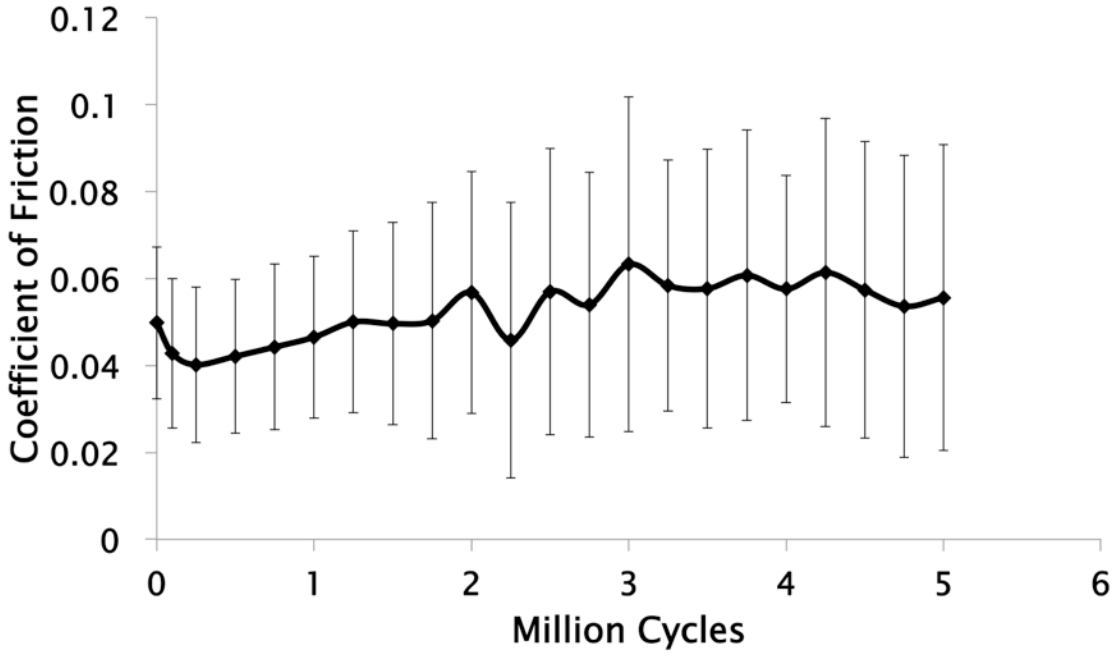

Figure 3-9) Average coefficient of friction of hydrogel articulation (n=5) is shown.

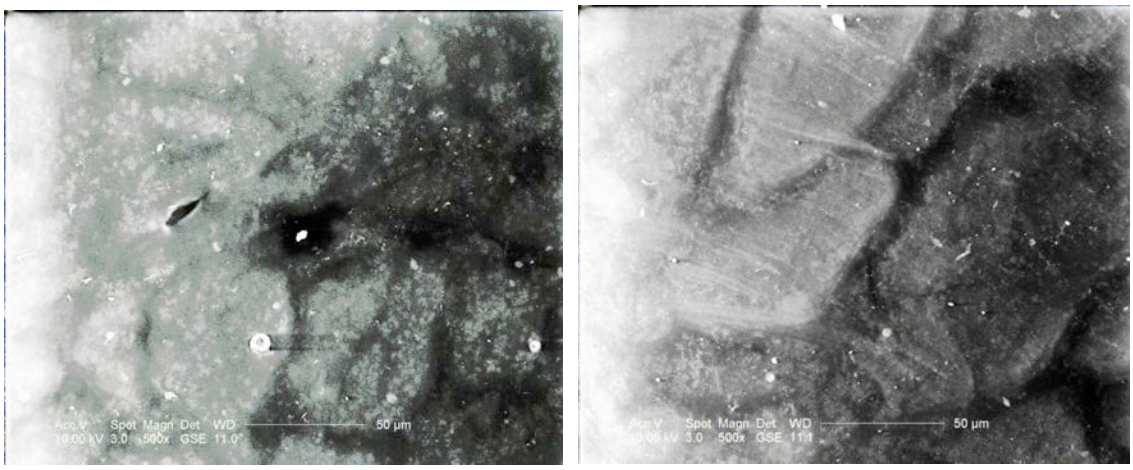

Figure 3-10) ESEM images of a- Non-articulating surface of disk b- Articulating surface of disk are shown. Images were taken at 500x magnification.

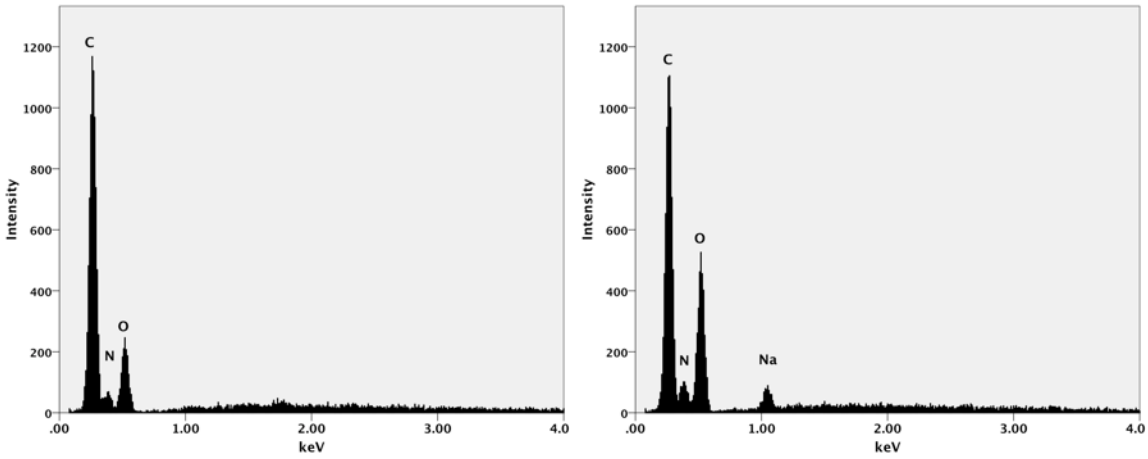

Figure 3-11) a- EDXA analysis of non-tested hydrogel is shown. b- EDXA analysis of tested hydrogel is shown

Discussion

As hydrogels are attractive materials for replacing damaged articular cartilage, accurate quantification of their tribological properties is crucial. However, quantifying wear of hydrogels is problematic [2, 8, 11, 12]. The objective of this study was to quantify the wear characteristics of hydrogel-on-hydrogel articulation and to assess the performance of submerged measurements in quantifying hydrogel wear. Our hypotheses

were: (1) Changes in magnitude of swelling would not affect the submerged weights; and (2) Submerged weights would be more precise than wet weights in characterizing volumetric wear of hydrogels.

Submerged measurements have been speculated to yield, on average, 10 times the maximum error gravimetric measurements tend to yield and as specimens get smaller, the precision of the balance becomes the limiting factor [23]. Another limitation, which pertains especially to hydrogels, is that as the density of the material becomes closer to that of water, the submerged mass per volume of material approaches zero. The motivation of this study was not to necessarily devise a method that would be more precise than gravimetric measurements, instead a method that would not be affected by swelling. Submerged weight was shown to be sufficiently reliable in quantifying mass of hydrogel as evidenced by the high correlation between submerged mass and dry weight, which is a highly reliable parameter devoid of effects of swelling. Submerged measurements were sensitive enough to differentiate between hydrogels of closely varying dry weights ranging from 2 and 3.5 mg. The regression model yielded a standard error of 0.05 mg when using dry weights to estimate the submerged mass (Figure 3). This precision is close to 0.01 mg, which is the precision of the balance used in this study. The linear relationship between submerged mass and wet weight in the soaking study yielded low standard errors ranging from 1 to 9 mg, which validated further that submerged weight was a reliable parameter for hydrogel quantification in distilled water, PBS and bovine serum. These standard errors corresponded to 0.1% – 0.8% of the average wet weight of specimens, which, in magnitude, matched the changes in wet weights of

specimens that were between 0.5% and 1% of initial wet weight. This error was attributed to changes in equilibrium swelling of hydrogel when soaked in different fluids.

This study did not support our hypothesis that changes in swelling would not affect the submerged weights since submerged weights of the tested and soak control specimens increased (Figures 4 and 5). The observation that submerged weights of soak compensation specimens had positively sloped best-fit lines (Figures 4 and 5), in the absence of mechanical damage or wear, showed that the increase in submerged weights of tested samples was not necessarily due to wear or mechanical damage. Submerged weights of soak control specimens yielded a smaller standard error of the mean compared to wet weights, 0.2% and 1.0% respectively. Since effects of swelling are expected to be uniform across soaking samples, submerged weights yielded less variable and more consistent results than wet weights. We postulated that the presence of sodium on the surface of the hydrogels, as detected by EDS, might have caused an increase in the submerged weights of specimens. Based on these findings, a pilot wear test in distilled water was conducted to avoid effects of salt entrapment while comparing submerged weights, wet weights and dry weights (Appendix 2).

This study supported the hypothesis that submerged weights were more precise than wet weights in characterizing volumetric wear of hydrogels. The pins were expected to wear faster than disks because they were exposed to cross-shear and the articulating surface of the pins were constantly under load for the duration of testing, which was expected to hinder rehydration and lubrication and facilitate wear, whereas only the portion of the articulating surface of disk in contact with the pin was under load at a given instant. Although wet weights were in disagreement with this prediction, the

submerged weights showed that the pins, on average, wore slightly while the disks ended up gaining minor weight (Table 2). In addition, the standard deviation in wear rate as measured by wet weights was four times the standard deviation as measured by submerged weights. Standard errors of the mean in wear rates based on submerged and wet weights were 3.7 and 14.6 mm^3 / million cycles respectively. Since specimens are of the same hydrogel formulation, large differences between wear rates of samples were not expected. Therefore, wear rates based on submerged weights were more reliable than wet weights. We postulated that the unexpected discrepancy between wear rates of stations based on wet weights could then be the result of the cumulative effect of both entrapped substances and changes in swelling. Despite their discrepancies, both measurement methods yielded hydrogel-on-hydrogel wear rates that were not statistically different from a wear rate of zero. However, coefficient of friction (Fig. 9) and surface roughness (Fig. 8) results indicated that surface topography of the tested hydrogel changed. Yet, visual inspection with SEM did not show any evidence of wear mechanisms that would otherwise indicate gross wear. These results suggested wear that was undetectable.

Differences in precision were used in this study to compare the two measurement methods because a gold standard method, which would enable comparisons also in accuracy between the methods, was not available for this study. Comparing dry weights before and after testing would have yielded results impervious to swelling and would help in quantifying the effect of salts entrapped in the specimens. However, fully dehydrating specimens before the wear test was not feasible since fully dehydrating hydrogels is known to affect their stiffness and wear resistance by inducing crosslinking [17, 18].

The wear rate of hydrogel calculated in our study was compared to wear rates of various hydrogels reported in literature to evaluate whether our results agree with those in the literature. Bavaresco et al. tested polyHEMA-coated pins on stainless steel disks under 2.4 MPa contact stress and reported wear rates in 0.005 mg/m range with static soak compensation, which is equivalent to 0.3 g / million cycles based on the wear path used in this study [6]. It should be noted that static soak compensation was not sufficient, in our study, to compensate for swelling of hydrogel during the wear test in contrast to the polyHEMA pins. Suciu et al. tested PVA for 0.1 million cycles under 1 MPa of contact stress and the lowest wear factor they reported was 10^{-6} mm^3 / Nm without soak compensation [12]. This corresponds to 5.9 mm^3/ million cycles when corrected for the load and wear track used in our study. Although the average wear rate of hydrogel articulation calculated in this study was smaller, the difference was not statistically significant based on submerged and wet weights ($p=0.12$; $p=0.97$), due to insufficient number of specimens. Katta et al. tested PVA/PVP for 0.1 million cycles under 2.9 MPa contact stress against CoCr and reported an average wear factor of 1.01E-6 ± 1.05E-7 mm^3 / (Nm) [7]. This wear factor corresponds to 6.0 ± 0.62 mm^3 / million cycles, which was higher than the wear rate calculated in this study, yet the difference was not statistically different based on submerged weights and wet weights ($p=0.11$; $p=0.97$). Finally, Yasuda et al. tested double network hydrogels [8] and Freeman et al. tested polyHEMA hydrogels [2], but they both reported maximum wear depth, indicative of wear, which is not comparable to wear rates in terms of volume that were presented in this study.

Previous studies analyzing wear of hydrogels [2, 6-8] presented only summarized wear data, which prevented monitoring of evolution of wear in order to discern effects of swelling. Sicui et al. published the wear data for each interval of the test and their results showed that hydrogel wear rates were still fluctuating until the end of the test at 0.1 million cycles [12]. In order to avoid complications related to gravimetric measurements of swellable materials, researchers employed various alternatives. Instead of mass, changes in articulating surface profile were monitored as indicative of wear [8, 9]. However, changes to roughness and surface profile may not easily be converted to wear volume that allows for comparisons with literature. In other studies, changes to sample dimensions were used to characterize wear [2, 11]. This approach could suffer from effects of creep and plastic deformation. Wear debris analysis has also been coupled with spectrophotometry [24] and used to quantify wear of hydrogels. This method requires a suitable chemical that would react with the dissolved hydrogel debris and involves complications due to calibration of spectrophotometer with concentration standards corresponding to known wear rates. The submerged measurement technique, which was proposed in our study, is of value because it is sufficiently precise and practical if performed repeatedly at each interval in order to decide whether the equilibrium wear rate is reached or more testing is needed.

References

[1] Peppas NA, Merrill EW. Development of semicrystalline poly (vinyl alcohol) hydrogels for biomedical applications. Journal of Biomedical Materials Research. 1977;11:423-34.
[2] Freeman ME, Furey MJ, Love BJ, Hampton JM. Friction, wear, and lubrication of hydrogels as synthetic articular cartilage. Wear. 2000;241:129-35.

[3] Caravia L, Dowson D, Fisher J, Corkhill P, Tighe B. A comparison of friction in hydrogel and polyurethane materials for cushion-form joints. Journal of Materials Science: Materials in Medicine. 1993;4:515-20.
[4] Bray JC, Merrill EW. Poly (vinyl alcohol) hydrogels for synthetic articular cartilage material. Journal of Biomedical Materials Research. 1973;7:431-43.
[5] Bodugoz-Senturk H, Macias CE, Kung JH, Muratoglu OK. Poly (vinyl alcohol)-acrylamide hydrogels as load-bearing cartilage substitute. Biomaterials. 2009;30:589-96.
[6] Bavaresco V, Zavaglia C, Reis M, Gomes J. Study on the tribological properties of pHEMA hydrogels for use in artificial articular cartilage. Wear. 2008;265:269-77.
[7] Katta JK, Marcolongo M, Lowman A, Mansmann KA. Friction and wear behavior of poly (vinyl alcohol)/poly (vinyl pyrrolidone) hydrogels for articular cartilage replacement. Journal of Biomedical Materials Research Part A. 2007;83:471-9.
[8] Yasuda K, Ping Gong J, Katsuyama Y, Nakayama A, Tanabe Y, Kondo E, et al. Biomechanical properties of high-toughness double network hydrogels. Biomaterials. 2005;26:4468-75.
[9] Northwood E, Fisher J. A multi-directional in vitro investigation into friction, damage and wear of innovative chondroplasty materials against articular cartilage. Clinical Biomechanics. 2007;22:834-42.
[10] Stammen JA, Williams S, Ku DN, Guldberg RE. Mechanical properties of a novel PVA hydrogel in shear and unconfined compression. Biomaterials. 2001;22:799-806.
[11] Bigsby R, Auger D, Jin Z, Dowson D, Hardaker C, Fisher J. A comparative tribological study of the wear of composite cushion cups in a physiological hip joint simulator. Journal of biomechanics. 1998;31:363-9.
[12] Suciu AN, Iwatsubo T, Matsuda M, Nishino T. A study upon durability of the artificial knee joint with PVA hydrogel cartilage. JSME International Journal Series C. 2004;47:199-208.
[13] Covert RJ. Durability evaluation of articular cartilage prostheses: Georgia Institute of Technology; 2003.
[14] Metters A, Anseth K, Bowman C. Fundamental studies of a novel, biodegradable PEG-b-PLA hydrogel. Polymer. 2000;41:3993-4004.
[15] Suggs LJ, Krishnan RS, Garcia CA, Peter SJ, Anderson JM, Mikos AG. In vitro and in vivo degradation of poly (propylene fumarate‐co‐ethylene glycol) hydrogels. Journal of Biomedical Materials Research. 1998;42:312-20.
[16] van Dijk-Wolthuis W, Hoogeboom J, Van Steenbergen M, Tsang S, Hennink W. Degradation and release behavior of dextran-based hydrogels. Macromolecules. 1997;30:4639-45.
[17] Thomas J, Gomes K, Lowman A, Marcolongo M. The effect of dehydration history on PVA/PVP hydrogels for nucleus pulposus replacement. Journal of biomedical materials research Part B, Applied biomaterials. 2004;69:135.
[18] Peppas NA, Merrill EW. Poly (vinyl alcohol) hydrogels: Reinforcement of radiation‐crosslinked networks by crystallization. Journal of Polymer Science: Polymer Chemistry Edition. 1976;14:441-57.
[19] Ding M, Odgaard A, Hvid I. Accuracy of cancellous bone volume fraction measured by micro-CT scanning. Journal of biomechanics. 1999;32:323-6.

[20] Sharp D, Tanner K, Bonfield W. Measurement of the density of trabecular bone. Journal of biomechanics. 1990;23:853-7.
[21] Pennings E, Grellner W. Precise nondestructive determination of the density of porous ceramics. Journal of the American Ceramic Society. 1989;72:1268-70.
[22] ASTM International PA U. F732 - Standard Test Method for Wear Testing of Polymeric Materials Used in Total Joint Prostheses. 2011.
[23] Pratten N. The precise measurement of the density of small samples. Journal of Materials Science. 1981;16:1737-47.
[24] Oka M, Ushio K, Kumar P, Ikeuchi K, Hyon S, Nakamura T, et al. Development of artificial articular cartilage. Proceedings of the Institution of Mechanical Engineers, Part H: Journal of Engineering in Medicine. 2000;214:59-68.

Conclusion

The previous chapters detailed the development of a methodology to characterize the tribological properties of a biphasic material for replacing damaged articular cartilage. In summary, biphasic cartilage models were employed to explore the correlations between the mechanical and tribological properties of a biphasic material. In addition, the lubrication mechanisms of the biphasic material were evaluated and compared to those of articular cartilage. Furthermore, Fourier transform infrared spectroscopy analysis and histology were used to assess the damage incurred on the opposing cartilage surface during *in vitro* wear testing against the biphasic material. Finally, submerged weight measurements were utilized to quantify wear of biphasic material.

In chapter 1, biphasic cartilage models were utilized to predict the mechanical response of a biphasic material in stress relaxation tests under confined and unconfined compression configurations. The effects of interstitial fluid pressurization, inherent matrix viscoelasticity and tension-compression nonlinearity on the bulk mechanical properties of the biphasic material were evaluated by linear biphasic, biphasic poroviscoelastic and linear biphasic with anisotropy models, respectively. The results of chapter 1 indicated that the simplest model we considered, i.e., the biphasic model with linear-elastic solid matrix (KLM), was sufficient to predict the material behavior of the family of tested hydrogels. Therefore, the effects of drag forces caused by fluid flow were dominant in the viscoelastic response of the material. Stribeck analysis of coefficient of friction at various combinations of velocity and load suggested that hydrogel on ceramic articulation was lubricated by a fluid film. Together, these findings suggested that, similar to articular cartilage, the biphasic material facilitated lubrication through

interstitial fluid pressurization. Furthermore, correlations between mechanical properties and coefficient of friction showed that biphasic materials with smaller aggregate moduli and larger permeability values than those of the hydrogels tested in this study would produce smaller coefficients of friction.

In chapter 2, *in vitro* wear of articular cartilage was microscopically characterized. Fourier Transform Infrared Spectroscopy (FTIRS) was employed, in tandem with histology, as a quantitative method to detect breakdown of matrix molecules before surface damage, such as clefts; fissures and fibrillations appeared. The effect of wear on multiple parameters relevant to the ultrastructure of articular cartilage was monitored simultaneously in order to determine *in vitro* wear mechanisms. FTIRS parameters related to collagen maturity and proteoglycan content were evaluated. The results from chapter 2 showed that beginnings of *in vitro* articular cartilage wear involved a decrease in collagen maturity and loss of proteoglycans. The collagen maturity parameter was the ratio of the infrared absorbance at 1660 cm^{-1} and the absorbance of 1690 cm^{-1}. These results suggested that *in vitro* wear testing of articular cartilage could have affected the secondary structure of collagen by disrupting the packing of triple helices. Although changes to the secondary structure of collagen could be detected by FTIRS, *in vitro* wear testing did not cause damage to the collagen network that was detectable by histological evaluation with H&E stain. Disruptions to the proteoglycan distribution, on the other hand, could be detected by both FTIRS analysis and histological evaluation. The effects of wear of cartilage against cartilage as control, and against CoCr and biphasic material as hemiarthroplasty materials were compared. Histological evaluation showed that tested control specimens had the thinnest proteoglycan deficient layer close to the surface

compared to cartilage pins that articulated against biphasic material, followed by cartilage pins that articulated against CoCr disks. Mechanical damage to the collagen ultrastructure due to wear was not visible on the surfaces or in the deeper zones of cartilage pins. FTIRS analysis, on the other hand, showed that cartilage on cartilage and cartilage on biphasic material articulation yielded higher collagen maturity than cartilage on CoCr articulation. In terms of proteoglycan content however, only cartilage on cartilage was higher than cartilage on CoCr articulation. In this dissertation, cartilage articulation against cartilage, biphasic material and CoCr might have represented three distinct stages of *in vitro* wear of articular cartilage. It was postulated that *in vitro* wear testing of cartilage first disrupted the secondary structure of collagen, i.e., the packing of triple helices, followed by proteoglycan loss from the matrix before surface fibrillation and clefts occurred.

In chapter 3, the performance of submerged measurement technique in quantifying hydrogel wear was evaluated. Submerged weights were shown to be reliable in quantifying mass of hydrogel with a standard error of 0.05 mg when using dry weights to estimate the submerged mass. Results from chapter 3 did not support our hypothesis that changes in swelling would not affect the submerged weights. However, Energy-dispersive X-ray Spectroscopy (EDS) revealed the presence of sodium on the surface of hydrogels. It was postulated that entrapped salts from the lubricant might have caused an increase in the submerged weights of specimens when testing was performed in bovine serum. Furthermore, wear testing results based on submerged weights and wet weights were compared. Standard errors of the mean in wear rates based on submerged and wet weights were 3.7 and 14.6 mm^3 / million cycles, respectively. Since specimens were of

the same hydrogel formulation, large differences between wear rates of individual samples were not expected and standard error was evaluated as a precision parameter. Therefore, submerged weights were found to be more precise than wet weights in characterizing volumetric wear of hydrogels. Finally, tribological properties of hydrogel on hydrogel articulation were characterized. The combination of coefficient of friction measurements and surface examinations by white light interferometry and by environmental scanning electron microscopy supported that wear generated in the current study was undetectable. Submerged weights compensated with dynamic soak controls yielded a wear rate of -1.4 ± 8.3 mm^3 / million cycles for hydrogel pin and disk couples, which was not statistically different than undetectable wear.

The contributions of this dissertation were: (1) the importance of interstitial fluid pressurization to the viscoelasticity and lubrication properties of this biphasic material, similar to articular cartilage, was demonstrated, (2) *in vitro* wear of articular cartilage was shown to initiate with a decrease in collagen maturity and loss of proteoglycans before histologically detectable damage on the structure of collagen network occurred, and (3) submerged measurement technique was shown to be more precise compared to wet weights for quantification of wear of biphasic materials.

Future studies should consider evaluating tribological properties of biphasic materials on joint simulators, which can simulate clinically relevant loading conditions in order to predict *in vivo* performance. Finally, instead of histological sectioning followed by FTIR microspectroscopy analysis, which were performed in the current study, Attenuated Total Reflectance - Fourier Transform Infrared Spectroscopy (ATR-FTIR) or infrared fiber optic probe should be considered for characterization of *in vitro* wear of

articular cartilage. These infrared modalities would enable non-destructive data acquisition at multiple time points and would enable the monitoring of evolution of *in vitro* cartilage wear based on the FTIRS parameters outlined in the current study.

Vita

Doruk Baykal, M.S.

Ph.D (in process)., Biomedical Engineering, Drexel University, 2013
M.S., Biomedical Engineering, Drexel University, 2010
B.S., Mechatronics Engineering, Sabanci University, Turkey, 2007

Drexel University Calhoun Fellowship, 2007-2012; Drexel University Provost Fellowship, 2007-2009; Sabanci University Success Scholarship, 2003-2007; Sakip Sabanci Full Scholarship for Academic Excellence, 2005-2007

Publications

Doruk Baykal; Mariya Tohfafarosh; Tina Arnholt; Cushla McGoverin; Kevin Mansmann; Nancy Pleshko; Steven M. Kurtz. "Microscopic Characterization of in vitro Wear of Articular Cartilage Against Hemiarthroplasty Materials". Submitted.

Baykal, D; Underwood, R; Mansmann, K; Marcolongo, M; Kurtz, S. "Evaluation of friction properties of hydrogels based on a biphasic cartilage model". Submitted.

Baykal, D., Siskey, R., Haider, H., Saikko, V., Ahlroos, T., Kurtz, S. "Advances in tribological testing of artificial joint biomaterials using multidirectional pin-on-disk testers". Journal of the Mechanical Behavior of Biomedical Materials, Under Review.

Baykal, D., Day, J., Jaekel, D., Katta, J., Mansmann, K., Kurtz, S. "Tribological Evaluation of Hydrogel Articulations for Joint Arthroplasty Applications". Journal of the Mechanical Behavior of Biomedical Materials, 2012. 14: p. 39-47.

Baykal D, Irrechukwu O, Lin PC, Fritton K, Spencer RG, Pleshko N. "Nondestructive Assessment of Engineered Cartilage Constructs Using Near-Infrared Spectroscopy". Applied Spectroscopy, 2010. 64(10): p. 1160-1166.

Appendix

1. **1) Derivation of the stress relaxation response of Biphasic Poroviscoelastic (BPVE) Model under confined compression configuration**

$\sigma^s = -\phi^s pI + \sigma^e$

$\sigma^f = -\phi^f pI$

$\pi^s = -\pi^f = K\left(v^f - v^s\right) = \frac{(\phi^f)^2}{k}\left(v^f - v^s\right)$

$\frac{\partial}{\partial t}\int \rho v\, dV = \int \rho b\, dV + \oint t_i\, dS + \int \pi\, dV$

$where\ \oint t_i\, dS = t_i \cdot n dS = \int \nabla \cdot \sigma\, dV$

$\dot{\rho} v + \rho \dot{v} = \rho b + \nabla \bullet \sigma + \pi$

$0 + 0 = 0 + \nabla \bullet \sigma + \pi$

$\nabla \bullet \sigma + \pi = 0;$ static conditions and no gravity

(intertial effects are much less than frictional effects)

$\nabla \bullet \sigma^f + \pi^f = 0$

$-\nabla \phi^f p - \frac{(\phi^f)^2}{k}\left(v^f - v^s\right) = 0$

$-k\nabla p = \phi^f \left(v^f - v^s\right)$ (1)

$\dot{m} = \int \frac{\partial}{\partial t}\rho\, dV = \rho J dV^0 = \left(\dot{\rho J}\right)$

$\left(\dot{\rho J}\right) = \dot{\rho} J + \rho \dot{J} = \dot{\rho} J + \rho \nabla \bullet v J = 0$

$\dot{p} + p\nabla \bullet v = 0$

$\nabla \bullet v = 0;$

$\nabla \bullet \left(\phi^s v^s + \phi^f v^f\right) = 0$

keep φ^f

$(1 - \phi^f) v^s + \phi^f v^f \rightarrow v^s - \phi^f v^s + \phi^f v^f$

$\nabla \bullet \left(v^s + \phi^f (v^f - v^s)\right) = 0$ (2)

Equation 1 is plugged into equation 2 to obtain:

$\nabla \bullet \left(v^s - k\nabla p\right) = 0$

since $v^s = du/dt$

$$\frac{\partial u}{\partial t} - k\nabla p = 0 \quad (3)$$

$$\sigma^t = \sigma^s + \sigma^f = -pI + \sigma^e$$
$$\nabla \bullet \sigma + \pi = 0$$
$$\nabla \bullet \left(-pI + \sigma^e\right) + \pi^s + \pi^f = 0$$
$$\nabla \bullet \left(-pI + \sigma^e\right) + 0 = 0$$
$$\sigma^e = -pI \rightarrow \nabla \bullet \sigma^e = \nabla p \quad (4)$$

Equation 4 is plugged into equation 3 to obtain:

$$\frac{\partial u}{\partial t} - k\nabla \cdot \sigma^e = 0 \quad (5)$$

For viscoelastic matrix properties:

$$\sigma^e = \underbrace{\lambda_{compression} \int g(t-\tau) \frac{\partial tr(\varepsilon_{kk})}{\partial \tau} \partial \tau}_{\text{bulk deformation}} + \underbrace{2G \int g(t-\tau) \frac{\partial e}{\partial \tau} \partial \tau}_{\text{shear deformation}}$$

$$g(t) = 1 + \int_0^\infty S(\tau) e^{-\frac{t}{\tau}} d\tau$$

$$S(\tau) = \begin{cases} \dfrac{c}{\tau}, & \tau_1 \le \tau \le \tau_2 \\ 0, & \tau \le \tau_1, \tau \ge \tau_2 \end{cases}$$

$$e_{ij} = \varepsilon_{ij} - \frac{1}{3}\varepsilon_{kk}\delta_{ij}$$

$$e_{33} = \varepsilon_{33} - \frac{1}{3}\left(\varepsilon_{11} + \varepsilon_{22} + \varepsilon_{33}\right) = \varepsilon_{33} - \frac{1}{3}\left(0 + 0 + \varepsilon_{33}\right)$$

$$e_{33} = \frac{2}{3}\varepsilon_{33}$$

$$tr(\varepsilon_{kk}) = \left(\varepsilon_{11} + \varepsilon_{22} + \varepsilon_{33}\right) = \left(0 + 0 + \varepsilon_{33}\right) = \varepsilon_{33} = \frac{\partial u}{\partial z}$$

$$\sigma^e = \lambda_{compression} \int g(t-\tau) \frac{\partial \frac{\partial u}{\partial z}}{\partial \tau} \partial\tau + 2G \int g(t-\tau) \frac{2}{3} \frac{\partial \frac{\partial u}{\partial z}}{\partial \tau} \partial\tau$$

$$\sigma^e = \lambda_{compression} \int g(t-\tau) \frac{\partial \frac{\partial u}{\partial z}}{\partial \tau} \partial\tau + 2G \int g(t-\tau) \frac{2}{3} \frac{\partial \frac{\partial u}{\partial z}}{\partial \tau} \partial\tau$$

$$\sigma^e = \left(\lambda_{compression} + \frac{4}{3} G \right) \int g(t-\tau) \frac{\partial \frac{\partial u}{\partial z}}{\partial \tau} \partial\tau;$$ deviatoric and dilation relaxations must be the same for this expression

$$\nabla \cdot \sigma^e = \left(\lambda_{compression} + \frac{4}{3} G \right) \int g(t-\tau) \frac{\partial \frac{\partial^2 u}{\partial z^2}}{\partial \tau} \partial\tau \quad (6)$$

Equation 6 is plugged into equation 5 to obtain:

$$\frac{\partial u}{\partial t} - k \left(\lambda_{compression} + \frac{4}{3} G \right) \int g(t-\tau) \frac{\partial \frac{\partial^2 u}{\partial z^2}}{\partial \tau} \partial\tau = 0$$

$$\left(\lambda_{compression} + \frac{4}{3} G \right) = H_A$$

$$\frac{\partial u}{\partial t} - k H_A \int_{-\infty}^{t} g(t-\tau) \frac{\partial \frac{\partial^2 u}{\partial z^2}}{\partial \tau} \partial\tau = 0 \quad (7)$$

The boundary conditions are listed below:

1. At bone intersection, z=h, u(h,t)=0
2. dp/dz=0 @z=h
3. At porous platen interface, p=0 @z=0

$$u_z(0,t) = u_a(t)$$

$$u_a = \begin{cases} v_0 t \ (t \le t_0) \\ v_0 t_0 \ (t > t_0) \end{cases}$$

4. $u_a(s) = v_o t - v_0(t - t_0)u(t - t_0)$

$$u_a(s) = \left(\frac{v_0}{s^2} - e^{-t_0 s}\frac{v_0}{s^2}\right)$$

$$\left.\begin{array}{l} u_a(0,s) = \frac{v_0}{s^2}\left(1 - e^{-t_0 s}\right) \\ u_z(1,s) = 0 \end{array}\right\} \text{ Boundary conditions}$$

Equation 7 is non-dimensionalized where spatial variables are normalized with respect to h and time is dimensionalized by Ha*k/h^2. Time domain is converted to Laplace domain.

The left hand side of the previous equation is the laplace convolution formula, $\int a(t-\tau)b(t)\,d\tau$ which is equivalent to A(s)B(s) in Laplace domain.

$$H_A \int_{-\infty}^{t} g(t-\tau)\frac{\partial \frac{\partial^2 \tilde{u}h}{\partial \tilde{z}^2 h^2}}{\partial \tau}\partial\tau = \frac{1}{k}\frac{\partial \tilde{u}h}{\partial \tilde{t}}\frac{H_A k}{h^2}$$

$$\int_{-\infty}^{t} g(t-\tau)\frac{\partial \frac{\partial^2 \tilde{u}}{\partial \tilde{z}^2}}{\partial \tau}\partial\tau = \frac{\partial \tilde{u}}{\partial \tilde{t}} \quad (8)$$

In this case, the multiplication is G(s)*d(d^{2}U/dz^2)/dt which is equal to:

$$G(s)\cdot s \cdot \frac{\partial^2 U(s)}{\partial z^2} - u(x,0)$$

$$G(s)\cdot s \cdot \frac{\partial^2 U(s)}{\partial z^2} \quad (9)$$

Laplace of g(t) is calculated next:

$$1+c\int_{\tau_1}^{\tau_2}\frac{1}{\tau}e^{-\frac{t}{\tau}}d\tau = 1+c\int_{\tau_1}^{\tau_2}-f'(t)d\tau$$

where

$$f(t)=e^{\frac{-t}{\tau}}$$

$$f'(t)=-\frac{1}{\tau}e^{\frac{-t}{\tau}}$$

since $\ell\{f'(t)\}=s\ell\{f(t)\}-f(0)$

$$\frac{1}{s}+c\int_{\tau_1}^{\tau_2}\left(-s\left(\frac{1}{s+\frac{1}{\tau}}\right)+1\right)\partial\tau \rightarrow \frac{1}{s}+c\int_{\tau_1}^{\tau_2}\left(\frac{-s\tau}{s\tau+1}+\frac{s\tau+1}{s\tau+1}\right)\partial\tau \rightarrow \frac{1}{s}+c\int_{\tau_1}^{\tau_2}\left(\frac{1}{s\tau+1}\right)\partial\tau$$

$$\frac{1}{s}+c\int_{\tau_1}^{\tau_2}\left(\frac{1}{s\tau+1}\right)\partial\tau \rightarrow \frac{1}{s}+c\cdot\frac{1}{s}\ln(s\tau+1)\Big|_{\tau_1}^{\tau_2} \rightarrow \frac{1}{s}+c\cdot\frac{1}{s}\ln\left(\frac{1+s\tau_2}{1+s\tau_1}\right) \quad (10)$$

Equations 9 and 10 are plugged into equation 8 to obtain:

$$\left(\frac{1+c\ln\left(\frac{1+s\tau_2}{1+s\tau_1}\right)}{s}\right)\cdot s\cdot\frac{\partial^2U(s)}{\partial\tilde{z}^2}=sU(s)-u(x,0)$$

$$\left(\frac{1+c\ln\left(\frac{1+s\tau_2}{1+s\tau_1}\right)}{s}\right)\cdot s\cdot\frac{\partial^2U(s)}{\partial\tilde{z}^2}=sU(s)$$

$$\frac{\partial^2U(s)}{\partial\tilde{z}^2}-\underbrace{\left(\frac{s}{1+c\ln\left(\frac{1+s\tau_2}{1+s\tau_1}\right)}\right)}_{f(s)}U(s)=0$$

Again, u(x,0)=0 in the first equation of this section is one of the initial conditions

Using boundary condition (4) @z=0;

$$\sigma = -pI + \sigma^s$$

$$\sigma = 0 + \sigma^s$$

Since p=0 @z=0, $\sigma_z = -P_A H(t) \rightarrow \sigma_z^s = -P_A H(t)$

$$\sigma_z^e = H_A \int g(t-\tau) \frac{\partial \frac{\partial u}{\partial z}}{\partial \tau} \partial \tau \quad (11)$$

Transforming equation 11 at z=0 to Laplace domain yields:

$$\frac{-P_A}{s} = H_A \frac{1}{f(s)} \cdot s \cdot \frac{\partial U(0,s)}{\partial \tilde{z}} - u(0,0)$$

$$\frac{-P_A}{s} = H_A \frac{1}{f(s)} \cdot s \cdot \frac{\partial U(0,s)}{\partial \tilde{z}} - 0$$

$$\frac{-P_A}{H_A} \frac{f(s)}{s^2} = \frac{\partial U(0,s)}{\partial \tilde{z}}$$

The following ODE is solved with the given boundary conditions

$$\frac{\partial^2 U(s)}{\partial \tilde{z}^2} - f(s)U(s) = 0$$

Since the second term has a negative coefficient, the proposed solution is in the form:

$$U(\tilde{z},s) = A(s)e^{\sqrt{f(s)}\tilde{z}} + B(s)e^{-\sqrt{f(s)}\tilde{z}} \quad (12)$$

The boundary and initial conditions are applied:

$$U(1,s) = A(s)e^{\sqrt{f(s)}} + B(s)e^{-\sqrt{f(s)}} = 0$$

$$\rightarrow B(s) = \frac{-A(s)e^{\sqrt{f(s)}}}{e^{-\sqrt{f(s)}}} = -A(s)e^{2\sqrt{f(s)}} \quad (13)$$

where $\tilde{z}$ =1 @ z=h; u(h,t)=0

$$U(0,s) = A(s) + B(s) = \frac{v_0}{s^2}\left(1 - e^{-t_0 s}\right)$$

$$A(s) - A(s)e^{2\sqrt{f(s)}} = \frac{v_0}{s^2}\left(1 - e^{-t_0 s}\right)$$

$$A(s) = \frac{v_0}{s^2} \frac{\left(1 - e^{-t_0 s}\right)}{1 - e^{2\sqrt{f(s)}}} \quad (14)$$

Equation 14 is plugged into equation 12:

$$\tilde{u}(\tilde{z},s)=\frac{v_0}{s^2}\frac{\left(1-e^{-t_0 s}\right)}{1-e^{2\sqrt{f(s)}}}e^{\sqrt{f(s)}\tilde{z}}-\frac{v_0}{s^2}\frac{\left(1-e^{-t_0 s}\right)}{1-e^{2\sqrt{f(s)}}}e^{2\sqrt{f(s)}\tilde{z}}e^{-\sqrt{f(s)}\tilde{z}}$$

$$\tilde{u}(\tilde{z},s)=-\frac{v_0}{s^2}\frac{\left(1-e^{-t_0 s}\right)}{1-e^{2\sqrt{f(s)}}}\left(e^{(2-\tilde{z})\sqrt{f(s)}}-e^{\sqrt{f(s)}\tilde{z}}\right)$$

$$\frac{\partial\tilde{u}}{\partial z}(\tilde{z},s)=\frac{v_0}{s^2}\frac{\left(1-e^{-t_0 s}\right)}{1-e^{2\sqrt{f(s)}}}\sqrt{f(s)}\left(e^{(2-\tilde{z})\sqrt{f(s)}}+e^{\sqrt{f(s)}\tilde{z}}\right)$$

$$\frac{\partial\tilde{u}}{\partial z}(\tilde{z},s)=\frac{v_0}{s^2}\frac{\left(1-e^{-t_0 s}\right)}{1-e^{2\sqrt{f(s)}}}\sqrt{f(s)}\left(e^{(2-\tilde{z})\sqrt{f(s)}}+e^{\sqrt{f(s)}\tilde{z}}\right)$$

$$\frac{\partial\tilde{u}}{\partial z}(0,s)=\frac{v_0}{s^2}\frac{\left(1-e^{-t_0 s}\right)}{1-e^{2\sqrt{f(s)}}}\sqrt{f(s)}\left(e^{2\sqrt{f(s)}}+1\right)$$

$$\frac{\partial\tilde{u}}{\partial z}(0,s)=-\frac{v_0}{s^2}\left(1-e^{-t_0 s}\right)\sqrt{f(s)}\coth(\sqrt{f(s)}) \quad (15)$$

$$F(s)=-H_{-A}\pi r_0^2\left.\frac{\partial u}{\partial z}\right|_{z=0}$$

Equation 15 is plugged into the force equation above to obtain the force response of the model in Laplace domain:

$$F(s)=H_{-A}\pi r_0^2\frac{v_0\sqrt{f(s)}}{s^2}\left(1-e^{-t_0 s}\right)\coth(\sqrt{f(s)})$$

where

$$f(s)=\frac{s}{1+c\ln\left(\frac{1+s\tau_2}{1+s\tau_1}\right)}$$

1. **2) Matlab scripts for parameter optimization and error analysis of BPVE model in confined compression**

confined_stressrelaxation_regression.m

```
material=2;
specimen=2;

trial_param1=[6; 0.13; 3; 0.1; 1]; %HA (*10^6) k (10^-16) c tao1 tao2
trial_param2=[5.4; 1.1]; %HA (*10^6) k (*10^-16)


time=eval(strcat('time',int2str(material),'_',int2str(specimen),'crop'));
stress=eval(strcat('stress',int2str(material),'_',int2str(specimen),'crop'));

hmatrix=[4.47 4.68 4.27 4.47 4.52; 4.24 4.2 4.55 4.19 4.25; 4.85 4.06 4.3 4.2 4.2];

options = optimset('DiffMinChange',1e-3, 'TolX', 1e-8,'MaxIter',1000);

[reg, fval]=fminsearch(@(trial_param1)
RMSE_confined(trial_param1,stress,time),trial_param1,options);

model=[time BPVE_confined_stressrelaxation_time([reg(1); reg(2); reg(3); reg(4);
reg(5)], time,h)];
r2(1)=coefficient_of_determination(stress,model(:,2));

plot(time, stress);
hold;
plot(time, model(:,2),'r');
xlabel('time (s)');
ylabel('stress (MPa)');

excel=[r2(1) sqrt(resnorm1) reg(1) reg(2) reg(3) reg(4) reg(5)];
```

RMSE_confined.m

```
function [rmse] = RMSE_confined(reg,stress,time)


if size(reg,1)==5
   y=BPVE_confined_stressrelaxation_time(reg, time);
else
   y=KLM_confined_stressrelaxation_time(reg, time);
end


n=size(y,1);

rmse=sqrt(1/n*(sum((y-stress).^2)));
```

BPVE_confined_stressrelaxation_time.m

```
function [stress] = BPVE_confined_stressrelaxation_time (parameters,time,h);


%h=0.00424;
v0=1.3*10^-6;
t0=h*0.1/v0;
%t0=376;

Ha=parameters(1,1)*10^6;
k=parameters(2,1)*10^-16;
c=parameters(3,1);
tao1=parameters(4,1);
tao2=parameters(5,1);

treal_to_t=Ha*k/h^2;

t=time.*treal_to_t;

t0_nond=t0*treal_to_t;
v0_nond=v0/treal_to_t/h;

stress=invlap('BPVE_confined_stressrelaxation_laplace',t,0,1e-9,v0_nond,t0_nond,c,
tao1,tao2).*Ha;
```

BPVE_confined_stressrelaxation_laplace.m

```
function f = BPVE_confined_stressrelaxation_laplace(s,v0,t0,c,tao1,tao2);

alpha=sqrt(s./(1+c*log((1+s.*tao2)./(1+s.*tao1))));


f=(v0./s.^2).*(1-exp(-t0.*s)).*alpha.*coth(alpha); %force

end
```

2. Verification of submerged measurement technique by dry weights following wear testing in distilled water

Introduction

Energy-dispersive X-ray Spectroscopy (EDS) analysis in chapter 3 showed that salts from the lubricant could be entrapped in the hydrogel matrix and could have

affected hydrogel measurements when testing was performed in bovine serum. In this study, wear testing of hydrogel on CoCr bearing couple was performed in distilled water to eliminate the effects of salt entrapment. Submerged weights were compared to dry and wet weights in order to verify the submerged measurement technique.

Methods

Pin shaped specimens of 9.53 mm diameter (n=3) were produced from a proprietary hydrogel (CyborGel, Formae Inc, Paoli, PA). Pins were desiccated at room temperature for 60 days until their weights stabilized. Subsequently, their dry weights were recorded. Following dehydration, the pins were rehydrated in distilled water.

Before wear testing, submerged weights and wet weights of the pins were recorded in accordance with the protocol described in chapter 3. Scratched CoCr disks (n=3) were used as counterface to ensure wear generation. Hydrogel on CoCr articulation was tested in distiller water using a Pin-on-disk tester. Applied axial load was 142 N, which corresponded to 2 MPa. Testing lasted 40000 cycles. The rest of the test parameters were described in chapter 3. At the end of the wear test, submerged and wet weights were recorded to calculate wear.

Following wear testing, the pins were desiccated in an oven at 95^0C for 24 hours and their final dry weights were recorded.

Results

Both dry weights and submerged weights yielded positive wear whereas results based on wet weights suggested undetected wear (Figure A-2-1). The average wear of hydrogel pins were 3% ± 0.5%, 1.3% ± 0.5% and -0.8% ± 0.2% as obtained by dry weights,

submerged weights and wet weights, respectively. Microscopy images of tested surfaces confirmed the generation of wear (Figure A-2-2). Pin #3, which yielded the largest wear by both submerged weights and dry weights, exhibited more severe surface damage compared to other tested pins.

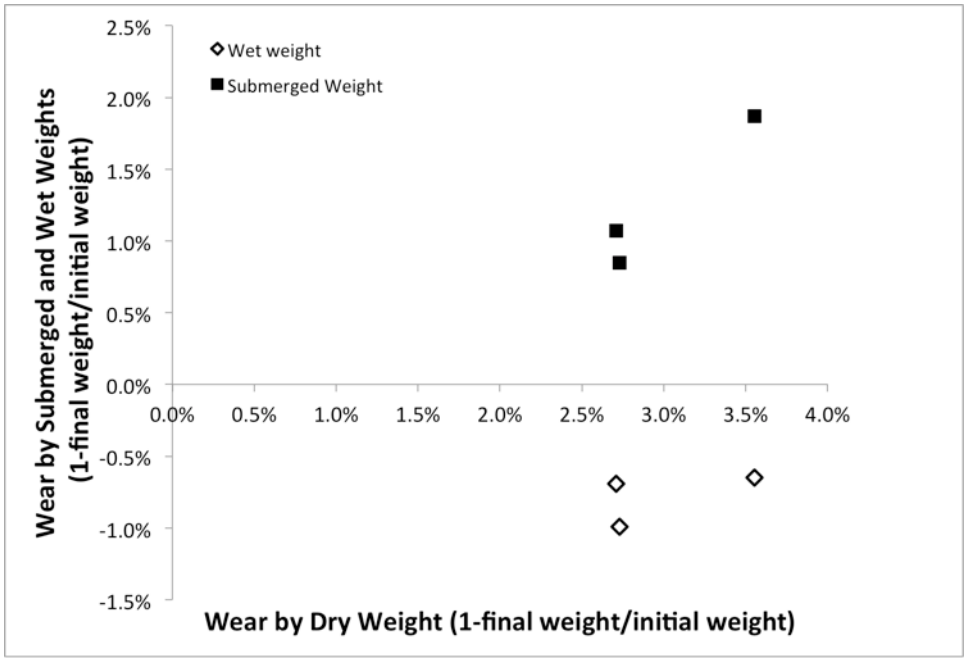

Figure A-1) Wear calculated by submerged and wet weights was plotted against wear calculated by dry weights.

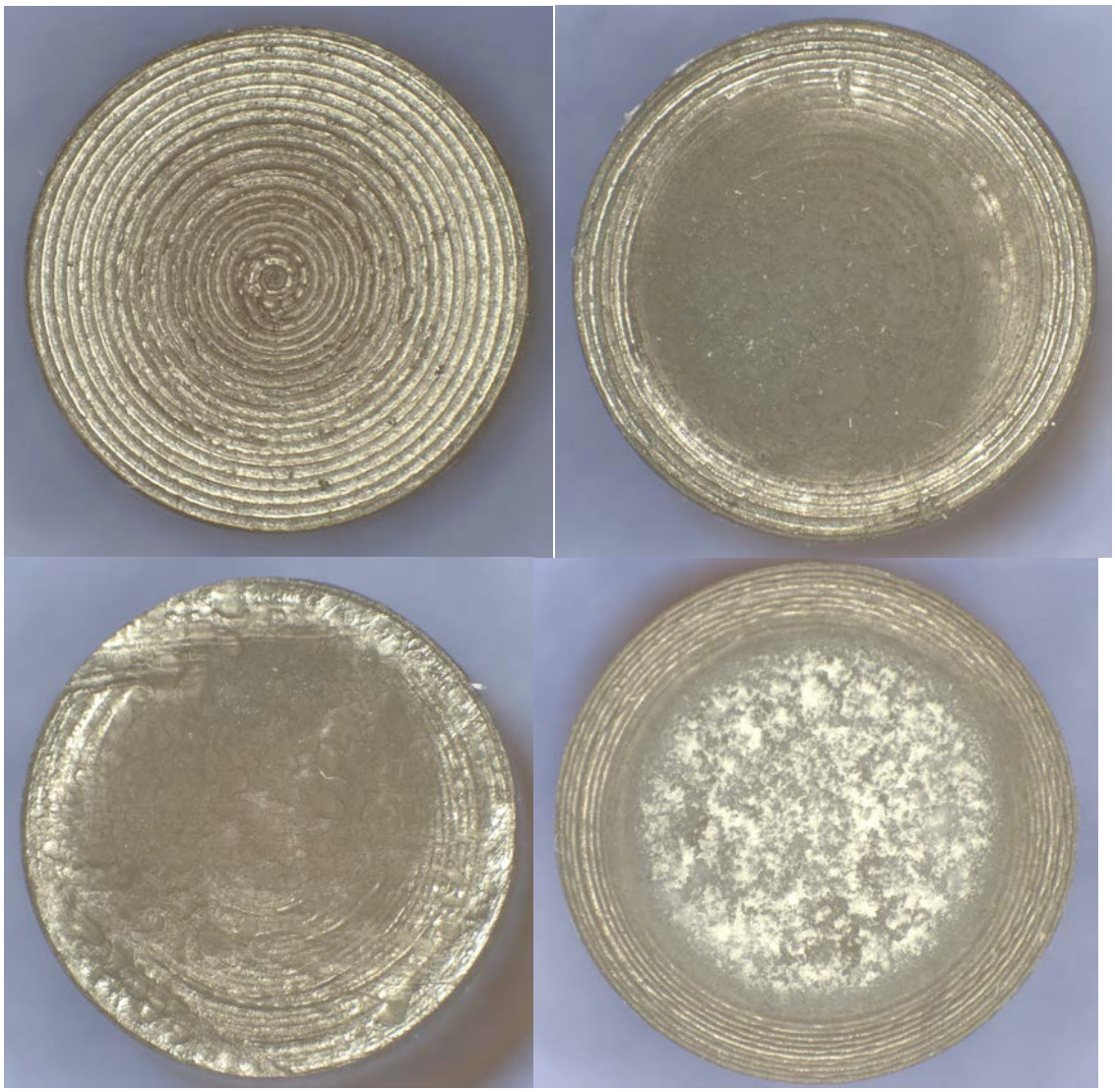

Figure A-2) a- Representative image of a pin surface before testing b- Surface of tested pin #1 c- Surface of tested pin #2 d- Surface of tested pin #3 were shown. Pin #3 showed severe surface damage.

Discussion

Submerged weights were shown to detect wear, which was confirmed by microscopy images, similar to dry weights. Wet weights, on the other hand, indicated an increase in weights, which could be due to increased swelling induced by broken crosslinks. The discrepancy between wear calculations by dry weights and submerged weights could be

due to having utilized two different methods to desiccate specimens before (at room temperature) and after testing (at elevated temperatures in an oven).